

## ABSTRACT

Title of thesis: Survey and Comparative Evaluation of  
Machine Learning Models For Performance  
Approximation of Tube-Fin Heat Exchangers

Rajath Subbappa  
Master of Science, 2021

Thesis directed by: Dr. Vikrant C. Aute  
Department of Mechanical Engineering

Abstract: Tube-fin heat exchangers (TFHXs) are omnipresent within the air-conditioning and refrigeration industry. Computationally expensive, physics-based models are conventionally used to conduct performance simulations, optimization, and design selection of such devices. In this thesis, a comparative evaluation of machine learning based regression techniques to predict the heat transfer and refrigerant pressure drop of TFHXs for different applications is conducted. Ridge Regression, Support Vector Regression (SVR) and Artificial Neural Network (ANN) models are trained and analysed. Results show that the baseline full-domain SVR and ANN models predict more than 90% of the test dataset within a 20% error band for 5 out of 6 application cases. Subsequently, an outcome-based comparison framework is proposed to understand the cost incurred by an ML model in achieving a predetermined degree of accuracy. As a result, reduced-domain ANN and SVR models with training times that are 2 to 3 orders of magnitude lower than baseline models with little to no degradation in prediction accuracy are obtained. The trained ML

models facilitate rapid exploration of the design space with significant reduction in engineering time to arrive at near optimal designs.

Survey and Comparative Evaluation of Machine Learning Models  
For Performance Approximation of Tube-Fin Heat Exchangers

by

Rajath Devendranath Subbappa

Thesis submitted to the Faculty of the Graduate School of the  
University of Maryland, College Park in partial fulfillment  
of the requirements for the degree of  
Master of Science  
2021

Advisory Committee:

Dr. Vikrant C. Aute, Advisor and Chair  
Professor Dr. Bao Yang  
Professor Dr. Mark Fuge

© Copyright by  
Rajath Devendranath Subbappa  
2021

## Dedication

To those who placed their belief in me, when I had none myself.

## Acknowledgments

I would like to take this opportunity to express my heartfelt gratitude towards Dr Vikrant Aute for giving me a wonderful but challenge-filled opportunity to conduct research at the Center for Environmental Energy Engineering (CEEE). Apart from serving as my research guide during my masters tenure, he also ensured that personal growth and comfort was never compromised. Thank you Dr. it has been an honor to have gotten the chance to learn from you.

To Dr. Bao Yang and Dr. Mark Fuge, I greatly appreciate the efforts taken to serve on my thesis committee.

I would like to thank Dr. Jiazhen Ling for always extending a helping hand in times of hardship, he always knew what I needed to overcome an obstacle. He was the perfect mediator between Dr. Vikrant and myself.

I wish to single out Dr. Daniel Bacellar for his unmatched professional and personal guidance. I will forever be grateful for the lessons imparted.

I have had the luxury of working beside some tremendous people. I will always be indebted to James Tancabel for engaging in numerous technical conversations with a bottomless pit of patience, Tanjebul Alam for his encouragement, suggestions and his love for Liverpool Football Club - "You'll never walk alone", Lalith Kannah for his companionship and timely help during the writing of this thesis and Dr. Ransisi Huang for taking great pain in teaching me the ropes of C#.

I am blessed to have made some amazing friends; Ajay, Harsha Naveen Das, and Shri Harsha, my housemates for the past two years, who always knew how to pick me up during times of uncertainty and doubt. I definitely do not thank them enough for it; Priyanka Prakash for her invaluable contributions to my thesis and my elder brother Varun for keeping me motivated during the final stages of my thesis.

Finally coming to the pillars of my life; my parents and my partner Shruthi. Without their motivation, guidance, support and presence this thesis would have been far from complete. I deeply apologize for all the time not spent with you. You are more than I could have deserved and making the three of you proud of my accomplishments is all that I will ever strive for.

# Table of Contents

Dedication	ii
Acknowledgements	iii
Table of Contents	v
List of Tables	vii
List of Figures	viii
List of Abbreviations	x
Chapter 1: Introduction	1
1.1 Background and Motivation	1
Chapter 2: Literature Review	5
2.1 Heat Exchanger Modeling Techniques	5
2.1.1 Lumped Modeling Approaches	7
2.1.2 Moving Boundary Modeling Approaches	8
2.1.3 Tube-by-Tube Modeling Approaches	10
2.1.4 Segment-by-Segment Modeling Approaches	11
2.2 Approximation Assisted Modeling (AAM)	12
2.3 Machine Learning Methods Adopted	14
2.3.1 Linear Regression	15
2.3.2 Support Vector Regression	19
2.3.3 Multi-Layer Feed Forward Neural Network	24
2.4 Machine Learning Approximation of Heat Exchangers	28
2.4.1 HX Performance Prediction	28
2.4.2 ML Estimation of Heat Exchanger Parameters	33
2.4.3 Identification of Two-Phase Flow Regimes	40
2.5 Summary	43
2.6 Research Gaps	45
2.7 Research Objectives	45
2.8 Research Tasks	46
2.9 Organization of Thesis	46
Chapter 3: ML Model Development of Single-Phase Heat Exchanger	48

3.1	Introduction . . . . .	48
3.2	Solution Methodology . . . . .	49
3.2.1	Design Space Identification . . . . .	50
3.2.2	Design Space Sampling . . . . .	51
3.2.3	Synthetic Data Generation . . . . .	52
3.2.4	Exploratory Data Analysis . . . . .	52
3.2.5	Data Pre-processing . . . . .	56
3.2.6	Hyperparameter Tuning . . . . .	59
3.2.7	Performance Metrics . . . . .	62
3.2.8	Model Training . . . . .	64
3.2.9	Data Pre-processing Outcome . . . . .	66
3.2.10	Model Testing . . . . .	68
3.2.11	Physical Verification of ML models . . . . .	71
3.3	Training Dataset Size Impact . . . . .	75
3.4	Outcome-based Comparison Framework . . . . .	76
Chapter 4: ML Model Development of Two-Phase Heat Exchangers		79
4.1	Introduction . . . . .	79
4.2	Solution Methodology . . . . .	80
4.2.1	Design Space Identification . . . . .	80
4.2.2	Design Space Sampling . . . . .	81
4.2.3	Synthetic Data Generation . . . . .	82
4.2.4	Exploratory Data Analysis . . . . .	82
4.2.5	Data Preprocessing . . . . .	86
4.2.6	Hyperparameter Tuning . . . . .	89
4.2.7	Model Training . . . . .	90
4.2.8	Model Testing . . . . .	90
4.3	Training Dataset Size Impact . . . . .	96
4.4	Outcome-based Comparison . . . . .	98
Chapter 5: Conclusion		99
5.1	Summary . . . . .	99
5.2	Conclusions . . . . .	100
5.3	Contributions . . . . .	102
5.4	Future Work . . . . .	103
Bibliography		104
Bibliography		104

## List of Tables

2.1	Kernel Functions . . . . .	23
2.2	Activation Functions . . . . .	26
3.1	Radiator Data . . . . .	52
3.2	Model Hyperparameters . . . . .	59
3.3	Kolmogorov-Smirnov Test Results . . . . .	62
3.4	Tuned Model Configuration . . . . .	64
3.5	Baseline Machine Learning Model Comparison . . . . .	68
3.6	Baseline Machine Learning Model Comparison . . . . .	70
3.7	Comparison of ML Model Performance for Sample Radiator . . . . .	73
4.1	Tube-Fin Condenser Data . . . . .	82
4.2	Tube-Fin Evaporator Data . . . . .	82
4.3	TF Condenser ML model tuned hyperparameters . . . . .	89
4.4	TF Evaporator ML model tuned hyperparameters . . . . .	89
4.5	TF Condenser Baseline ML Models Comparison . . . . .	91
4.6	TF Evaporator Baseline ML Models Comparison . . . . .	91
4.7	TF Condenser Baseline ML Models Comparison . . . . .	93
4.8	TF Evaporator Baseline ML Models Comparison . . . . .	94

## List of Figures

2.1	Control Volumes Based on Modeling Approach [15]	6
2.2	Machine Learning Types	14
2.3	Ordinary Least Squares Estimation [43]	16
2.4	Ridge Estimate vs Ordinary Least Squares Estimate [43]	18
2.5	Lasso Estimate vs Ordinary Least Squares Estimate [43]	19
2.6	SVR Representation [47]	21
2.7	Typical Multi-Layer Feed Forward Neural Network [48]	24
2.8	Information Processing within Neuron	25
2.9	Heat Exchanger Application Area	43
2.10	Machine Learning Model applied	43
2.11	HX Performance Prediction Studies	44
3.1	Flowchart of ML Modeling	49
3.2	Radiator Design Space	50
3.3	Machine Learning Model Output	50
3.4	Variable Distribution	53
3.5	Correlation Matrices	55
3.6	Box-Cox Transformation	58
3.7	k-Fold Cross Validation [44]	60
3.8	Comparison of Statistical Moments	62
3.9	Comparison of Statistical Moments	63
3.10	Artificial Neural Network Training Behavior	65
3.11	Data Pre-processing Outcome	67
3.12	Heat Load Prediction Verification Plots	69
3.13	Pressure Drop Prediction Verification Plots	71
3.14	Sample Radiator Design Space	72
3.15	Parametric Analysis	73
3.16	Pairwise Comparison of HX design	74
3.17	Radiator Training Dataset Size Impact	76
3.18	Outcome-based Comparison Framework	77
3.19	ML Model Appropriateness	78
4.1	Condenser Design Space	80
4.2	Evaporator Design Space	81
4.3	Machine Learning Model Output	81
4.4	TF Condenser Variable Distribution	83

4.5	TF Evaporator Variable Distribution . . . . .	84
4.6	Correlation Matrices for TF Condenser . . . . .	86
4.7	Correlation Matrices for TF Evaporator . . . . .	87
4.8	Yeo-Johnson Transformation . . . . .	88
4.9	TF Condenser Heat Load Prediction Verification Plots . . . . .	92
4.10	TF Evaporator Heat Load Prediction Verification Plots . . . . .	93
4.11	TF Condenser Pressure Drop Prediction Verification Plots . . . . .	94
4.12	TF Evaporator Pressure Drop Prediction Verification Plots . . . . .	95
4.13	Condenser Training Dataset Size Impact . . . . .	97
4.14	Evaporator Training Dataset Size Impact . . . . .	97
4.15	ML Model Appropriateness . . . . .	98

## Nomenclature

### English Symbols

$\Delta P$	Pressure Drop [Pa]
$\Delta T$	Temperature difference [K]
$b$	Bias term in Neural Networks [-]
$C$	Shrinkage term in Support Vector Regression [-]
$D$	Diameter [m]
$exp$	Exponent [-]
$G$	Mass flux [ $\text{kgm}^{-2}\text{s}^{-1}$ ]
$h$	Enthalpy [ $\text{Jkg}^{-1}$ ]
$K$	Number of folds in K-fold cross validation [EA]
$k$	Kernel function [-]
$L$	Lagrangian [-]
$m$	Refrigerant charge [kg]
$max$	Maximize, Maximum [-]
$min$	Minimize, Minimum [-]
$N$	Speed [RPM]
$Nu$	Nusselt number [-]
$P$	Pressure [Pa]
$Q$	Heat load or Heat exchanger capacity [W]
$R$	Correlation coefficient [-]

$R^2$	Coefficient of determination [-]
$Re$	Reynolds number [-]
$T$	Matrix transpose, Temperature [K]
$UA$	Overall heat conductance [WK <sup>-1</sup> ]
$V$	Velocity [ms <sup>-1</sup> ]
$w$	Neural network weights [-]
$X$	Design Variable (Model input)
$x$	Observation, Refrigerant quality [-]
$Y$	Response (Model output)

### Acronyms

$1D$	One Dimension
$2D$	Two Dimension
$AAM$	Approximation Assisted Modeling
$AC$	Air Conditioning
$ANN$	Artificial Neural Network
$BP$	Back Propagation
$CFD$	Computational Fluid Dynamics
$CV$	Cross Validation
$DOE$	Design of Experiments
$ELU$	Exponential Linear Unit
$htc$	Heat transfer coefficient [Wm <sup>-2</sup> K <sup>-1</sup> ]
$HVAC\&R$	Heating Ventilation Air Conditioning and Refrigeration
$HX$	Heat eXchangers
$KNN$	K-Nearest Neighbors
$LMTD$	Log-Mean Temperature Difference [K]
$LR$	Linear Regression
$MAPE$	Maximum Absolute Percentage Error [%]

<i>MFR</i>	Mass Flow Rate [ $\text{kgs}^{-1}$ ]
<i>ML</i>	Machine Learning
<i>MLFFN</i>	Multi Layer Feed Forward Neural Network
<i>NTU</i>	Number of Transfer Units
<i>Nu</i>	Nusselt Number
<i>ReLU</i>	Rectified Linear Unit
<i>RMAE</i>	Relative Mean Absolute Error [%]
<i>RMSE</i>	Root Mean Square Error
<i>RR</i>	Ridge Regression
<i>SGD</i>	Stochastic Gradient Descent
<i>SVM</i>	Support Vector Machine
<i>SVR</i>	Support Vector Regression
<i>TF</i>	Tube Fin
<i>TFHX</i>	Tube Fin Heat Exchanger
<i>VCC</i>	Vapor Compression refrigeration Cycle

### **Greek symbols**

$\alpha$	Void Fraction, Lagrange Multiplier for Inequality Constraints, Kernel Parameter in Sigmoid Kernel, Parameter in ELU Activation Function
$\beta$	Regression Coefficients or Weights
$\Delta$	Difference
$\epsilon$	Effectiveness, Tube Width in SVM
$\eta$	Lagrange Multiplier for Equality Constraints
$\gamma$	Kernel Parameter in Sigmoid Kernel
$\lambda$	Shrinkage Term in RR
$\phi$	Activation function for Neural Network
$\Sigma$	Summation

$\sigma$  Standard Deviation, Fin thickness, Kernel Parameter in Gaussian Kernel

$\xi$  Slack Variables in SVM

### **Subscript**

*air* Air

*cond* Condensation

*db* Dry Bulb

*delta* Degree of Superheat [K]

*evap* Evaporation

*in* Inlet

*ref* Refrigerant

*water* Water

*wb* Wet Bulb

### **Superscript**

*air* Air

*ref* Refrigerant

*water* Water

## Chapter 1: Introduction

### 1.1 Background and Motivation

The United States Energy Information Administration (EIA) estimates that by the year 2050, the energy use for Air Conditioning (AC) systems will grow faster than any other end use in the building sector (commercial and residential) [1]. In the year 2020, the building sector consumed 37.7 quadrillion BTU (quads), thereby accounting for roughly 39% of the energy consumption of the United States [1]. A further breakup of the 37.7 quads revealed that Heating, Ventilation, Air Conditioning and Refrigeration (HVAC&R) systems accounted for 60% of the residential and 47% of the commercial energy intake respectively. At the heart of every AC system is the Vapor Compression refrigeration Cycle (VCC). In addition, food and beverage processing establishments, pharmaceutical industries and scores of other industrial establishments have a deep need for temperature and humidity control. This need is satisfied again by the VCC. In short, the importance of this cycle cannot be exaggerated.

Since, air-to-refrigerant Heat eXchangers (HX) make up two of the four key components of the VCC, they largely dictate the performance and cost of HVACR systems. Westphalen et al. [2] highlighted the impact heat transfer enhancement

(htc) on the air-side of a condenser has on energy consumption. The authors showed that, doubling the air-side heat transfer coefficient could reduce cycle energy consumption by 10-15%, consequently decreasing the building energy consumption by 4.6-6.9%. Thus, it is clear that the need of the hour is an improvement in HX performance either through novel product design, or via rigorous mathematical optimization.

A-priori knowledge of favorable regions (performance wise) within the design space is highly sought after in areas of design optimization and system integration. The pool of prospective designs is quite significant to begin with; but when these designs are required to be chosen in conjunction with other system components, the number of combinations increase considerably and consequently the duration of HX simulations is compounded. In this view, it is indisputable that there exists a requirement for accurate yet quick prediction models. Such tools are therefore of great prominence during design comparisons, and more so with ever-increasing design complexity.

The complexity in HX analysis stems from the interactions between fluid flow and heat transfer processes along with the effects of complex geometry. This demands a high level of detail that is usually synonymous with physics based HX models. In order to make these models more convenient to solve, reasonable but restrictive assumptions are made [3].

Rather than attempting to understand the laws of physics as is the case with conventional techniques [4], [5], Machine Learning (ML) models are capable of determining the causal relationship between the inputs (features) and outputs (targets)

pertaining to a HX simulation [6]. These models are characterized by simple computational steps, accompanied by a large number of repeated computational cycles.

Despite their black-box nature, ML models have been widely used for their speed and accuracy to predict the performance of complex systems [7]. Keeping in mind our intention of obtaining rapid but accurate HX designs for a given set of system requirements, it is certainly attractive to implement ML models in our performance predictions of HXs. In addition to predicting steady-state systems with a high level of precision [8–10], ML models have yielded satisfactory results when simulating transient systems [11]. Sen and Yang [12] conducted tests that dealt with dynamic heating and cooling of air across a tube-fin HX (TFHX). They developed an Artificial Neural Network (ANN), that was able to predict the outlet temperatures of water and air in close agreement to experimental results. Furthermore, an aggressive advancement of these techniques makes them all the more viable in the solving of complex thermal problems.

That being said, ML techniques can hardly be considered a panacea to resolve the existing challenges in the field of HVACR. An in-depth, physical understanding of the phenomena that is being statistically modeled, will forever be relevant since reliable ML models deeply rely on being fed with the appropriate mechanistic parameters. Moreover, a sound theoretical understanding is a means of critically analyzing the ML model output. What may sometimes be numerically correct may have no practical meaning whatsoever. The following are disadvantages inherent to ML techniques:

- (i) Extensive data required to develop accurate models.
- (ii) Training and tuning of ML models can be time-consuming, and in some cases the procedure involves trial-and-error.
- (iii) Extra attention is required to prevent ML models from overfitting to the training data.
- (iv) ML models cannot guarantee reliable performance beyond the training data used [13], i.e., they cannot be extrapolated.

## Chapter 2: Literature Review

The role of Machine Learning (ML) in heat transfer studies has been on the rise for over the past two and a half decades. A result of vigorous advances in artificial intelligence and computer hardware, is a set of ML algorithms which are being developed to efficiently map process inputs to output(s). Prior to thoroughly reviewing the impact of ML in the field of heat transfer, it would be fitting to briefly review conventional Heat eXchanger (HX) modeling techniques so as to provide the necessary background for the utilization of ML not as an alternative, but as an ally to conventional procedures in the solution of heat transfer challenges prevalent today.

### 2.1 Heat Exchanger Modeling Techniques

Air-to-refrigerant HXs have been actively investigated for several years now. The aim during the modeling and design optimization phase is to come up with a prototype that is 90% correct [14]. Thus, apart from the performance enhancement of HXs, there lies a strong emphasis on the improvement of their modeling, simulation, and optimization. To accurately predict HX performance, several simulation approaches have been formulated. Based on their accuracy and computational time,

they can be broadly classified as lumped parameter approach, moving boundary approach, tube-by-tube approach, and segment-by-segment approach 2.1. At the heart of each technique is a fundamental heat transfer calculation method that is exercised on a control volume of varying resolution. The calculation methods used widely are:

- (i) Logarithmic Mean (UA-LMTD) or Arithmetic Mean Temperature Difference (UA-AMTD).
- (ii) Effectiveness Number of Transfer Units ( $\epsilon$ -NTU).
- (iii) Conservation of Energy.

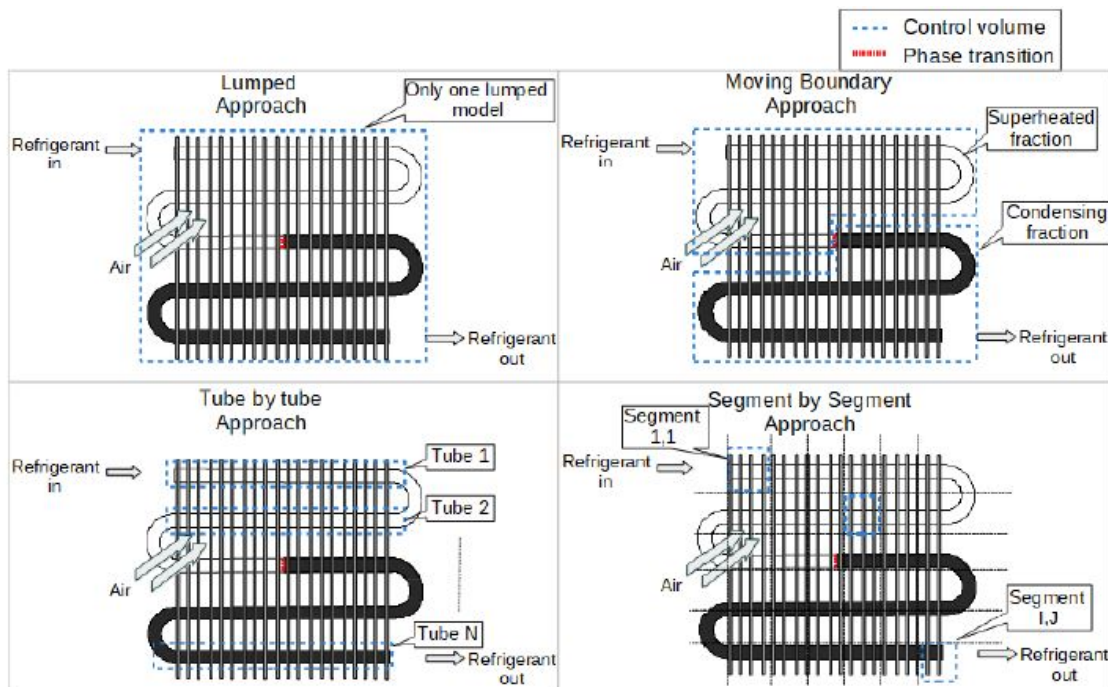


Figure 2.1: Control Volumes Based on Modeling Approach [15]

### 2.1.1 Lumped Modeling Approaches

The lumped modeling approach is by far the simplest among the four approaches mentioned above. Several researchers have employed the lumped approach in their HX analyses [16–20].

Parise [16] developed a vapor compression heat pump simulation model by employing simple lumped models for the condenser and evaporator. The overall conductances (UA) of the HX are treated as constant input parameters based on the arithmetic overall temperature differences of the fluids participating in the heat exchange. It is worth mentioning that the values of UA do account for the two-phase region in addition to single-phase. Jin and Spitler [19] presented a vapor compression heat pump model in which the evaporator and the condenser were modeled using the  $\epsilon$ -NTU method on a lumped basis. Constant UA values for the evaporator and condenser were derived from manufacturer’s data. The measured condenser and evaporator values of Q were on average 12% and 17% lower than the model-predicted rates respectively. A compact HX model which adopted the lumped approach was developed by Zhou et al. [20]. The model is capable of calculating Q and  $\Delta P$  whose values were then validated using experimental data. The results show that the RMAE for Q and  $\Delta P$  is 7.6% and 2.9% respectively. While the predicting capabilities of the model seem attractive, care should be taken before utilizing this approach since the correlations of j and f factors are required to be of a certain functional form. Additionally, dehumidification is not considered in this approach.

Though computationally inexpensive, the lumped approach possesses the following inherent drawbacks:

- (i) Phase transition and local thermophysical properties are not considered which may result in inaccurate predictions.
- (ii) The predetermined empirical parameters used to represent overall heat transfer coefficients in the two-phase region require careful tuning.
- (iii) Additionally, these parameters rely on manufacturer provided HX performance data which may not always be present.

### 2.1.2 Moving Boundary Modeling Approaches

The moving boundary modeling approach takes into consideration refrigeration phase change as part of its analysis in addition to dehumidification on the air-side. In this approach, the HX is divided into single-phase and two-phase zones. Once such a discretization has been made, the lumped approach is exercised on each zone. The following are works based on this approach [21–26].

Braun et al. [21] devised effectiveness models for cooling coils through the introduction of air saturation specific heat. In their modeling approach, they analyze the case of a combined wet and dry surface through a bifurcation of the HX outer surface area into wet and dry zones. Abdelaziz et al. [24] adopted a moving boundary HX modeling approach to obtain accurate but fast models as part of their transient simulations of household refrigeration systems. The result of the authors’

efforts was a highly generalized model suitable for both condensers and evaporators. Bell [25] used the moving boundary approach in the modeling of TFHXs. The  $\epsilon$ -NTU method was applied to each zone, wherein both fluids were assumed to have constant specific heat values. Average heat transfer coefficients on the air and refrigerant sides were considered. Qiao et al. [26] presented an advanced HX model based on the moving boundary approach to dynamically simulate VCCs. The model was used to predict the occurrences during the start-up of an R410A flash tank vapor injection cycle. A close agreement between experimental data and modeling results were noticed. Furthermore, the results of this dynamic boundary model were compared against that of the finite volume (segment-by-segment) model. Apart from prediction accuracy being upheld, the former was able to outpace the latter by a factor of 3.

The moving boundary approach exhibits a superiority in prediction accuracy over the lumped approach. At the same time, computationally speaking, it is relatively inexpensive. The approach however, has the following drawbacks:

- (i) The temperature difference between the participating fluids are taken to be constant over an entire single or two-phase zone, which may lead to inaccuracies in predictions.
- (ii) Air or refrigerant flow maldistribution cannot be accounted for.
- (iii) From a system level transient simulation point of view, the moving boundary approach cannot be used in cases which include zero incoming flow [26]. In such cases a segment-by-segment approach should be adopted.

### 2.1.3 Tube-by-Tube Modeling Approaches

Post the initial consideration that each HX tube is a separate control volume, the lumped approach is applied to each tube to solve for HX performance [27–31]. This approach is capable of handling refrigerant-side and air-side 1D (transverse to the air flow) maldistributions in addition to accounting for refrigerant phase change.

Domanski [27], [28] presented a simulation model for a plate fin air-to-refrigerant HXs. The heat transfer was calculated using the UA-LMTD method for each tube, analyzed separately in a sequential manner. Refrigerant distribution is determined by a sequential analysis of each split point and associated branches. Air distribution data is needed at discrete points on the coil face to handle 1D nonuniform air distribution. Finally, tubes in which phase change occurs can be identified and the fraction of tube length associated with each phase can be calculated. Liu et al. [30] developed a general steady state model of TFHXs based on graph theory. With the aid of a directed graph and graph-based search algorithms, the model is capable of simulating complex refrigerant circuitry in addition to heat conduction through fins. On a control volume level (tube in this case) where energy balance equations are exercised, the authors' have presented a computational algorithm that is iterative in nature. The refrigerant  $\Delta P$  is calculated by solving the momentum equation at each control volume in a sequential manner along the flow path. The model predicts experimental  $Q$  and  $\Delta P$  values within deviations of  $\pm 10\%$  and  $\pm 20\%$  respectively. Richardson [31] conducted modeling of a cross flow TFHX (condenser) by representing the entire length of the tube as a single segment followed by the application of

lumped  $\Delta P$  and heat transfer correlations. The  $\epsilon$ -NTU method was implemented to determine heat transfer for a given control volume. Heat transfer calculations of the different phases were conducted separately with the help of correction factors. In order to improve the simulation efficiency, multiple tube passes are combined into a single pass with arrangements being made to offset errors arising out of such a simplification.

While the tube-by-tube approach does away with the major disadvantage of the moving boundary approach, one shortcoming is:

- (i) 2D air maldistribution cannot be handled.

#### 2.1.4 Segment-by-Segment Modeling Approaches

A significant difference in air profile exists along the length of a HX tube [32], [33]. This necessitates a finer control volume approach resulting in widespread application of the segment-by-segment method [4, 34–40]. Similar to the previous approach this approach too subdivides a segment when phase transition occurs.

Rossi [34] developed a heat pump simulation model named ACMODEL. To ensure the convergence of a solver within a tight tolerance, the segment-by-segment approach was adopted. Heat transfer calculations were done using the  $\epsilon$ -NTU method. A distributed simulation model for steady-state prediction of evaporator coils with complex circuitry was developed by Liang et al. [35]. The UA-LMTD method was made use of to calculate the performance of individual control volumes. Jiang et al. [4] developed a general-purpose simulation and design tool for air-to-refrigerant

HXs. They adopted a segment-by-segment modeling approach enabling an efficient handling of 2D air maldistribution as well as heterogeneous refrigerant flow patterns within the HX. A junction tube connectivity matrix was defined to account for complex refrigerant circuitry. The  $\epsilon$ -NTU method was employed at each segment for heat transfer calculations, and further subdividing of segments was carried out in cases of phase transition. Singh et al. [39] formulated an air-to-refrigerant fin-tube HX that is capable of accounting for tube-to-tube heat conduction. This model was based on the solution methodology of Jiang et al [4] and includes two approaches to solve for the tube-to-tube conduction. The UA-LMTD method was exercised on individual control volumes. Both approaches were validated against experimental data and were found to be in close agreement. In a recent work by Sarfraz et al. [40], a fin discretized model was developed which eliminates the need to iteratively compute tube wall temperature resulting in a reduction in computational cost.

## 2.2 Approximation Assisted Modeling (AAM)

As was detailed in the previous section, most of today's engineering (read as HX) analyses consists of running complex physics-based models via computer programs. Despite continuous improvements in computing power, the cost of running many such codes (simulations) is significantly high. In addition, the process of query and response is a trial and error approach to engineering design since the true functional relationship of the input and output vectors may never truly be understood.

Thus, optimal solutions may never be arrived at in a timely manner [41].

To address the above concerns, AAM has been advocated by [41, 42]. Approximations of the mechanistic models are constructed, resulting in metamodels that are more efficient to run and at the same time which attempt to understand the functional relationship between the design variables and responses. AAM comprises the following steps:

- (i) Choosing an experimental design to generate data, e.g. Latin Hypercube, Random Selection etc. Data could be subsequently generated either experimentally or in a synthetic fashion.
- (ii) Metamodeling, or fitting an appropriate model to the data generated previously, e.g. Linear Regression (LR), Artificial Neural Network (ANN) etc. This step is termed “Model Training”.
- (iii) Verification of model performance through random-sample evaluation or cross-validation, where performance is indicated by error metrics such as Root Mean Square Error (RMSE), Standard Deviation ( $\sigma$ ), Relative Mean Absolute Error (RMAE), Maximum Absolute Percentage Error (MAPE) etc. This step is termed “Model Testing”.

## 2.3 Machine Learning Methods Adopted

One such powerful AAM technique is ML which has been the topic of intense research over the last two decades or so [7]. ML techniques have been widely used for their speed and accuracy to predict performances of complex systems across various disciplines. The non-linear relationship between the cause-and-effect factors of a HX can be correlated with minimal error using certain ML methods [6]. ML approaches can be broadly categorized as shown in fig. 2.2

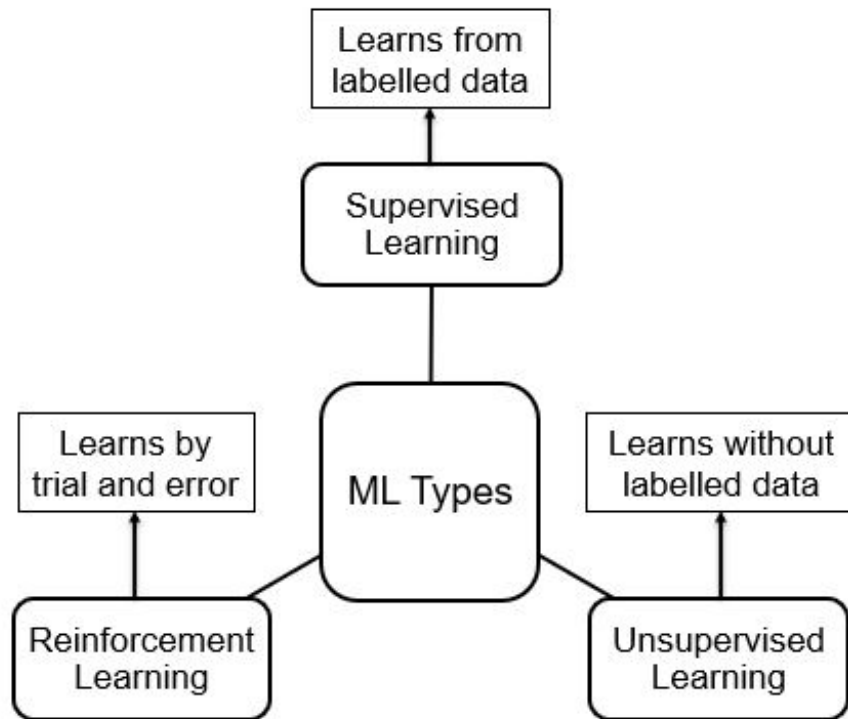


Figure 2.2: Machine Learning Types

This thesis focuses on the implementation of supervised ML techniques, namely, Linear Regression (LR), Support Vector Regression (SVR), and Artificial Neural Networks (ANN); particularly Multi-Layer Feed Forward Neural Networks (MLFFN).

The reasons for their use are:

- (i) These techniques have been relatively well understood [43]
- (ii) Availability of extensive open-source libraries to develop models based on these techniques [44], [45].
- (iii) Several researchers have successfully utilized these techniques in their prediction of heat transfer phenomena. This is elaborated in section 2.4.

### 2.3.1 Linear Regression

Linear models describe a continuous response variable as a function of one or more predictor variables. Linear regression is a statistical tool used to create a linear model by assuming that the regression function  $E(Y|\mathbf{X})$  is linear in the inputs  $\mathbf{X}$ .

Suppose  $\mathbf{X}^T = (X_1, X_2, \dots, X_p)$  is an input vector and we want to predict a real-valued scalar output  $Y$ . The form taken by the linear regression model is

$$Y = f(\mathbf{X}) = \beta_0 + \sum_{j=1}^p X_j \beta_j \quad (2.1)$$

where,

$\beta_j$ , = unknown coefficients,  $j = 0 \dots p$ .

Since we are involved in the use of supervised ML techniques, we typically possess a training dataset of  $N$  designs (observations);  $\{(\mathbf{x}_1, y_1) \dots (\mathbf{x}_n, y_n)\}$ . Each observation  $\mathbf{x}_i = (X_{1i}, X_{2i} \dots X_{pi})^T$  is a vector of  $p$  features for the  $i^{th}$  case, while its corresponding response is  $y_i$ . The aim of linear regression is to estimate the values

of the coefficients  $\beta_j$  from the training data so as to minimize the Residual Sum of Squares (RSS). This estimation method known as the Ordinary Least Squares (OLS) method happens to be the most popular estimation method [43] and can be represented as:

$$RSS(\beta) = \min_{\beta} \left\{ \sum_{i=1}^N (y_i - f(\mathbf{x}_i))^2 \right\} = \min_{\beta} \left\{ \sum_{i=1}^N \left( y_i - \beta_0 - \sum_{j=1}^p X_{ij} \beta_j \right)^2 \right\} \quad (2.2)$$

Fig. 2.3 illustrates the OLS method in an  $\mathbb{R}^{p+1}$  dimensional space occupied by the data pairs  $(\mathbf{X}, Y)$ . The residuals are represented by the vertical distances between the true points (red markers) and the function  $f(\mathbf{X})$  (denoted by the plane).

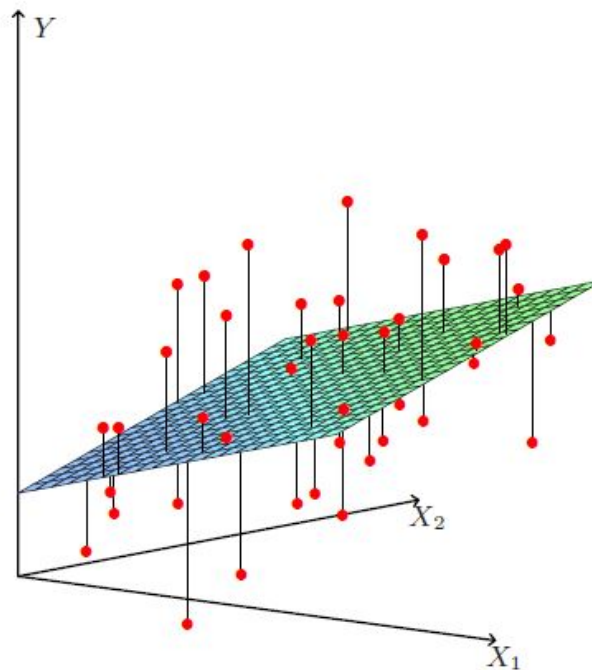


Figure 2.3: Ordinary Least Squares Estimation [43]

Oftentimes, predictions from the OLS estimate have high prediction variance. Prediction accuracy can be improved by choosing a subset of our predictors or more

preferably, employing shrinkage methods. Shrinkage methods such as Ridge Regression, Lasso Regression and Least Angle Regression are preferred to subset selection methods since they penalize or “shrink” the size of the regression coefficients, sacrificing high bias for low variance. On the other hand, subset selection is a discrete process, which in turn may introduce high prediction variability.

### 2.3.1.1 Ridge Regression

Ridge regression (RR) is a technique used to estimate the regression coefficients. Its objective is to minimize a penalized RSS instead of just the RSS as is done in OLS. The penalty term imposed here is an L2 norm of the regression coefficients multiplied by a constant shrinkage term  $\lambda$ . RR can be expressed as:

$$Ridge(\hat{\beta}_{ridge}) = \min_{\beta} \left\{ \sum_{i=1}^N (y_i - \beta_0 - \sum_{j=1}^p X_{ij}\beta_j)^2 + \lambda \sum_{j=1}^p \beta_j^2 \right\} \quad (2.3)$$

Larger the value of  $\lambda$ , greater will be the shrinkage. Geometrically, RR for  $\mathbf{p} = \mathbf{2}$  is illustrated in fig. 2.4.

The ellipses represent contours of the OLS estimate with the innermost point having the least RSS. The circumference of the blue circle represents the penalty term imposed. During RR we attempt to simultaneously minimize sizes of the ellipse as well as the circle. Thus, the ridge estimate is the point of intersection between the two.

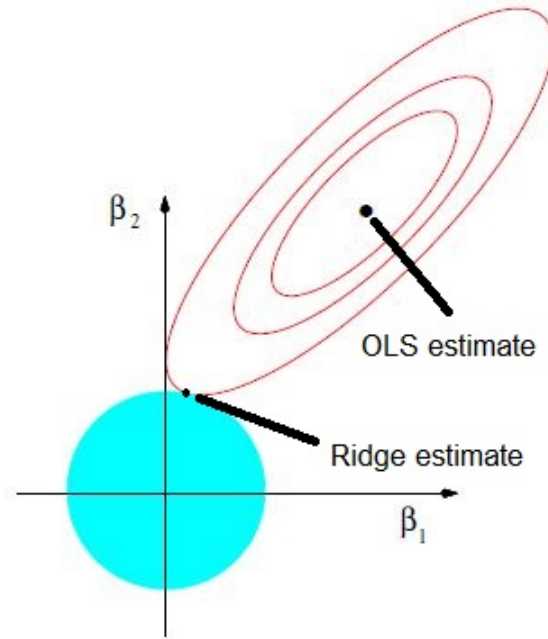


Figure 2.4: Ridge Estimate vs Ordinary Least Squares Estimate [43]

### 2.3.1.2 Lasso Regression

Like the RR, the Lasso Regression is a shrinkage method too. The main difference lies in the penalization of the coefficients. Lasso does so with an L1 norm multiplied by a constant shrinkage term  $\lambda$  instead. As a result, some of the coefficients can be exactly shrunk to zero. Lasso regression can be expressed as:

$$Lasso(\hat{\beta}_{lasso}) = \min_{\beta} \left\{ \sum_{i=1}^N (y_i - \beta_0 - \sum_{j=1}^p X_{ij} \beta_j)^2 + \lambda \sum_{j=1}^p |\beta_j| \right\} \quad (2.4)$$

Geometrically, Lasso for  $\mathbf{p} = \mathbf{2}$  is illustrated in fig. 2.5. In this case the diamond represents the penalty term imposed, and the ellipses represent contours of the OLS estimate. For the same reasons as in RR, the lasso estimate is the point of intersection between the two.

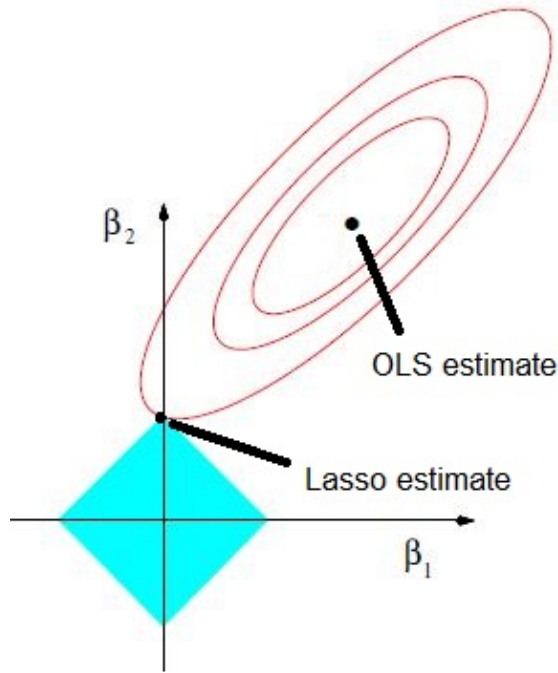


Figure 2.5: Lasso Estimate vs Ordinary Least Squares Estimate [43]

## 2.3.2 Support Vector Regression

Support Vector Regression (SVR) is a particular implementation of Support Vector Machines (SVM) which were initially used for carrying out classification tasks. For regression purposes the  $\epsilon$ -SVR [46] is commonly employed.

### 2.3.2.1 Linear Regression Using SVR

Suppose  $\mathbf{X}^T = (X_1, X_2, \dots, X_p)$  is the vector of  $p$  inputs, the goal of this methodology is to find an approximation function  $f(\mathbf{X})$  that will have at most a deviation of  $\epsilon$  from each of the true target values. In other words, errors within the threshold “ $\epsilon$ ” are not considered. At the same time, the function  $f(\mathbf{X})$  must be as flat as possible [47], i.e. we seek a small  $\beta$  which represents the model coefficients.

Consider a training data of  $N$  designs (observations);  $\{(\mathbf{x}_1, y_1) \dots (\mathbf{x}_n, y_n)\}$ .

For the linear case:

$$f(\mathbf{X}) = \boldsymbol{\beta} \cdot \mathbf{X} + \beta_0 \quad (2.5)$$

where  $\boldsymbol{\beta} = [\beta_1, \beta_2 \dots \beta_n]$  is the vector of model coefficients.

In order to achieve both the aforementioned goals, we formulate this as a convex optimization problem:

$$\begin{aligned} \min \quad & \frac{1}{2} \|\boldsymbol{\beta}\|^2 \\ \text{subject to} \quad & y_i - \boldsymbol{\beta} \cdot \mathbf{x}_i - \beta_0 \leq \epsilon \\ & \boldsymbol{\beta} \cdot \mathbf{x}_i + \beta_0 - y_i \leq \epsilon \end{aligned} \quad (2.6)$$

A key assumption in the above formulation is that there exists a function  $f(\mathbf{X})$  that approximates all the input pairs  $(\mathbf{x}_1, y_1)$  with an  $\epsilon$  precision. However, we may want to allow for some slackness to cope with constraints that have been violated. Thus, we introduce slack variables  $\xi$  and  $\xi^*$ . The formulation now becomes:

$$\begin{aligned} \min \quad & \frac{1}{2} \|\boldsymbol{\beta}\|^2 + C \sum_{i=1}^N (\xi_i + \xi_i^*) \\ \text{subject to} \quad & y_i - \boldsymbol{\beta} \cdot \mathbf{x}_i - \beta_0 \leq \epsilon + \xi_i \\ & \boldsymbol{\beta} \cdot \mathbf{x}_i + \beta_0 - y_i \leq \epsilon + \xi_i^* \\ & \xi_i, \xi_i^* \geq 0 \end{aligned} \quad (2.7)$$

where  $C$  is a constant term which determines the trade-off between the flatness of the function and the extent to which deviations greater than  $\epsilon$  are tolerated.

Fig. 2.6 illustrates the problem graphically. Only those points that fall outside the shaded region contribute to the cost function. This contribution is equal to  $\xi_i - |\epsilon|$ .

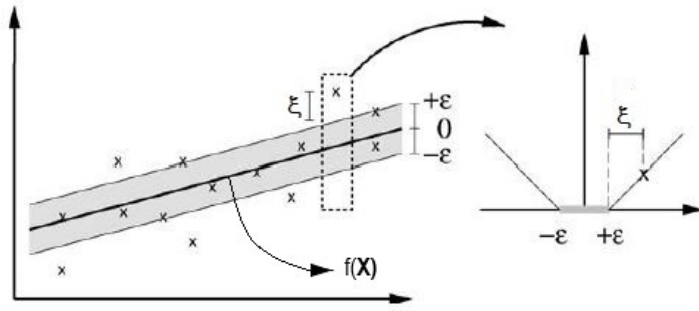


Figure 2.6: SVR Representation [47]

The problem formulation in 2.7 can be expressed as a Lagrangian function as:

$$\begin{aligned}
 L(\boldsymbol{\beta}, \beta_0, \xi_i, \xi_i^*) &= \frac{1}{2} \|\boldsymbol{\beta}\|^2 + C \sum_{i=1}^N (\xi_i + \xi_i^*) - \sum_{i=1}^N \alpha_i (\epsilon + \xi_i - y_i + \boldsymbol{\beta} \cdot \mathbf{x}_i + \beta_0) \\
 &\quad - \sum_{i=1}^N \alpha_i^* (\epsilon + \xi_i^* + y_i - \boldsymbol{\beta} \cdot \mathbf{x}_i - \beta_0) - \sum_{i=1}^N (\eta_i \xi_i + \eta_i^* \xi_i^*)
 \end{aligned} \tag{2.8}$$

The necessary optimality conditions for the above problem are as follows:

$$\frac{\partial L}{\partial \boldsymbol{\beta}} = \boldsymbol{\beta} - \sum_{i=1}^N (\alpha_i - \alpha_i^*) \mathbf{x}_i = 0 \tag{2.9}$$

$$\frac{\partial L}{\partial \beta_0} = \sum_{i=1}^N (\alpha_i^* - \alpha_i) = 0 \tag{2.10}$$

$$\frac{\partial L}{\partial \xi_i} = C - \alpha_i - \eta_i = 0 \tag{2.11}$$

$$\frac{\partial L}{\partial \xi_i^*} = C - \alpha_i^* - \eta_i^* = 0 \quad (2.12)$$

Expressing the problem in 2.7 in its dual form, we get:

$$\begin{aligned} \max \quad & -\frac{1}{2} \sum_{i=1}^N (\alpha_i - \alpha_i^*)(\alpha_j - \alpha_j^*)(\mathbf{x}_i \cdot \mathbf{x}_j) \\ & - \epsilon \sum_{i=1}^N (\alpha_i - \alpha_i^*) + \sum_{i=1}^N y_i (\alpha_i - \alpha_i^*) \\ \text{subject to} \quad & \sum_{i=1}^N (\alpha_i - \alpha_i^*) = 0 \\ & (\alpha_i, \alpha_i^*) \in [0, C] \end{aligned} \quad (2.13)$$

Rewriting equation 2.9 as:

$$\boldsymbol{\beta} = \sum_{i=1}^N (\alpha_i - \alpha_i^*) \mathbf{x}_i \quad (2.14)$$

Finally, equation 2.5 can be rewritten as:

$$f(\mathbf{X}) = \sum_{i=1}^N (\alpha_i - \alpha_i^*) (\mathbf{x}_i \cdot \mathbf{X}) + \beta_0 \quad (2.15)$$

### 2.3.2.2 Nonlinear Regression Using SVR

As a result of expressing the SVR function in its dual form, we can approximate nonlinear functions by replacing the dot product of the training vectors with a nonlinear transformation of the input vectors. This transformation is carried out via kernel functions and is represented as  $k(\mathbf{x}_i \cdot \mathbf{X})$ , where  $\mathbf{x}_i$  and  $\mathbf{X}$  are input vectors. Table 2.1 lists some of the commonly used kernel functions which can conveniently

Table 2.1: Kernel Functions

Linear	$k(\mathbf{x}_i \cdot \mathbf{X}) = (\mathbf{x}_i^T \mathbf{X})$
Polynomial	$k(\mathbf{x}_i \cdot \mathbf{X}) = (\mathbf{x}_i \cdot \mathbf{X})^n$
Gaussian	$k(\mathbf{x}_i \cdot \mathbf{X}) = \exp(-\frac{\ \mathbf{x}_i - \mathbf{X}\ ^2}{2\sigma^2})$
Sigmoid	$k(\mathbf{x}_i \cdot \mathbf{X}) = \tanh(\alpha(\mathbf{x}_i \cdot \mathbf{X}) + \gamma)$

be substituted into equation 2.15 as:

$$f(\mathbf{X}) = \sum_{i=1}^N (\alpha_i - \alpha_i^*) k(\mathbf{x}_i \cdot \mathbf{X}) + \beta_0 \quad (2.16)$$

In this manner SVR can approximate nonlinear functions while simultaneously maintaining the simplicity and elegance of linear SVR approximations. Following are the salient features of the SVR

- (i) The regression coefficients can be expressed as a linear combination of the training data.
- (ii) The optimization problem is a quadratic programming problem with linear constraints and a positive definite Hessian matrix. This ensures a unique global optimum solution.
- (iii) Though it is widely acknowledged that SVR provides a means for addressing the curse of dimensionality, its training time complexity increases rapidly with the training dataset size.

### 2.3.3 Multi-Layer Feed Forward Neural Network

Multi-Layer Feed Forward Neural Network (MLFFN) or Multi-Layer Perceptrons are a sub-category of Artificial Neural Networks (ANN), used to conduct regression as well as classification tasks. MLFFN are massively parallel systems with a large number of simple interconnected processors called neurons. Multiple layers of neurons with nonlinear activation or transfer functions enable the network to learn the linear and/or nonlinear relationship between the inputs and output(s). A typical MLFFN is as shown in fig. 2.7.

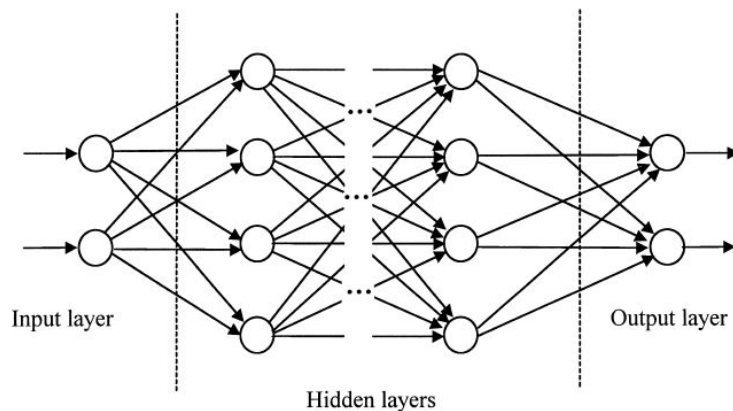


Figure 2.7: Typical Multi-Layer Feed Forward Neural Network [48]

It typically consists of neurons aligned along an input layer, one or more hidden layers and an output layer. Fully connected networks are among the most widely used MLFFN [11] wherein each neuron belonging to a layer is fully interconnected with each neuron present in the succeeding layer via connectors that represent the weights of the ANN. While the number of neurons or perceptrons in the input and output layers depend upon the number of independent and dependent variables involved in our problem, the number of hidden layers and the number of

neurons in each hidden layer is dependent upon the complexity of the phenomenon we are attempting to model, and is usually arrived at through trial and error. The computation occurring within a neuron is depicted in fig. 2.8.

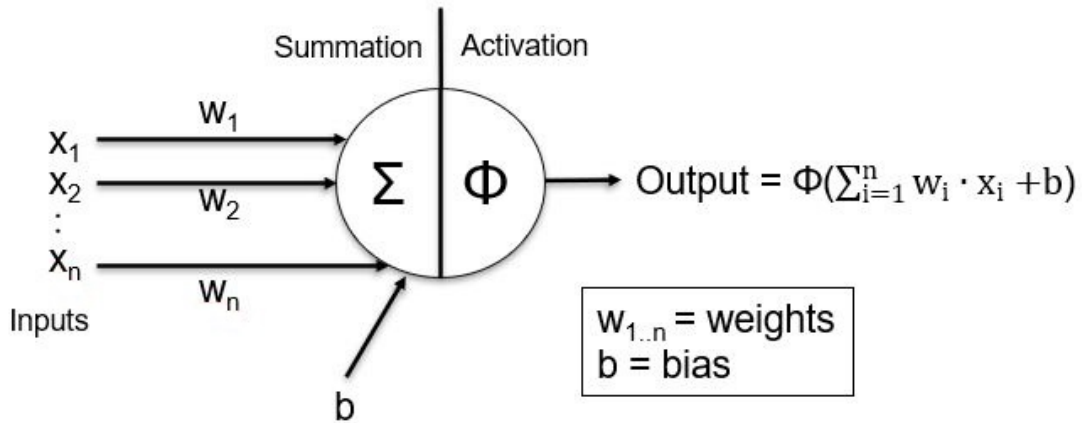


Figure 2.8: Information Processing within Neuron

Starting from the first hidden layer, for a particular set of coefficients (weights and biases), the neuron first calculates the weighted sum of its inputs followed by a transformation of the sum through a chosen activation function 2.2. Barring perceptrons contained in the final layer, the output from each perceptron in each hidden layer(s) is fed as input to the neurons in the subsequent layer. In this manner, the network is traversed in the forward direction, resulting in an estimated value of the target variable. Rarely is it observed that an untrained network produces satisfactory estimates of the output in one forward run. Therefore, an effective training or learning procedure is needed. Back-Propagation (BP) is one such learning method where the weights and bias terms are corrected layer by layer in the reverse direction. This training procedure is carried out until the optimizer yields results that satisfy a termination criterion.

Table 2.2: Activation Functions

Linear	$f(\mathbf{x}) = x$
Sigmoid	$f(\mathbf{x}) = \frac{1}{1+\exp(-x)}$
Tan Hyperbolic (tanh)	$f(\mathbf{x}) = \frac{2}{1+\exp(-2x)} - 1$
ReLU	$f(\mathbf{x}) = \begin{cases} 0 & \text{for } \mathbf{x} < 0 \\ x & \text{for } \mathbf{x} \geq 0 \end{cases}$
ELU	$f(\mathbf{x}) = \begin{cases} \alpha(\exp(\mathbf{x} - 1)) & \text{for } \mathbf{x} < 0 \\ x & \text{for } \mathbf{x} \geq 0 \end{cases}$

Typically in an ANN, a non-deterministic algorithm such as Stochastic Gradient Descent (SGD) or its variants are used to find the optimal weights and bias terms. The weights are initialized to random values (usually between 0 and 1) and the network is traversed in the forward direction yielding an estimate of the output. Depending upon the value of the cost function (e.g., RMSE for regression and cross-entropy for classification), the coefficients are adjusted via BP so as to minimize the loss. Training the network by performing one forward run and one BP on the entire dataset is termed an epoch. Generally, several epochs are needed to obtain a capable MLFFN model. For best results, it is necessary that the input training

data be normalized.

Additionally, hyperparameter tuning is another necessity in achieving precise prediction models. The hyperparameters generally associated with an MLFFN are:

- (i) Number of hidden layers.
- (ii) Number of nodes per hidden layer.
- (iii) Activation function to be used.
- (iv) Training procedure.
- (v) Coefficient initialization scheme.
- (vi) Optimizer and its hyperparameters.

## 2.4 Machine Learning Approximation of Heat Exchangers

It has been observed that a majority of the published works belong to one or more of the following areas:

- (i) HX Performance Prediction.
- (ii) Estimation of HX Parameters.
- (iii) Identification of Two-Phase Flow Regimes.

### 2.4.1 HX Performance Prediction

Over the last two decades, numerous ML techniques have been utilized to build models with the intention of predicting HX performance. These have been reviewed in great detail by [6,49,50]. As tube-fin HXs are the focus of this study, the following paragraphs highlight ML investigations pertaining to tube-fin HXs only.

Several authors have modeled TFHXs using ANN of varying network architectures [8, 51–58]. Diaz et al. [51] were one of the earlier practitioners of ANN applied to HXs. Their neural network was able to accurately predict the heat transfer from hot water to externally flowing air in a single row tube-fin HX. The authors show that their predictions were superior in comparison to predictions made by a conventional power law correlation. No geometrical parameters were considered as inputs to the model, thereby restricting its scope of prediction. Pachecho Vega et al. [52] developed a fully connected MLFFN to predict the heat transfer of a tube-fin evaporator. A methodology to estimate the prediction error from ANN trained with

limited data is presented with the objective of determining if there are sufficient data points to aid in ANN predictions. In addition, the authors claim that their procedure can help determine where further testing is necessary within the design space. It is important to note that the predictions made by the developed MLFFN were on the same dataset used for its training as opposed to using a separate verification dataset. In a related study conducted by the same authors [53], they established that the predictions of sensible and total Chilton-Colburn ‘j’ factors using ANN were superior to the predictions made by prominent correlations of [59], [60]. The authors further recommended the direct prediction of heat transfer instead of intermediate parameters such as ‘j’ factors.

Ding et al. [54] highlighted the hybrid capabilities of ANN, by using them in conjunction with an approximate integral model to predict the performance of a tube-fin condenser. The pairing of the two methodologies resulted in a simpler ANN structure as well as the representation of the nonlinear factors that were not considered in the approximate integral model. The RMAE in heat transfer predictions was found to be less than 1%. The performance prediction of a gas cooler as part of a Carbon Dioxide transcritical cycle was conducted by Wu et al. [8]. Apart from accurately predicting performance, they examined the impact of the input design variables on the model output. The deviation between predicted and experimental data was found to be less than 5%. Tan et al. [55] predicted the performance of a tube-fin HX as well as the exit air temperature by developing two separate ANNs. The study involved blocking off various percentages of the HX face area. Additionally, they utilized a Self-Organizing-Map Neural Network to classify the extent to

which inlet air was obstructed at the face of a HX due to fouling. The RMAE pertaining to heat transfer predictions were 1.8% and 5.1% for the ANN and non-linear regression respectively. Yang et al. [56] utilized dimensionless Pi-groups as inputs and outputs to the ANN model used to evaluate tube-fin condenser performance. It was shown that the dimensionless ANNs outperformed dimensional ANNs in some test cases, while the opposite was true for the remaining test cases. Nevertheless, the dimensionless ANNs exhibited greater generality than their dimensional counterparts. Parallel flow condensers with R134a to be used in electric vehicles were investigated by Tian et al. [57]. An ANN was built to predict  $Q$ , outlet refrigerant temperature, and  $\Delta P$  on the air and refrigerant sides. The authors reported that the RMAE for all the predicted parameters were less than 1.3%. Impact of geometry was neglected in this modeling effort, as only the fluid inlet states were varied.

Kumra et al. [61] compared SVR and ANN models in their prediction of heat transfer by a wire-on-tube HX. Their results show that the SVR model yielded better predictions on a held-out validation dataset. No mention of the NN architecture or its training is made. Yan et al [62] predicted the heat dissipated by an automotive radiator as a function of HX geometry with the aid of an SVR model. The hyperparameters were tuned using a modified artificial fish swarm algorithm. The results obtained were shown to be superior to predictions of LR and ANN. Details of the LR and ANN models used as well as their training procedure and training time have not been presented by the authors. Fitness of three approximation assisted modeling techniques were compared by Huang et al. [63] based on their ability to accurately and quickly simulate HXs as well as VCCs. On the HX level the metamodels ap-

proximated change in enthalpy and  $\Delta P$ . The Kriging metamodel was observed to perform exceedingly well. An overall RMAE of 4.46% was attained in addition to speeding up the tube-fin HX simulation by a factor of 60-170.

A handful number of evaluation studies on evaporative condensers have been carried out by researchers with the aid of ML techniques [64–67]. Reichert et al. [66] made use of ANN as an intermediate simulation tool to generate data related to the working of an evaporative condenser. The data generated by the ANN was then used to develop Design of Experiment predictive models to estimate the evaporative condenser heat rejection and its overall heat transfer coefficient (htc). The authors claim that nonlinearity effects were not dominant, thereby expressing heat rejection rate and overall htc as linear functions of the relevant parameters. Behnam et al. [67] conducted a comparative study of four different ML methods to predict the Q and overall htc of an evaporative condenser. The results showed that the ANN performed the best, and was followed by SVR and Random Forest models. The study deemed the use of Decision Tree models ineffective in the prediction of the aforementioned parameters.

Similar to the trend observed for heat transfer predictions, ANNs have been extensively used to predict fluid Pressure Drop ( $\Delta P$ ) in both single and two-phase flows. [10, 68–73]. Alizadehdakhel et al. [68], investigated two-phase  $\Delta P$  of water in tubes of various orientations. They compared prediction results of CFD and ANN. On the test dataset it was found that CFD results were marginally better. The authors however, advocate the use of ANN due to its satisfactory performance and convenience of use. Bar et al. [69] developed ANNs using three different BP

optimization techniques to predict the two-phase  $\Delta P$  in U-bends. The sigmoid activation function combined with the Levenberg-Marquardt optimization algorithm was found to yield the least value of RMAE of 9%. Zendehboudi and Li [70] leveraged the robustness inherent to ML ensembling in the prediction of condensation  $\Delta P$  of R134a in inclined tubes. Encouraging results were obtained from three of the four methodologies adopted, but the authors advocated for the use of the more robust methodology which combined the prediction capabilities of ANN, SVR and Adaptive Neuro Fuzzy Inference System. Khosravi et al. [10] compared the capabilities of three different ML techniques in their prediction of  $\Delta P$  during evaporation of R407C. The ML techniques used were MLFFN, SVR, and a group method of data handling ANN. While the prediction of all three techniques were satisfactory, the authors claim that the group method of data handling ANN outperformed the other two. Maldonado et al. [72] developed an ANN to predict frictional  $\Delta P$  during flow boiling of zeotropic mixtures through minichannels, subject to cryogenic conditions. The model outperformed other well-known correlations across all flow regimes. Flow boiling  $\Delta P$  in mini/microchannels was investigated by Qiu et al. [73]. The authors employed several supervised ML techniques in their study to determine the most suitable regression function to a consolidated database gathered from 21 sources. While all the ML models employed in this study outperform a reliable conventional correlation [74], the ANN was found to be the most adept approach for this problem.

A similar study was also conducted by Ardam et al. [75] to predict the flow boiling  $\Delta P$  of R134a in a horizontal microfin tube. The Random Forest algorithm that was utilized in this study, yielded an RMAE of 6.41%, which the authors

present to be superior to the predictions made by a physical model proposed by Shannak [76].

Oh et al. [77] optimized the design of a parallel flow HX via a second order response surface methodology. The HX was optimized for maximum JF factor (a criterion that represents both heat transfer and  $\Delta P$  simultaneously). The proposed methodology yielded a design with improved values of JF factor. Sun and Zhang [78] evaluated the thermal performance of elliptical tube-fin HXs. With the aid of response surface methodology and DOE the authors were able to identify the interacting effects of the tube axis ratio, air velocity and internal fluid volumetric flow rate on the overall performance of the HX.

## 2.4.2 ML Estimation of Heat Exchanger Parameters

HX parameters such as heat transfer coefficient, friction factor, void fraction and fouling factor are key aspects considered during HX design, simulation, and optimization. The investigations listed below leverage ML principles to accurately approximate such parameters.

### 2.4.2.1 Heat Transfer Coefficient

Neural Networks have the distinction of being known as universal approximators [79], thereby making them very popular among researchers in the prediction of Heat Transfer Coefficient (htc) [80–88] and other HX parameters as will be seen in later subsections. Jambunathan et al. [80] presented one of the earliest applications

of ANN to the transient simulation of air-side convective htc. Encouraging results were obtained by the authors in their predictions, however it should be noted that there was no held-out test or validation dataset to evaluate the realistic performance of the model. Ghajar et al. [81] developed an ANN to accurately predict the single-phase internal convective htc for transitional flow in a horizontal circular straight tube under uniform heat flux boundary condition. The proposed correlation fared better than their previous least squares correlation. Majority of the data points were predicted within a deviation of 5%. Demir et al. [82] have utilized ML to study alternative refrigerants (R600A). The authors predicted the internal convective htc using an ANN whose predictions were found have an RMAE less than 4%, thereby outperforming noteworthy correlations of Shah [89] and Travis [90]. A single correlation to predict the Nusselt number (Nu) during boiling and condensation of R134a flowing through smooth and microfin tubes was developed by Balcilar et al. [84]. The correlation is shown to predict experimental Nu values within a deviation of  $\pm 30\%$ . Similar work by Ewim et al. [88] was conducted to predict condensation htc of R134a inside enhanced inclined tubes. The ANN predictions were able to predict the trends of experimental htc as a function of inclination angle, vapor quality and refrigerant mass flux. Saturated flow-boiling htc in mini/microchannels of varying cross sections was predicted with the aid of an ANN developed by Qiu et al. [86]. Experimental data from 50 sources, covering 16 fluids were collected to train and validate the model. The capability of the developed ANN model was compared against a prominent physics-based correlation [91], and it is observed that the ANN with an RMAE of 14.3% performed better than the physics-based correlation whose

RMAE equalled 27.37%. Zhou et al. [87] applied ML techniques to predict the flow condensation htc. The data for the model training and testing was amassed from 37 distinct sources covering 17 different fluids. Among the models compared, the ANN (RMAE = 6.8%) and the XGBoost (RMAE = 9.1%) models outperformed the rest regardless of the condensation flow regime. Results from the study showed that the optimal ANN and XGBoost models yielded more accurate predictions than the widely used correlation [92].

Tam et al. [93] built upon their previous work [81], by predicting the single-phase internal convective htc for transitional horizontal flow using an SVR model. The htc predictions were comparable to the ANN developed earlier with a majority of the experimental data being predicted within an error band of  $\pm 5\%$ . However, the SVR model has an added benefit of yielding a unique correlation unlike ANNs. As a natural extension to the aforementioned work [93], Tam et al. [94], developed an SVM htc for turbulent gas-liquid two-phase flow in vertical pipes. Their results showed that a majority of the data was predicted within a deviation of  $\pm 5\%$ , while at the same time outperforming a prominent empirical correlation developed to predict the same.

#### 2.4.2.2 Friction Factor

The following works have successfully approximated friction factor ( $f$ ) in HXs using ANNs [95–98]. Nasr and Khalaj [95] investigated corrugated tubes combined with twisted tape inserts as means of enhancing heat transfer. They further devel-

oped an ANN to predict the heat transfer and  $f$ . Predictions of  $h_{tc}$  were made with an RMAE less than 2.9% and corresponding  $f$  RMAE was found to be less than 0.36%. Cebi et al. [97] developed several ANNs to predict the  $f$  associated with buoyancy aided and buoyancy opposed single-phase flows in smooth and microfin tubes, under cooling heating and isothermal conditions. Apart from obtaining encouraging results, the authors were able to conclude that geometry and mass flow had a greater impact than the direction of heat transfer on  $f$ . Zhang et al. [99] applied ANNs in an interesting manner by utilizing it to pick out the dominant parameters that correlate two-phase friction multiplier and  $\alpha$ . The Laplace constant or confinement number was found to be highly dominant and improved correlations for two-phase frictional  $\Delta P$  and  $\alpha$  are developed as functions of the Laplace constant.

Najafi et al. [100] attempted to predict single-phase  $f$  and two-phase flow multipliers in microfin tubes with the aid of ML techniques. K-Nearest Neighbors and Random Forest algorithms-both supervised ML approaches, were used for single-phase and two-phase predictions respectively. The model predictions were compared against well-known correlations found in the literature, and results showed that the ML models fared better. Additionally the authors pointed out the trade-offs between model accuracy and complexity by employing a varying number of features as model inputs.

Several authors have conducted investigations that seek to predict both  $h_{tc}$  as well as frictional  $\Delta P$  in HXs [9, 101–105]. Xie et al [102], recommend the usage of ANNs to predict the air-side  $Nu$  and  $f$  for TFHXs having large diameter tubes arranged along relatively higher number of tube banks. Moreover, three different

types of fins were used in this study. The ANN yielded superior prediction in comparison to reference correlations used in the study. In order to reduce variance and avoid overfitting, an ensemble method was adopted by Pai et al. [103] to predict single-phase Nu and f through 35 distinct channel cross sections. Lopez-Belchi et al. [104] advocated the use of ANNs as a tool to predict the condensation htc and  $\Delta P$  within minichannels. Additionally, a grouping method was utilized in order to identify the minimum number of variables required to develop a satisfactory model.

Thermal-hydraulic performance of compact heat exchangers was predicted by Peng and Ling [9] by adopting SVR. Predictions of j and f factors were slightly better than that of an ANN whose hyperparameters and network architecture were tuned based on trial and error (as is the norm with ANN). Moreover, the training time for ANN was significantly longer. However, one point of concern with this work, is that normalization of data was done before splitting into training and testing data subsets. This could lead to exaggerated results of prediction accuracy from the SVR model. Hughes et al. [105] performed a thermo-fluid investigation of condensation heat transfer. As part of their study, they developed and compared conventional as well as ML models to predict condensation htc and  $\Delta P$ . Results demonstrate that the random forest regression model performs significantly better than the other conventional and ML models considered.

### 2.4.2.3 Void Fraction

Malayeri et al. [106] developed a radial basis function ANN to predict  $\alpha$  in vertical upward flows at elevated temperatures. The inputs to the model were dimensionless groups. The results of this investigation highlight similar trends across experimental results and the ANN predictions. Azizi et al. [107] investigated the ability of ANNs to predict the  $\alpha$  of a gas-liquid two phase flow in horizontal and inclined pipes (upward and downward). The model predictions were compared against seventeen  $\alpha$  correlations from the literature, and in each case, it was found that the ANN outperformed the correlations irrespective of the flow pattern. The  $\alpha$  of gas-liquid flows in minichannels was predicted by Hua jun Li et al. [108] with the aid of a SVR model. The  $\alpha$  data was first classified into one of four flow regimes - bubble, slug, stratified or annular flows. Subsequently one of the four developed SVR models was used to make predictions for  $\alpha$ .

### 2.4.2.4 Fouling Factor

An ANN was built by Riverol and Napolitano [109] to predict the internal fouling factor in a tubular HX. An RMAE of 2.3% was obtained between predicted and true experimental results. However key details regarding network architecture were missing. SVM was employed to predict internal HX fouling by Sun et al. [110]. The authors claim that the SVM outperforms the radial basis function model. However, details related to the radial basis function model and clear description of the error metrics used are absent from this communication. In an extensional work by

the same authors [111], they exercised the particle swarm optimization algorithm to tune the hyperparameters of the SVR model. While the authors claim that the optimized SVR produced better results, the value of RMAE reported in this investigation is larger than the corresponding value present in [110]. Davoudi and Vaferi [112] simulated the fouling factor in single tube HXs with the aid of an ANN. The Pearson correlation coefficient was used to identify feature importance. However, it should be noted that the Pearson correlation coefficient does not take into account interaction between the inputs while determining the feature importance. Additionally the model output is the fourth root of the fouling factor. Nevertheless, results show that the RMAE = 5.4%. Internal, external and overall fouling resistance in a cross-flow HX was investigated by Sundar et al. [113]. The authors developed a fouling prediction framework with an ANN at its core, whose mean absolute prediction errors were under  $10^{-4}$  KW<sup>-1</sup>.

#### 2.4.2.5 Miscellaneous HX Parameters

Kurt and Kayfeci [114] predicted the thermal conductivity of ethylene glycol-water solutions with the aid of an ANN. The authors encourage the use of ANN to predict thermal conductivity of liquids since their predictions were in close agreement with experimental data. The normal boiling point of refrigerants widely used in HVAC&R was predicted successfully by Deng et al. [115] with the aid of ANN combined with Genetic Algorithm for network optimization. The ANN model was found to be highly accurate and was also capable of distinguishing all the isomers of

a particular refrigerant. Baghban et al. [116] developed a least squares SVM and a ANFIS to predict the dew point temperature of moist air at atmospheric pressure. The two models had their hyperparameters optimized using a genetic algorithm. While both models performed well, the authors recommend the usage of least squares SVM since it mapped the data most effectively. KNN was employed by Krishnayatra et al. [117] to predict the thermal performance of fins used in conjunction with an axial TFHX. The HX possessed primary fins (in contact with tube) and secondary fins (in contact with primary fins). The model was able to predict upwards of 80% of the test data within an absolute deviation of 10%. Giannetti et al. [118] developed an ANN to accurately predict the two-phase flow distribution in the header of a microchannel HX. The input parameters to the model were relevant dimensionless numbers such as Reynolds number, Froude number, Capillary number and void fraction. The developed ML model was compared against other prominent models related to the phenomena (two-phase flow distribution) and results show that the ANN outperforms contemporary models.

### 2.4.3 Identification of Two-Phase Flow Regimes

Accurate identification of the two-phase flow regime is crucial for accurate modeling and prediction of the dynamic nature of two-phase flow systems. Conventional methods of predicting two-phase flow regimes include flow regime maps which are unfortunately not universal [50]. Since several ML models have displayed great effectiveness in classification problems we can leverage this innate quality to

conveniently and precisely identify the flow regime of a two-phase fluid.

Mi et al. [119, 120] classified vertical two-phase flow into one of four flow regimes, namely bubbly flow, slug flow, churn flow and annular flow. The authors did so with the aid of a supervised ANN and unsupervised self-organizing neural network maps. In the former work, both the neural networks were trained from signals emitted by an impedance void-meter while in the latter, the impedance results of a verified two-phase flow simulation model were used. Across both works it was shown that the ANNs were able to satisfactorily classify the flow regimes in agreement with the flow regime map of Mishima and Ishii. However, some disagreements or misclassifications exist around the transition regions. An on-line flow regime identification approach has been developed by Tambouratzis and Pazsit [121] by combining a statistical-operator driven feature extraction method with an ensemble of self organizing maps (unsupervised ANNs). The original inputs are a set of radiography images. The vertical flow was classified into bubble, slug, churn or annular flows with accuracies greater than 87.7%. For the same set of radiography images used in the earlier study [121], Tambouratzis and Pazsit [122] developed a generalized regression ANN (GRANN). Apart from exercising the same feature extraction method employed in the earlier study, the authors also carried out counter-clustering resulting in a decrease of the training set. The authors claim that overall, the GRANN was able to deliver at worst, similar classification accuracies than previous studies but at significantly quicker rates of prediction.

Kreitzer et al. [123] employed a supervised ANN to identify flow regimes in horizontal two-phase R134a adiabatic flow. The inputs to the ANN were pre-processed

electrical capacitance tomography results. The results showed that the authors' technique was able to classify with an accuracy of 99% the two-phase flow regime into bubble, plug, slug, intermittent or annular flows. Seal et al. [124] conducted an investigation to classify the condensation flow pattern of R134a refrigerant flowing in inclined tubes. They developed an ANN capable of categorizing flow into one among ten different regimes with more than 98%. Prior to classification, principal component analysis was employed to ensure dimensionality reduction.

Identification of air-water two phase flow regimes was conducted by Zhou et al. [125] with the combined usage of an effective image pre-processing technique and SVMs (used as a classifier). In addition, the rough sets theory was utilized to reduce the dimensionality of the flow regime samples (images). The results of the paper demonstrate that the SVM had a higher classification accuracy than a BP ANN. Hobold and da Silva [126] successfully classified the existent flow regimes during boiling heat transfer via low speed visualization over a large captured area. Dimensionality reduction was accomplished by the use of Principal Component Analysis. Finally, classification was carried out with the aid of a Support Vector Classifier and an ANN resulting in over 93% accuracy.

## 2.5 Summary

The literature survey conducted can be summarized in two ways:

- (i) Based on the application area of the ML investigations (fig. 2.9).
- (ii) Based on the type of ML model applied (fig. 2.10).

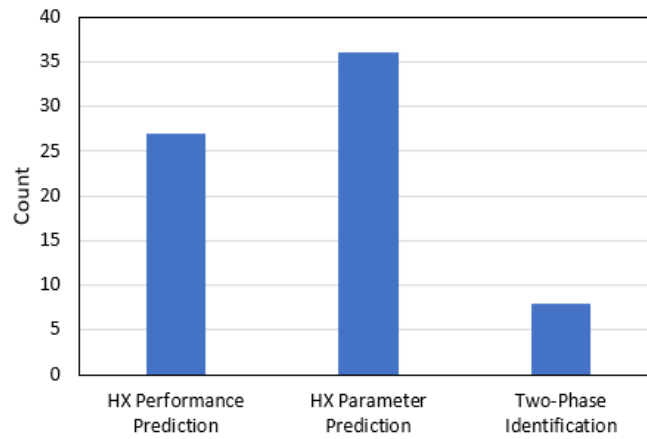


Figure 2.9: Heat Exchanger Application Area

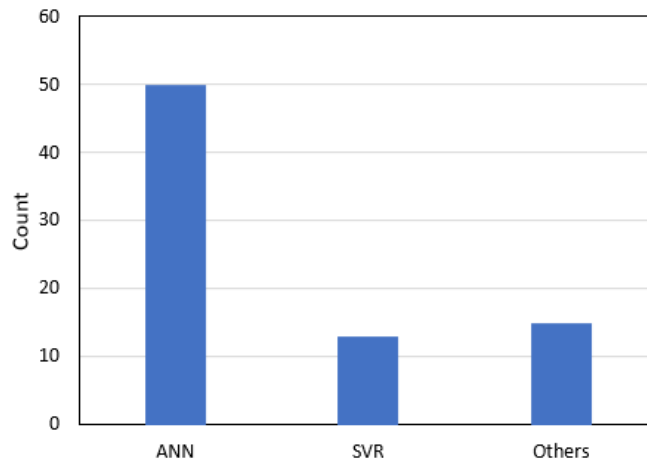


Figure 2.10: Machine Learning Model applied

Since the focus of this thesis is to accurately predict TFHX performance, the tabulated figure below describes in greater detail ML investigations pertaining to this activity. These have been previously introduced in section 2.4.1.

Reference	Application	ML Model	Output = f(model inputs)	Input Summary	Result
Diaz et al. (1999)	Air-Water TFHX	ANN	$Q = f(\text{MFR}_{\text{air}}, \text{MFR}_{\text{water}}, T_{\text{in}}^{\text{air}}, T_{\text{in}}^{\text{water}})$	Operating conditions	MAPE = 3.7%
Vega et al. (2001)	Air-Water TFHX	ANN	$Q = f(7 \text{ Geometry and } 4 \text{ Operating Parameters})$	Geometry & operating conditions	RMSE of percentage errors < 1.5%
Vega et al. (2001)	Air-Water TFHX	ANN	$Q = f(\text{Re}_{\text{air}}, T_{\text{in},\text{db}}^{\text{air}}, T_{\text{in},\text{wb}}^{\text{air}}, T_{\text{in}}^{\text{water}}, \sigma)$	Geometry & operating conditions	RMAE = 2.69%
Ding et al. (2004)	TF Condenser	ANN	$Q = f(\sigma, \text{MFR}_{\text{ref}}, V_{\text{air}}, P_{\text{cond}}, \Delta T_{\text{deht}}, T_{\text{in},\text{db}}^{\text{air}})$	Geometry & operating conditions	RMAE < 1%
Ertunc & Hosoz (2006)	Evap Condenser	ANN	$Q = f(\text{Load Requirement}, \text{MFR}_{\text{air}}, \text{MFR}_{\text{water}}, T_{\text{in},\text{db}}^{\text{air}}, T_{\text{in},\text{wb}}^{\text{air}})$	Geometry & operating conditions	RMAE = 1.9%
Wu et al. (2008)	Transcritical CO2 Gas Cooler	ANN	$Q, \Delta P = f(\text{MFR}_{\text{ref}}, V_{\text{air}}, P_{\text{cond}}, T_{\text{in}}^{\text{ref}}, T_{\text{in},\text{db}}^{\text{air}})$	Operating conditions	RMAE < 5%
Ertunc & Hosoz (2008)	Evap Condenser	ANN & ANFIS	$Q = f(\text{MFR}_{\text{ref}}, \text{MFR}_{\text{air}}, \text{MFR}_{\text{water}}, T_{\text{in},\text{db}}^{\text{air}}, T_{\text{in},\text{wb}}^{\text{air}}, P_{\text{cond}}, T_{\text{in}}^{\text{ref}})$	Operating conditions	ANN RMAE = 2.59% ANFIS RMAE = 0.56%
Tan et al. (2009)	Air-Brine TFHX	ANN	$Q = f(\text{MFR}_{\text{ref}}, \text{MFR}_{\text{air}}, T_{\text{in}}^{\text{ref}}, T_{\text{in},\text{db}}^{\text{air}}, \text{Face Area}, \text{Concentration})$	Operating conditions	RMAE < 1.8%
Kumra et al. (2013)	Wire-Tube HX	SVR	$Q = f(7 \text{ Geometry and } 5 \text{ Operating Parameters})$	Geometry & operating conditions	RMAE < 0.2%
Tian et al. (2014)	MC Condenser	ANN	$Q, \Delta P = f(\text{MFR}_{\text{ref}}, V_{\text{air}}, P_{\text{cond}}, T_{\text{in}}^{\text{ref}}, T_{\text{in},\text{db}}^{\text{air}}, T_{\text{in},\text{wb}}^{\text{air}})$	Geometry & operating conditions	0.24% < RMAE < 1.32%
Zendehboudi & Li (2017)	Condenser	ANN+SVR+ANFIS	$\Delta P = f(G_{\text{ref}}, T_{\text{cond}}, x, \text{Inclination Angle})$	Operating conditions	$R^2 = 0.9993$
Garcia et al. (2018)	Evaporator	ANN	$\Delta P = (P_{\text{evap}}, x, G_{\text{ref}}, D)$	Geometry & operating conditions	RMAE < 6.11%
Khosravi et al. (2018)	Evaporator	GMDH-ANN, ANN, SVR	$\Delta P = (P_{\text{evap}}, x, G_{\text{ref}}, D)$	Geometry & operating conditions	GMDH R = 0.99, ANN R = 0.99, SVR R = 0.92
Maldonado et al. (2019)	Evaporator	ANN	$\Delta P = (\text{Re}_{\text{ref}}, x, G_{\text{ref}}, \text{Tube Roughness}, \text{Refrigerant})$	Geometry, operating conditions & refrigerant	RMAE = 8.3%
Huang et al. (2019)	TFHX, Plate HX and Coaxial HX	Kriging	$\Delta h, \Delta P = f(P_{\text{in}}, h_{\text{in}}, \text{MFR}_{\text{ref}})$	Operating conditions	RMAE < 2% for TFHXs
Datta et al. (2019)	TF Evaporator	ANN	$Q = (\text{refrigerant charge}, N_{\text{compressor}}, N_{\text{blower}})$	Operating conditions	5% < RMAE < 6.49%
Yan et al. (2020)	TF Radiator	SVR	$Q = f(6 \text{ Geometry Parameters})$	Geometry	RMAE = 1.8%
Alizadehdakheel et al. (2020)	TFHX	ANN	$\Delta P = f(V_{\text{gas}}, V_{\text{liquid}}, \text{Inclination Angle})$	Geometry & operating conditions	$R^2 = 0.9985$
Reichert et al. (2020)	Evap Condenser	ANN	$Q = f(T_{\text{in}}^{\text{water}}, T_{\text{in},\text{db}}^{\text{air}}, T_{\text{in},\text{wb}}^{\text{air}}, T_{\text{in}}^{\text{ref}}, \text{MFR}_{\text{air}}, \text{MFR}_{\text{water}})$	Operating conditions	$R^2 = 88\%$
Behnam et al. (2021)	Evap Condenser	ANN, SVR, RF	$Q = f(\text{MFR}_{\text{ref}}, \text{MFR}_{\text{air}}, T_{\text{in},\text{db}}^{\text{air}}, T_{\text{in},\text{wb}}^{\text{air}}, T_{\text{cond}}, T_{\text{in}}^{\text{water}})$	Geometry & operating conditions	ANN RMSE = 0.01, SVR RMSE = 0.01, RF RMSE = 0.03
Qiu et al. (2021)	Evaporator	ANN, XGBoost etc	$\Delta P = f(23 \text{ Dimensionless Parameters})$	Geometry, operating conditions & refrigerant	ANN RMAE = 9.58%, XGBoost RMAE = 10.38%

Figure 2.11: HX Performance Prediction Studies

## 2.6 Research Gaps

While there is no dispute that there has been extensive application of ML to heat transfer, and more so to HX operation, a survey of the literature suggests that there exist areas that warrant attention:

- (i) Most HX performance investigations do not considered a comprehensive set of features.
- (ii) Impact of refrigerant is considered in only 2 HX performance prediction studies.
- (ii) Lack of systematic framework to conduct a fair comparison.

## 2.7 Research Objectives

In lieu of the gaps described in section [2.6](#), the following make up the objectives of this thesis:

- (i) Predict performance of single and two-phase HXs with a high degree of accuracy.
- (ii) Determine the cost-accuracy appropriateness of a ML model applied to a particular problem.

## 2.8 Research Tasks

The following are crucial so as to accomplish the research objectives put forth in section 2.7

- (i) A thorough review of the literature.
- (ii) Generate the data required for ML modeling via sampling techniques and a general-purpose air-to-refrigerant HX simulation tool [4].
- (iii) Develop accurate and reliable Machine Learning models.
- (iv) Design a framework to fairly evaluate suitability of chosen Machine Learning models on a given problem.

## 2.9 Organization of Thesis

With the research objectives as the guiding principles of this thesis, the organization of the thesis is as follows; Chapter 2 begins with a brief review of conventional HX modeling approaches. Presented next is an introduction to the ML models implemented in this thesis, namely, Linear Regression models, Support Vector Regression models and Artificial Neural Networks. This is followed by a detailed review of the relevant ML investigations applied to HXs. Chapter 3 presents an ML-based performance approximation of a single-phase HX. A comparison of the ML models evaluated on their prediction accuracy, computation expense, and their reliance upon available dataset size and design variables is conducted. A second series of

systematic comparisons are made based upon model behavior to changes in design space. Chapter 4 involves a similar analysis applied to two-phase HXs instead. Finally, chapter 5 consists of concluding remarks, contributions and scope for future work.

## Chapter 3: ML Model Development of Single-Phase Heat Exchanger

### 3.1 Introduction

Those HXs in which no phase transition occurs on either side of the HX are termed single-phase HXs. The primary mode of heat transfer in these devices is generally through single-phase forced convection (between fluid and HX surface). One such type of HXs belonging to this class is a radiator. A radiator is typically a source of heat to its environment, achieved either directly through space heating or indirectly through fluid cooling as observed in automotive radiators and dry cooling towers.

Tube-fin radiators stand out from other radiator designs such as flat-panel and sectional radiators due to their compact structure, high heat dissipation efficiency and low production costs [127]. A survey of investigations on radiator design and operation revealed their impact on energy consumption and consequently guides the designer towards potential opportunities for energy savings [128–130]. Therefore, there is no dispute that there exists a strong need for accurate simulation tools capable of calculating the performance of a given design. Models built using ML techniques can effortlessly fulfil this need. Further design optimization can be performed once ML models that inspire a high degree of confidence are developed.

## 3.2 Solution Methodology

Following up on the premise that ML models can be viewed as an alternative method to estimate HX performance, the steps taken to arrive at acceptable predictive ML models are shown in fig. 3.1.

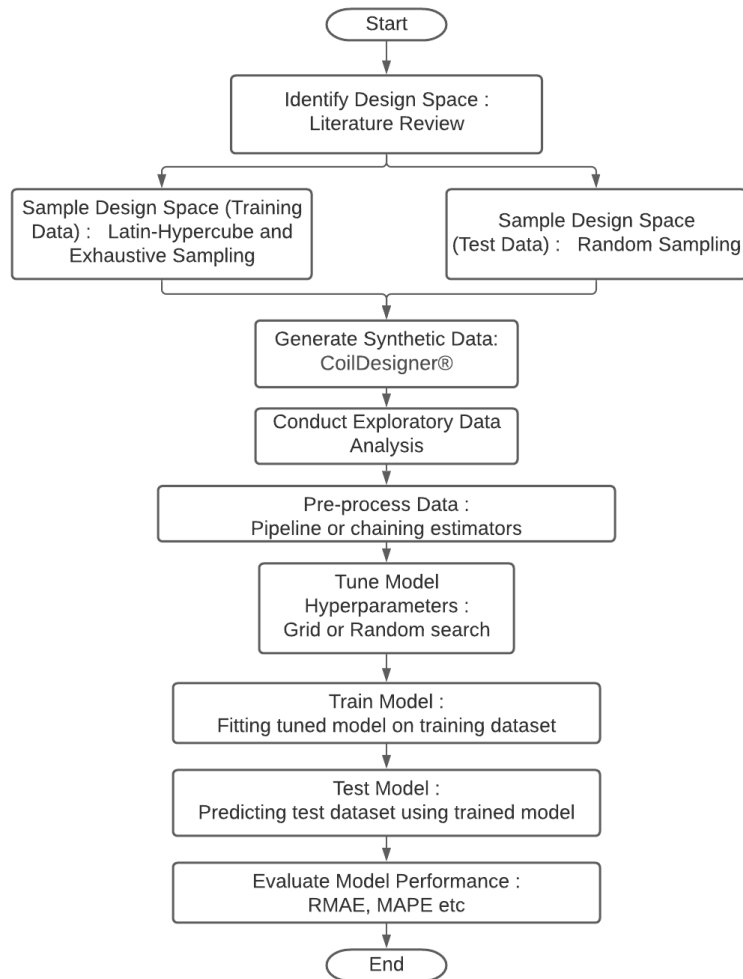


Figure 3.1: Flowchart of ML Modeling

### 3.2.1 Design Space Identification

The design space considered for the radiator modeling is shown in fig. 3.2. The design space is essentially an N-dimensional space of model inputs, with each point in this space corresponding to a valid HX design. Also present is a list of parameters that can assume only a single value for this problem.

Variables (Model Inputs)				Parameters		
Variables	Units	Range	Nature	Parameter	Units	Value
Tubes per Bank	EA	10 - 100	Discrete	Refrigerant	-	Water
Tubes per Bank per Circuit (flow configuration)	EA	1 - 4	Discrete	Refrigerant Pressure	bar	5.0
Tube Banks	EA	1 - 4	Discrete	Air Temperature	K	294.15
Tube Length	m	0.25 - 2	Continuous	Air RH	%	10
Fins per Inch	inch <sup>-1</sup>	11 - 20	Continuous	Fin Type	-	Flat plate
Air Velocity	ms <sup>-1</sup>	0.5 - 3	Continuous	Fin Thickness	mm	0.1
Refrigerant Temperature	K	338.15 - 353.15	Continuous	Tube OD	mm	9.525
Refrigerant Mass Flux	kgm <sup>-2</sup> s <sup>-1</sup>	200 - 800	Continuous	Tube Thickness	mm	0.26
				Horizontal Spacing	mm	22
				Vertical Spacing	mm	25.4
				Circuitry Type	-	Full Counter Flow

Figure 3.2: Radiator Design Space

The list of responses attempted to be predicted accurately is shown in fig. 3.3.

Response (Model Output)	Units
Heat Load	W
Refrigerant $\Delta P$	Pa

Figure 3.3: Machine Learning Model Output

Research objective number 1 (section 2.6), expresses the intent to consider a design space that encompasses the entire set of geometrical parameters and operating conditions (for both fluids) as considered in the physics-based HX simulation tool [4]. On the other hand, another equally important objective is to cover a vast operating

range for each design variable so as to include a wide array of practical HX designs. Data pertaining to the radiator design space has been obtained from standard guidelines [131] in addition to data made publicly available from an Original Equipment Manufacturer [132].

### 3.2.2 Design Space Sampling

Design space sampling involves conducting a series of properly designed experiments with the aim of generating a desired amount of data. An experimental design comprises a number of factors (design variables) set at specified levels. Assignment of levels to the factors is based upon the type of experimental design adopted. Since it is preferred to have the ML models learn the entire landscape of the design space, training data is collected through a combination of exhaustive, full factorial and Latin Hypercube sampling [41], [133]. While the discrete variables were sampled exhaustively, Latin Hypercube and full factorial (levels corresponding to minimum and maximum) experimental design were exercised on the continuous variables. In addition to collecting training data, we also require validation or testing data to gauge model performance. A competent model is one that produces acceptable solutions throughout the design space. Therefore, a testing dataset that is randomly sampled over the entire design space is chosen. Details of the relevant datasets are shown in table 3.1

Table 3.1: Radiator Data

Application	Training dataset size	Testing dataset size
Tube-fin Radiator	167716	72000

### 3.2.3 Synthetic Data Generation

As mentioned in section 2.4, the focus of this thesis is limited to supervised ML models. To enable model learning it is a must to provide them with labeled values of output for given input designs. These labeled outputs, corresponding to the training and test datasets are obtained via CoilDesigner<sup>®</sup> [4].

### 3.2.4 Exploratory Data Analysis

Exploratory Data Analysis (EDA) is the approach of analyzing the dataset at hand most commonly through data visualization techniques such as histograms, pairplots, correlation matrices etc. The reasons for undertaking an EDA at all stages of our modeling exercise are as follows:

- (i) To gain a deeper understanding of the data, thereby laying the foundation for subsequent modeling steps.
- (ii) To monitor and debug model performance.
- (iii) To communicate the results of our study.

Prior to carrying out any modeling related activities a good starting point is to investigate the extent of spread and sparsity of our data. A convenient way of conducting this analysis is through the use of histograms.

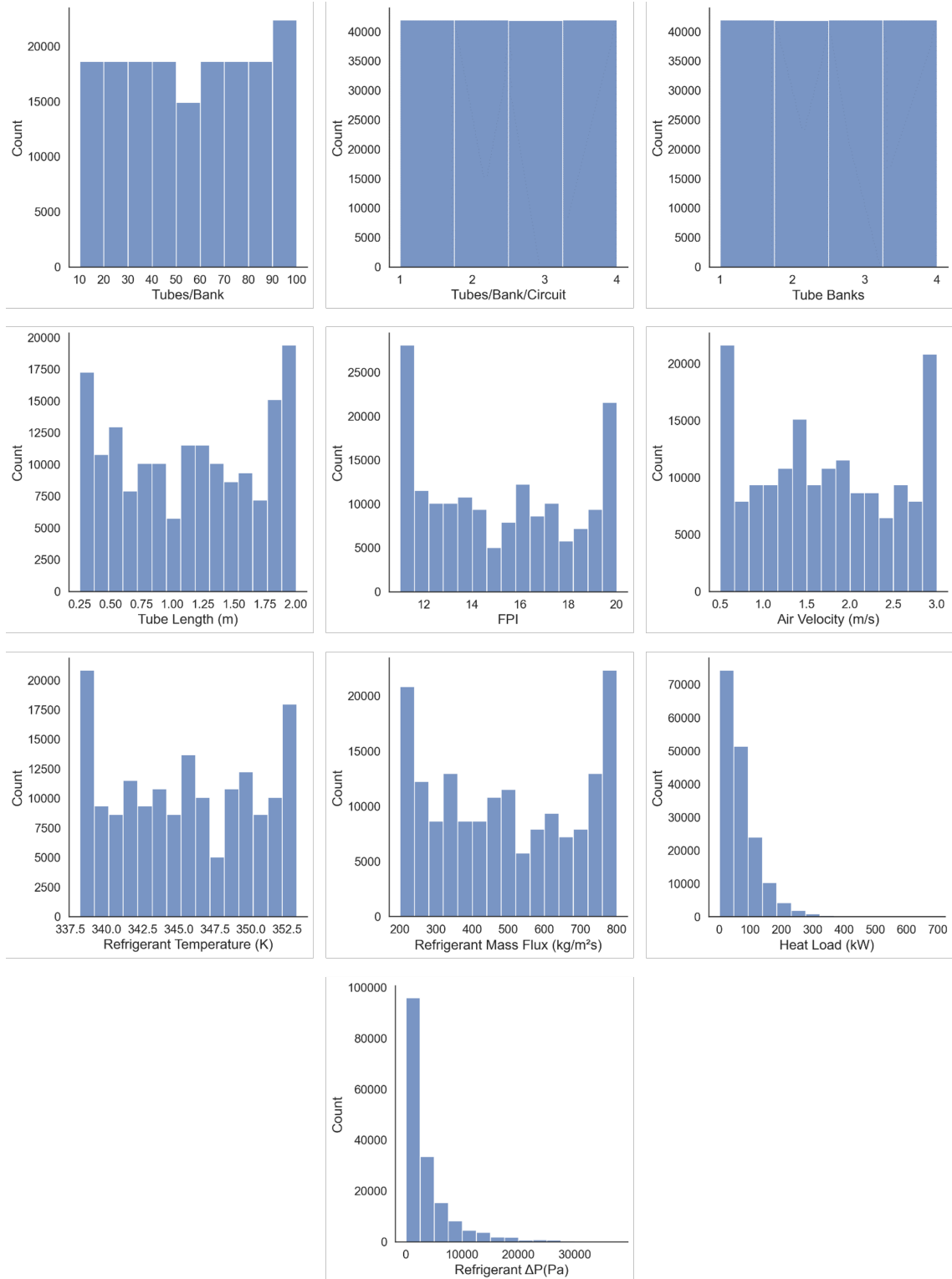


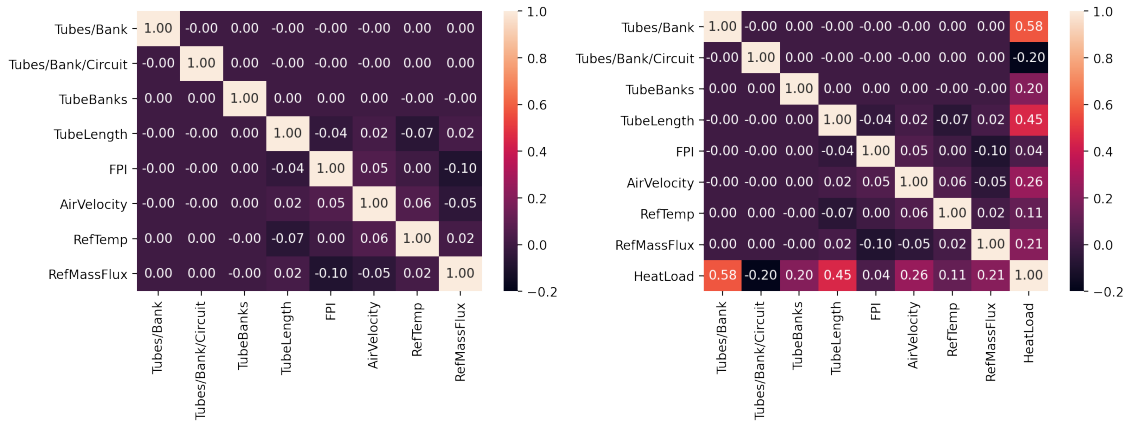
Figure 3.4: Variable Distribution

From the set of histograms shown in fig. 3.4, the following insights can be drawn:

- (i) The design variables exhibit a fair spread over their individual ranges.
- (ii) Data representation at the boundaries is larger due to the adoption of the full factorial DOE as described in section 3.2.2.
- (iii) (iii) The distribution of heat load and Refrigerant  $\Delta P$  is observed to be heavily positively skewed.

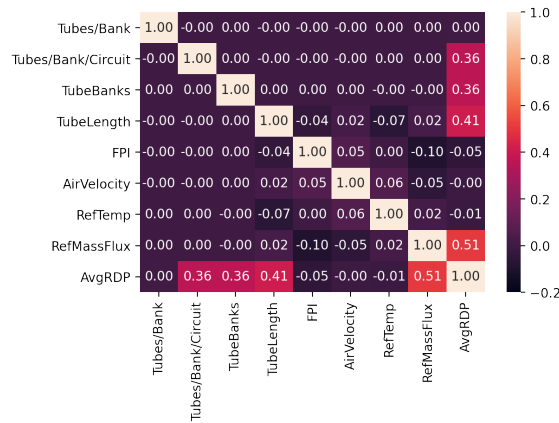
In addition to investigating the distribution of the design and response variables, it is good practice to check for the existence of multicollinearity among the design variables in a multiple regression analysis such as ours. It is undesirable to have a correlation among the independent variables because they result in high variance of the OLS estimates of the regression coefficient [134]. Ultimately unreliable regression models are arrived at. One such means of determining the bivariate correlation between two variables is the Pearson correlation coefficient ( $r$ ) [135] represented on a heatmap in fig. 3.5. The  $r$  values range from -1 to +1, with -1 indicating a strong negative correlation, and +1 indicating a strong positive correlation. An  $r$  value of 0 indicates a lack of correlation. A close inspection of fig. 3.5a reveals the absence of multicollinearity between the design variables. Several physics-based insights can be obtained by observing figs. 3.5b and 3.5c. Occurrences that make intuitive sense, such as refrigerant  $\Delta P$  being directly proportional to the refrigerant mass flux, or tubes per bank per circuit have been identified by the correlation matrix. However, an attempt to conclude upon the relative importance of the design variables on the

model output must be discouraged since an explanation of the interactive effects of two or more design variables on the response variable cannot be provided by merely examining the r values.



(a) Input-Input Relationship

(b) Input-Output(Q) Relationship



(c) Input-Output( $\Delta P$ ) Relationship

Figure 3.5: Correlation Matrices

### 3.2.5 Data Pre-processing

Data pre-processing involves a series of activities that take in real-world data with the aim of encoding it so as to significantly improve the generalization capabilities of the ML modeling algorithm. A well-structured training dataset is the product of the sub activities that comprise data pre-processing. Out of the several factors affecting the performance of an ML model, Kotsiantis et al. [136] assert data pre-processing to exert the greatest bearing. Data pre-processing is a broad umbrella encompassing several processes such as instance selection, outlier detection, imputation , discretization, normalization, transformation, feature selection and feature construction. The steps adopted as part of this study are:

- (i) Instance selection
- (ii) Data Normalization
- (iii) Data Transformation

#### 3.2.5.1 Instance Selection

Broadly speaking instance selection involves data reduction to primarily handle noise within the data. Erroneous simulation results which amounts to 0.02% of the total synthetic data generated (see section 3.2.3) are removed as part of this step.

### 3.2.5.2 Data Normalization

A multiple regression problem is composed of features whose values generally differ in their orders of magnitude. Normalization is exercised so as to rescale the features within a consistent range of values thereby minimizing the bias imposed by the ML model from one feature to another. For this problem the Min-Max normalization technique is exercised on each of the numerical variables, resulting in values being calculated within [0,1] as follows:

$$x_{new} = \frac{x_{old} - x_{min}}{x_{max} - x_{min}} \quad (3.1)$$

Convenient data normalization is performed using the Scikit-learn `MinMaxScaler` function [44]. In addition to the features, data normalization is also imposed on the model outputs. While normalization between [0,1] is directly imposed on Heat load-Q, refrigerant  $\Delta P$  is handled indirectly, as will be explained in 3.2.5.3. Finally, care is taken to ensure inverse scaling is carried out within the same range of response variable values as observed in the training dataset.

### 3.2.5.3 Data Transformation

Fig. 3.4 highlights the skewness exhibited by the refrigerant  $\Delta P$  distribution. Works in the literature [137, 138] advocate the mapping of a non-Gaussian distribution towards more Gaussian-like distributions so as to aid in superior model predictions. The Box-Cox transformation [139] is one such mapping function that

enables us to transform skewed data to a normalized, Gaussian like distribution.

The transformation is defined as follows:

$$x_i(\lambda) = \begin{cases} \frac{x_i^\lambda - 1}{\lambda} & \text{if } \lambda \neq 0 \\ \ln(x_i) & \text{if } \lambda = 0 \end{cases} \quad (3.2)$$

where,  $x_i$  is value of a numerical variable, and  $\lambda$  is a transformation parameter determined through the maximum likelihood estimation over the entire dataset to be transformed. Graphically the transformation is observed in fig. 3.6.

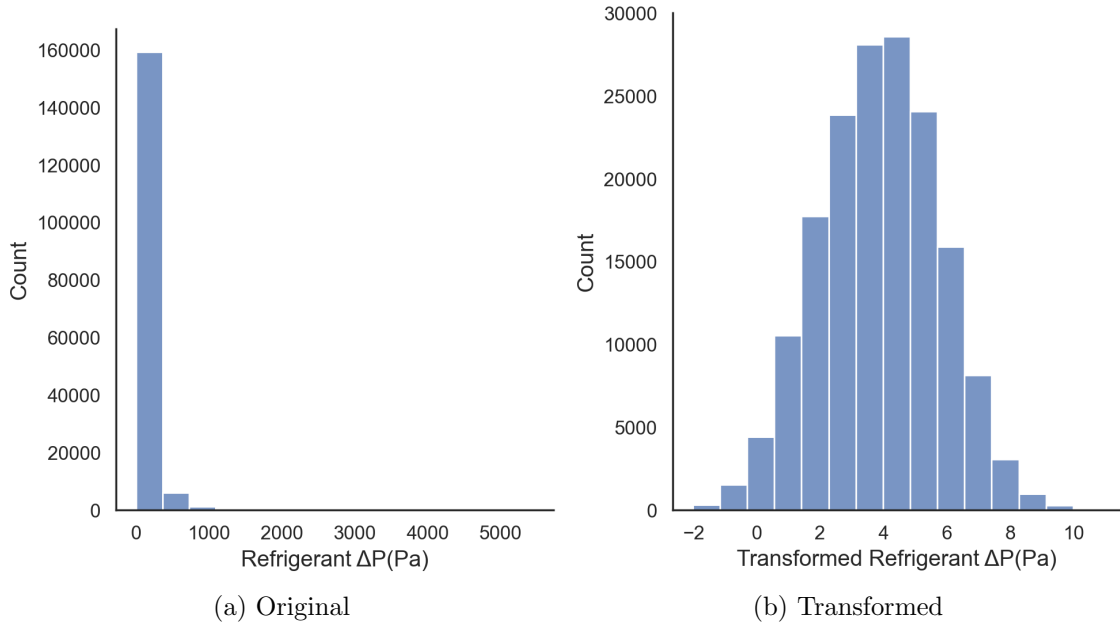


Figure 3.6: Box-Cox Transformation

In this analysis the Box-Cox transformation was implemented over the values of refrigerant  $\Delta P$  through Scikit-learn’s PowerTransformer function [44]. The improvement resulting from such a transformation is shown in section 3.2.9.

### 3.2.6 Hyperparameter Tuning

Unlike the weights of an ML regression model, hyperparameters have to be specified prior to the model training. The hyperparameters pertaining to the ML models used in this study are shown in table 3.2. The process of designing the ideal ML model architecture with the optimal set of configured hyperparameters is defined as hyperparameter tuning. Tuning of hyperparameters is considered a key component of ML modeling due to the direct relevance it bears on the model performance. A thorough review of the state-of-the-art techniques as applied to hyperparameter optimization is presented in [140]. Steps on how to conduct hyperparameter tuning is demonstrated both theoretically and through practical experiments. Several techniques such as grid search, random search, genetic algorithm, particle swarm optimization and Bayesian optimization are benchmarked as part of this investigation.

Table 3.2: Model Hyperparameters

Model	Hyperparameters	Nature
Ridge Regression	Regularization parameter	Continuous
SVR	Deviation tolerance ( $\epsilon$ )	Continuous
	Regularization parameter ( $C$ )	Continuous
	Kernel function	Categorical
	Kernel coefficient ( $\gamma$ )	Continuous
ANN	Hidden layer neurons	Discrete
	Activation function	Categorical
	Batch size	Discrete
	Weight initialization scheme	Categorical

Bergstra and Bengio [141] provided empirical evidence to prove that random search is capable of yielding solutions that are as good if not better than solutions arrived at by the widely used grid search at a fraction of the compute time. Hence, these two methods are adopted as part of this study by leveraging the implementations provided by Scikit-learn [44] - an open source ML library.

Cross validation (CV) [142] plays a significant role by evaluating the performance of each model configuration during hyperparameter tuning. k-fold CV is one of the more straightforward approaches wherein, the original training dataset is divided into ‘k’ equal subsets or folds. This is followed by an assignment of ‘k-1’ folds to train the model, while the held-out single fold is used to test the trained model. This procedure is repeated ‘k’ number of times, thereby presenting an opportunity for each fold to act as a validation dataset once. The working of k-fold CV where  $k = 5$  is shown in fig. 3.7

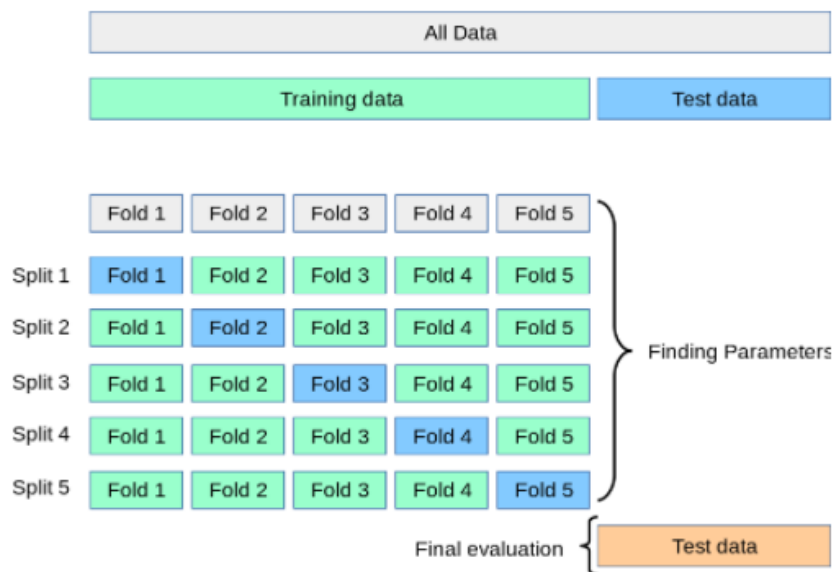


Figure 3.7: k-Fold Cross Validation [44]

On one hand k-fold CV is a valuable procedure that lends itself to the estimation of an unbiased out-of-sample error for a particular model, however, on the other hand, it significantly increases computational expense since it necessitates training the model ‘k’ number of times. This drawback is further magnified when we are working with large datasets. It is therefore desired to conduct CV on a subset of the training data, while ensuring that the sampled subset is a fair representation of the superset from which it is derived. A comparison of the statistical moments shown in figs. 3.8 and 3.9 provides an indication of the statistical similarity between the two datasets on all counts as well as the required degree of confidence to use the randomly sampled subset for the purpose of CV. Furthermore, the two sample Kolmogorov-Smirnov (K-S) test [143] is used to determine if two samples or datasets come from the same probability distribution. For the radiator case, the results of the K-S test are shown in table 3.3. At a significance level of 0.95, the K-S statistic for each feature is lower than the corresponding critical value. This is an indication that the random subset and the original dataset are drawn from the same probability distribution, and that the former is indeed a good representation of the latter. The tuned hyperparameters for Q and  $\Delta P$  models are presented in table 3.4.

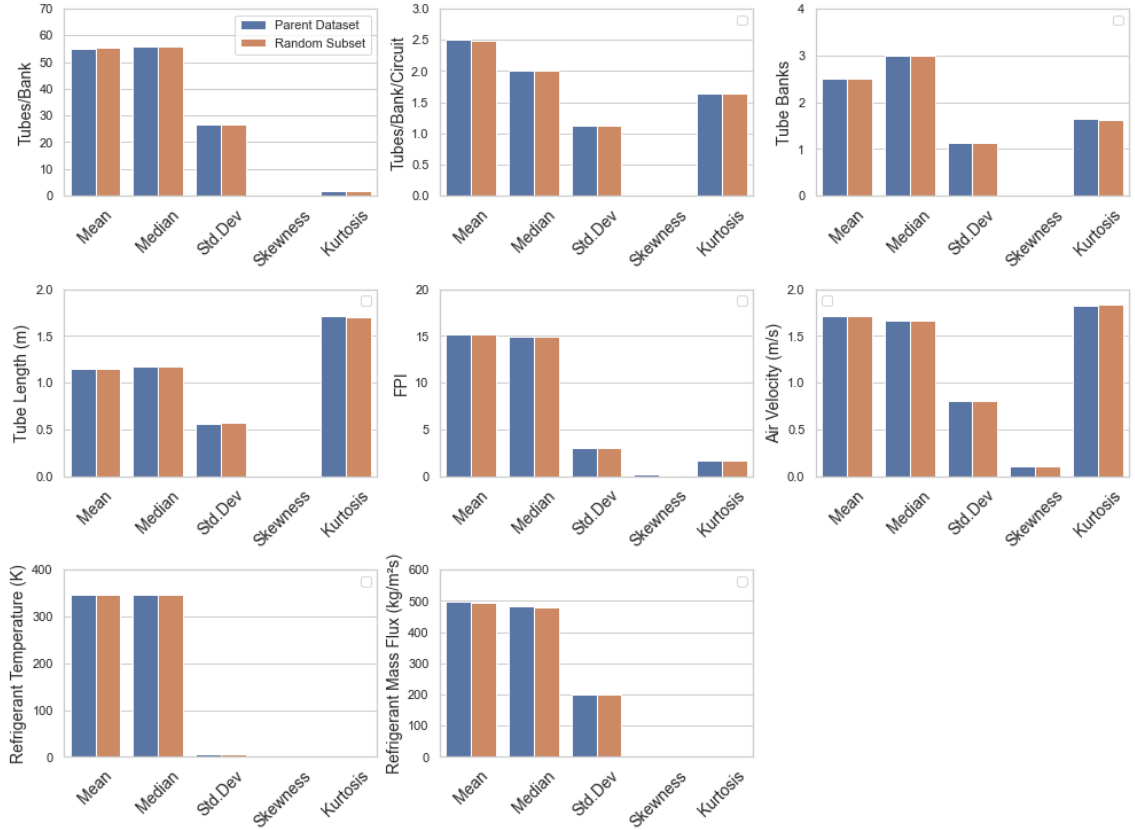


Figure 3.8: Comparison of Statistical Moments

Table 3.3: Kolmogorov-Smirnov Test Results

Feature	K-S Statistic	Critical value
Tubes/Bank	0.0097	0.013 at $\alpha = 0.05$
Tubes/Bank/Circuit	0.0045	
Tube Banks	0.0036	
Tube Length	0.01	
FPI	0.01	
Air Velocity	0.0097	
Refrigerant Temperature	0.0097	
Refrigerant Mass Flux	0.0094	

### 3.2.7 Performance Metrics

The performance metrics used to ascertain accuracy of the ML models are:

Metric	Tubes/Bank		
	Original Data	Subset	Deviation
Mean	55.08	55.45	0.68%
Median	56.00	56.00	0.00%
Std.Dev	26.84	26.73	0.39%
Skewness	-0.01	-0.03	0.03
Kurtosis	1.76	1.77	0.34%

Metric	Tubes/Bank/Circuit		
	Original Data	Subset	Deviation
Mean	2.50	2.49	0.33%
Median	2.00	2.00	0.00%
Std.Dev	1.12	1.12	0.13%
Skewness	0.00	0.00	0.00
Kurtosis	1.64	1.64	0.21%

Metric	Tube Length		
	Original Data	Subset	Deviation
Mean	1.14	1.15	0.73%
Median	1.17	1.17	0.46%
Std.Dev	0.57	0.57	0.39%
Skewness	-0.01	-0.03	0.02
Kurtosis	1.72	1.70	0.77%

Metric	FPI		
	Original Data	Subset	Deviation
Mean	15.20	15.23	0.23%
Median	14.96	14.96	0.00%
Std.Dev	3.03	3.04	0.52%
Skewness	0.15	0.14	0.01
Kurtosis	1.66	1.65	1.07%

Metric	Refrigerant Temperature		
	Original Data	Subset	Deviation
Mean	345.52	345.43	0.095
Median	345.54	345.49	0.051
Std.Dev	4.80	4.81	0.18%
Skewness	0.03	0.06	0.02
Kurtosis	1.75	1.75	0.23%

Metric	Refrigerant Mass Flux		
	Original Data	Subset	Deviation
Mean	496.53	494.08	0.49%
Median	484.83	479.93	1.01%
Std.Dev	200.07	199.11	0.48%
Skewness	0.06	0.07	0.01
Kurtosis	1.65	1.66	0.43%

Metric	Tube Banks		
	Original Data	Subset	Deviation
Mean	2.50	2.50	0.05%
Median	3.00	2.00	33.33%
Std.Dev	1.12	1.12	0.57%
Skewness	0.00	0.00	0.00
Kurtosis	1.64	1.63	0.89%

Metric	Air Velocity		
	Original Data	Subset	Deviation
Mean	1.71	1.71	0.17%
Median	1.67	1.67	0.00%
Std.Dev	0.80	0.80	0.17%
Skewness	0.10	0.11	0.01
Kurtosis	1.82	1.83	0.75%

Figure 3.9: Comparison of Statistical Moments

(i) Relative Mean Absolute Error (RMAE)

$$RMAE = \frac{1}{N} \sum_{i=1}^N \frac{|(y_{true} - y_{predicted})|}{y_{true}} \times 100 \quad (3.3)$$

(ii) Maximum Absolute Percentage Error (MAPE)

$$MAPE = \max_i \frac{|(y_{true} - y_{predicted})|}{y_{true}} \times 100 \quad \text{for } i = 1 \dots N \quad (3.4)$$

Table 3.4: Tuned Model Configuration

Model	Hyperparameters	Nature	Tuned Value/Category	
			Q	$\Delta P$
RR	Regularization parameter	Continuous	0.38	0.5
SVR	Deviation tolerance ( $\epsilon$ )	Continuous	0.005	0.01
	Regularization parameter (C)	Continuous	2.3	0.51
	Kernel function	Categorical	RBF	RBF
	Kernel coefficient ( $\gamma$ )	Continuous	0.84	0.26
ANN	Activation function	Categorical	sigmoid	sigmoid
	Batch size	Discrete	16	16
	Weight initialization scheme	Categorical	normal	uniform
	Network architecture	[-]	8-6-1	8-7-4-1

(iii)  $\sigma_{error}$  - Standard Deviation of Absolute Errors

$$\sigma_{error} = \sigma\left(\frac{1}{N} \sum_{i=1}^N |(y_{true} - y_{predicted})|\right) \quad (3.5)$$

(iv)  $\beta_N$  - Percentage of data points predicted within  $\pm N\%$  deviation

(v) Training time - The time taken in seconds for a given model to be trained over the entire HX training dataset

(vi) Prediction time - The time taken in seconds for a trained ML model to predict the output of each HX design contained in the test dataset

### 3.2.8 Model Training

Model training or fitting of supervised ML algorithms can be informally described as determining the best possible mapping for a given set of model inputs and known model outputs. A more formal explanation of the manner in which the

supervised ML methods considered in this thesis are trained is provided in sections 2.3.1, 2.3.2 and 2.3.3. From an application standpoint, once hyperparameter tuning is successfully complete (section 3.2.6), the next step is to fit the configured model to the training data. This is realized by utilizing the vast functionalities made available through open-source ML libraries [44, 45]. Furthermore, the entire computational load was borne by an Intel<sup>®</sup> Xeon<sup>®</sup> E3-1245, 3.5 GHz processor with 4 cores and 16 GB of installed RAM.

Despite the objective of model training being universal across all ML techniques, the procedure however, is not. While RR and SVR training is fairly straightforward, ANN training requires further attention to prevent occurrences of either overfitting or non-converging ANN weight updates. Measures to tackle these scenarios include but are not limited to early termination of training [6] and the introduction of a time-based learning rate schedule [144]. The effect of implementing these measures is observed by investigating plots of training behavior as shown in fig 3.10.

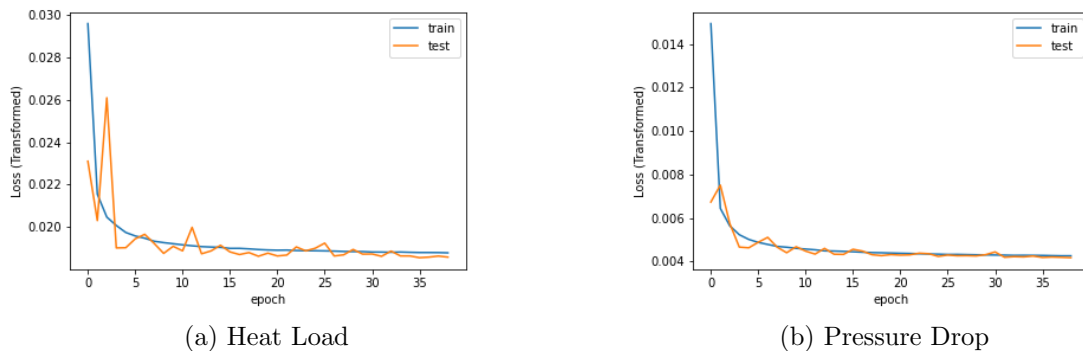


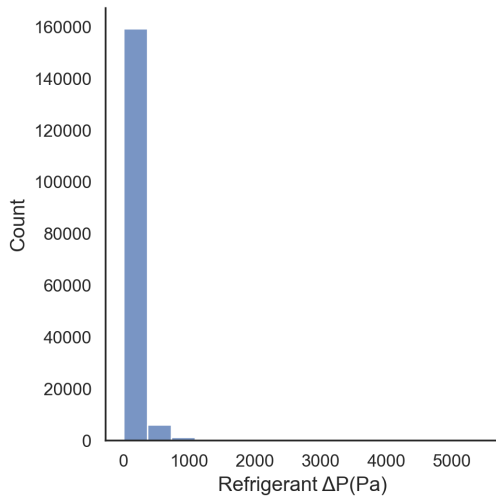
Figure 3.10: Artificial Neural Network Training Behavior

A few modeling insights may be drawn from the plots in fig. 3.10. The absence

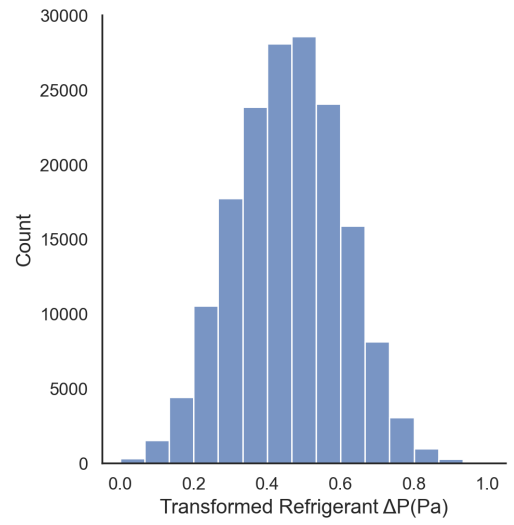
of deviation in the trends of train and test loss curves reveal a lack of overfitting to the training data; as was desired. In addition, the usefulness of introducing a learning rate schedule is also witnessed. The amplitude in the oscillations of the test loss curve (more pronounced in fig. 3.10a) is observed to drastically decrease as the number of training epochs advance.

### 3.2.9 Data Pre-processing Outcome

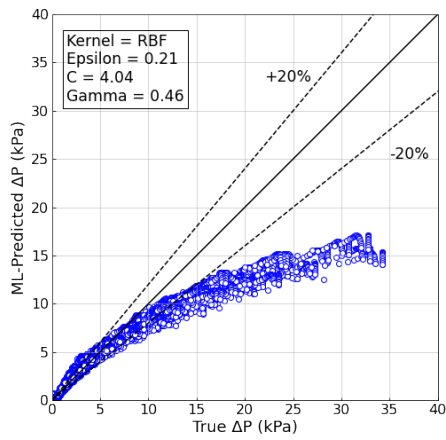
Section 3.2.5 advocates the utilization of several data pre-processing steps to improve the predictive capabilities of ML models. The advantages of conducting the steps described in section 3.2.5 prior to model training and testing is highlighted here. A comparison of the SVR predictions of radiator refrigerant  $\Delta P$  with and without pre-processing of data is shown below (see fig. 3.11). Additionally, the transformation of the refrigerant  $\Delta P$  distribution from highly positively skewed to a more Gaussian-like distribution is also exhibited (see fig. 3.11). 3.11e provides further numerical evidence of the improvement in performance due to the adoption of steps described in section 3.2.5.



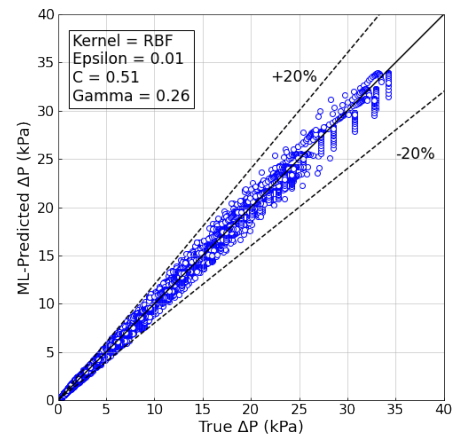
(a) Without Data Pre-processing



(b) With Data Pre-processing



(c) Without Data Pre-processing



(d) With Data Pre-processing

	RMAE (%)	$\beta_{20}$ (%)
Without Data Pre-processing	30	75.1
With Data Pre-processing	3.5	99.9

(e) Numerical Comparison

Figure 3.11: Data Pre-processing Outcome

### 3.2.10 Model Testing

A culmination of the various procedures described in sections 3.2.1 - 3.2.8 is an ML model which is expected to predict HX performance on unseen data. The performance of the developed ML models (RR, SVR and ANN) on the test dataset of the TF Radiator (see table 3.1) is compared by simultaneously examining their individual verification plots and corresponding performance metrics. It must be noted that unless specified, each performance metric pertains to the test dataset. For a comparison of predictions of  $Q$ , the reader is directed to table 3.5 and fig. 3.12. Shown within each plot is a textbox of the tuned hyperparameters.

Table 3.5: Baseline Machine Learning Model Comparison

Heat Load Prediction			
Metric	RR	SVR	ANN
RMAE [%]	23.4	2.6	4.2
MAPE [%]	412.6	22.4	59.1
$\sigma_{error}$ [W]	58.5	15.8	247.8
$\beta_5$ [%]	12.8	86.8	70.8
$\beta_{20}$ [%]	52.1	99.9	99.2
Training Time [s]	1.3	4355	1041
Prediction Time [s]	0.002	49.6	1.3

Although the computation expense associated with SVR is a point of concern, it yields the most accurate predictions. RR imposes minimal computation expense, but results in inaccurate predictions. A favorable balance between prediction accuracy and computation expense is achieved using ANN.

The robustness of each ML technique can be assessed using  $\sigma_{error}$ , which is determined as a result of performing 5-fold cross validation (CV). In concurrence with

other works in the literature [145], [146], it is noticed that ANN suffers from high variances in prediction. This is attributed to the backpropagation (BP) learning algorithm being a gradient method that cannot guaranteed global minimum. Additionally, all models exhibit relatively high values of MAPE, indicating the existence of region(s) in the design space where prediction capability is poor.

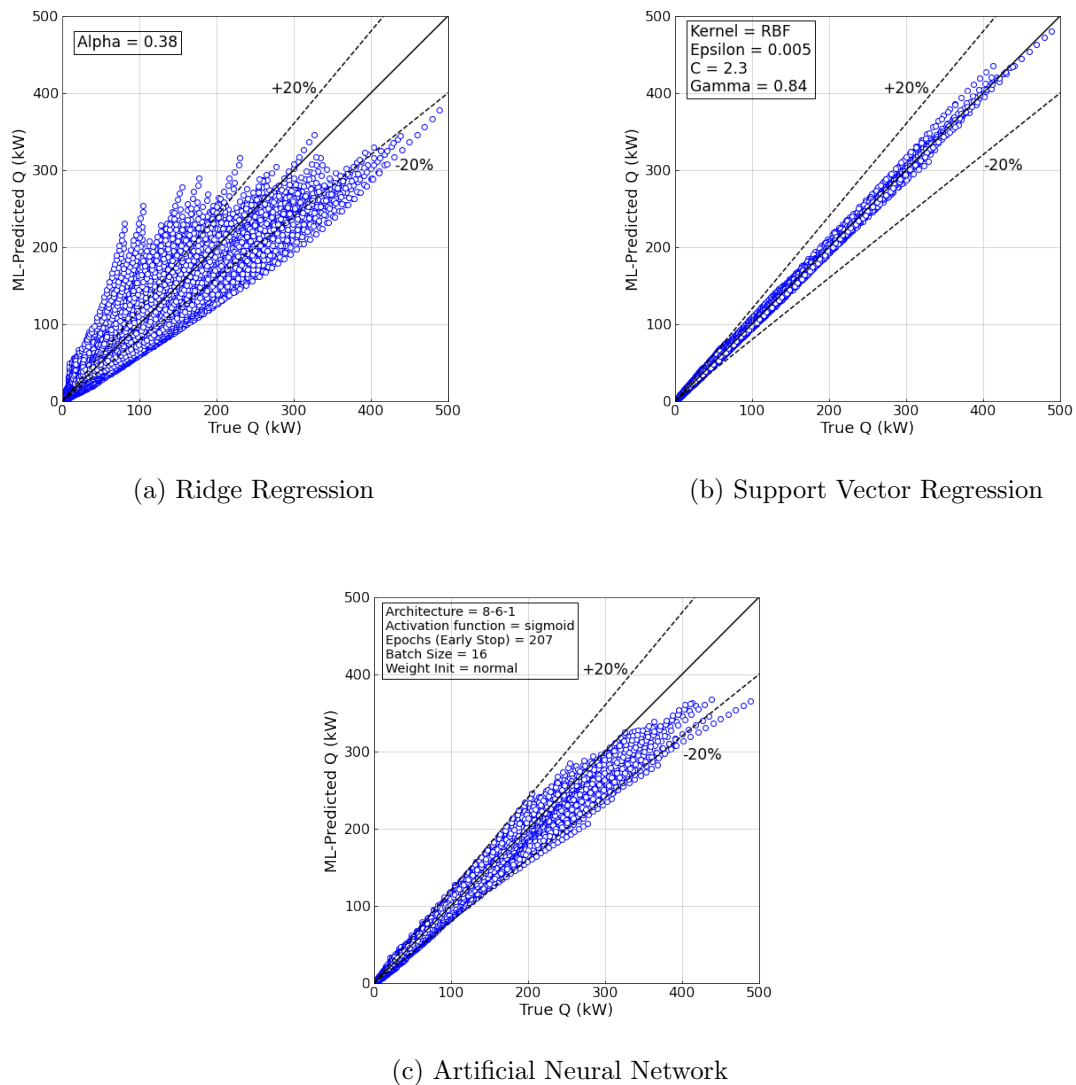


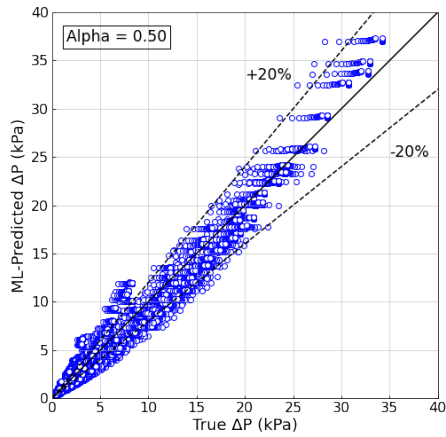
Figure 3.12: Heat Load Prediction Verification Plots

Results relevant to  $\Delta P$  predictions are presented in table 3.6 and fig. 3.13

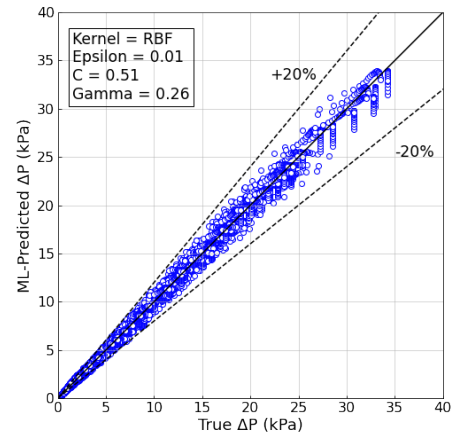
In the case of refrigerant  $\Delta P$ , results show that ANN outperforms SVR. As with heat load predictions, RR yields poor predictions. Though the predictions resulting from the SVR are encouraging, there is a degradation relative to its corresponding heat load predictions. Additionally, the robustness of ANN predictions in this case is comparable to the other models, further increasing its standing as an effective approximator.

Table 3.6: Baseline Machine Learning Model Comparison

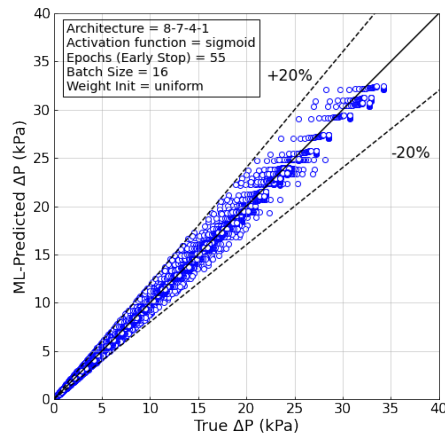
Pressure Drop Prediction			
Metric	RR	SVR	ANN
RMAE [%]	18.4	3.7	1.8
MAPE [%]	131.1	27	25.5
$\sigma_{error}$ [Pa]	1.4	4.1	13.1
$\beta_5$ [%]	15.4	73	93
$\beta_{20}$ [%]	60.3	99.9	99.9
Training Time [s]	1.1	5604	289
Prediction Time [s]	0.001	44.4	1.3



(a) Ridge Regression



(b) Support Vector Regression



(c) Artificial Neural Network

Figure 3.13: Pressure Drop Prediction Verification Plots

### 3.2.11 Physical Verification of ML models

Section 3.2.10 highlights the ability of ML models to predict a large set of points accurately. In order to further enhance their reputation as capable estimators, it is necessary for these ML models to capture heat transfer and refrigerant  $\Delta P$  trends as physics-based models do.

### 3.2.11.1 Parametric Analysis

To this end, a sample radiator design as shown in fig. 3.14 is considered. Parametric analyses are conducted to investigate the impact of tube length on heat load and refrigerant  $\Delta P$  respectively. Figs. 3.15a and 3.15b show the variation in heat load and refrigerant  $\Delta P$  as calculated by a physics-based HX model [4] and ML models (SVR and ANN) for various tube lengths. While, there does exist a clear deviation in prediction it is evident that both ML models predict physical trends of heat load and refrigerant  $\Delta P$  in accordance with the physics-based HX model.

Sample Radiator Design			Parameters		
Variables	Units	Value	Parameter	Units	Value
Tubes per Bank	EA	60	Refrigerant	-	Water
Tubes per Bank per Circuit	EA	4	Refrigerant Pressure	bar	5.0
Tube Banks	EA	4	Air Temperature	K	294.15
Tube Length	m	0.25 – 2 (steps of 0.25m)	Air RH	%	10
Fins per Inch	inch <sup>-1</sup>	16.7	Fin Type	-	Flat plate
Air Velocity	ms <sup>-1</sup>	2.6	Fin Thickness	mm	0.1
Refrigerant Temperature	K	347	Tube OD	mm	9.525
Refrigerant Pressure	Pa	500000	Tube Thickness	mm	0.26
Refrigerant Mass Flux	kgm <sup>-2</sup> s <sup>-1</sup>	600, 800	Horizontal Spacing	mm	22
			Vertical Spacing	mm	25.4
			Circuitry Type	-	Full Counter Flow

Figure 3.14: Sample Radiator Design Space

Further comparison of each ML model relative to the true heat load and  $\Delta P$  values is shown in table 3.7. In accordance with the results of a physics-based HX model [30], the ML models also seem to predict heat load with a greater degree of accuracy than refrigerant  $\Delta P$ .

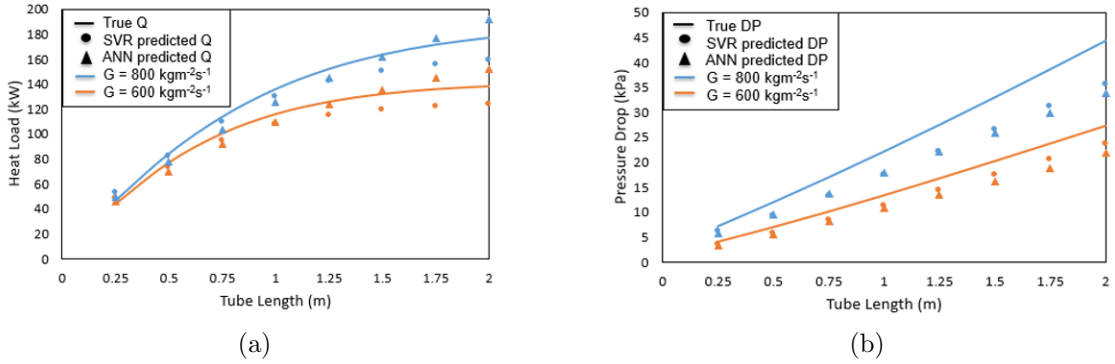


Figure 3.15: Parametric Analysis

Table 3.7: Comparison of ML Model Performance for Sample Radiator

Heat Load (kW)			Pressure Drop (kPa)		
SVR	RMAE [%]	7.9	SVR	RMAE [%]	17.5
	MAPE [%]	13.6		MAPE [%]	22.1
ANN	RMAE [%]	6.4	ANN	RMAE [%]	20.4
	MAPE [%]	11.4		MAPE [%]	23.7

### 3.2.11.2 Pairwise Comparison

Evolutionary algorithms are effective methods of solving multi-objective optimization problems. Many of these algorithms comprise a non-dominated sorting procedure which is conducted to determine the relative quality of designs [147]. In other words, feasible designs are compared pairwise to identify the design that yields a more favorable objective function(s) value. Thus, it is desired to investigate if ML models display exact comparative trends of HX performance as exhibited by physics-based models. In this thesis, a pairwise comparison of HX designs is carried out as follows:

- (i) For  $n = 1 \dots N$ , consider  $\binom{n}{2}$  HX designs, where  $N$  values are randomly chosen

from the test dataset (physics-based HX model predictions).

- (ii) Pair the HX design as  $(\mathbf{X}_{n,1}, \mathbf{X}_{n,2})$ ,  $n = 1 \dots N$ .
- (iii) Calculate their corresponding objective function values which are then represented as  $(Q_{n,1}, Q_{n,2})$ ,  $n = 1 \dots N$ .
- (iv) Count the number of cases where  $Q_{n,1} > Q_{n,2}$ ,  $n = 1 \dots N$ , from test dataset (true values), SVR ANN predictions, .
- (v) Repeat the above four steps ‘m’ times and calculate mean number of cases satisfying the criterion  $Q_{n,1} > Q_{n,2}$ ,  $n = 1 \dots N$ , for SVR and ANN predictions.

The number of cases from the test dataset, SVR and ANN predictions are further compared. It is desired that the SVR and ANN predictions exhibit the same comparative trend as predicted by the physics-based HX model for each case considered. For  $N = 1000$ ,  $m = 10$ . The same set of radiator designs which have been considered thus far as part of this study is used for the pairwise comparison. The results for heat load and refrigerant  $\Delta P$  are as shown in fig. 3.16.

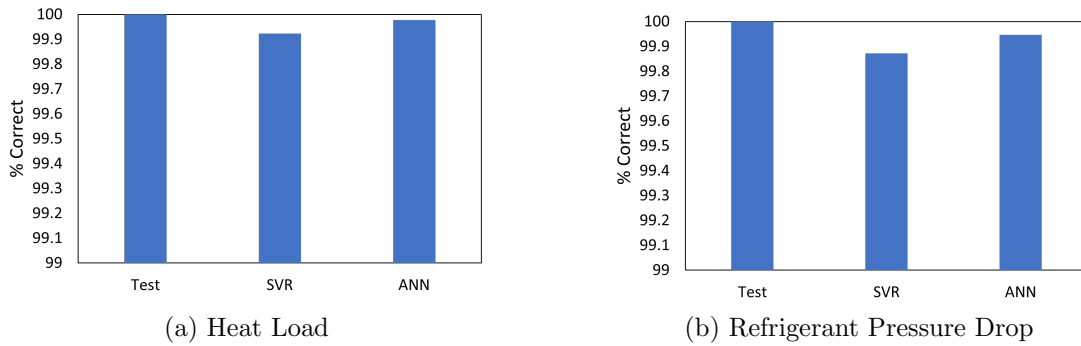


Figure 3.16: Pairwise Comparison of HX design

Fig. 3.16 indicates the percentage of total cases where the SVR and ANN models produce the exact same comparative trend as yielded by the physics-based model [4]. For heat load and refrigerant  $\Delta P$ , it is noticed that both the ML models achieve a prediction accuracy  $> 99.8\%$ .

### 3.3 Training Dataset Size Impact

Thus far, the prediction capability of the ML models have been gauged by training these models over the entire training dataset. These models are termed as baseline models in this study. Kotsiantis et al. [136] state that as the amount of data available to a model grows, the rate of increase in its prediction accuracy tends to slow down. Therefore, from the available training dataset, random subsets of varying sizes are made available to the models during the training phase. Subsequently, the corresponding variation in performance and training time is observed in fig. 3.17 where  $\alpha$  represents the percentage of the original training dataset size chosen at random. Contrary to the findings of section 3.2.10 it is seen that the prediction accuracies achieved by the reduced-domain SVR and ANN models differ significantly. Consistent with the observations of Mohanraj et al. [6], the ANN model is seen to suffer from a performance degradation at low values of  $\alpha$ , while the same is not true in the case of the SVR. Moreover, when the models are trained on significantly small dataset sizes, the time required to train the SVR is found to be lower than the corresponding time required for ANN training.

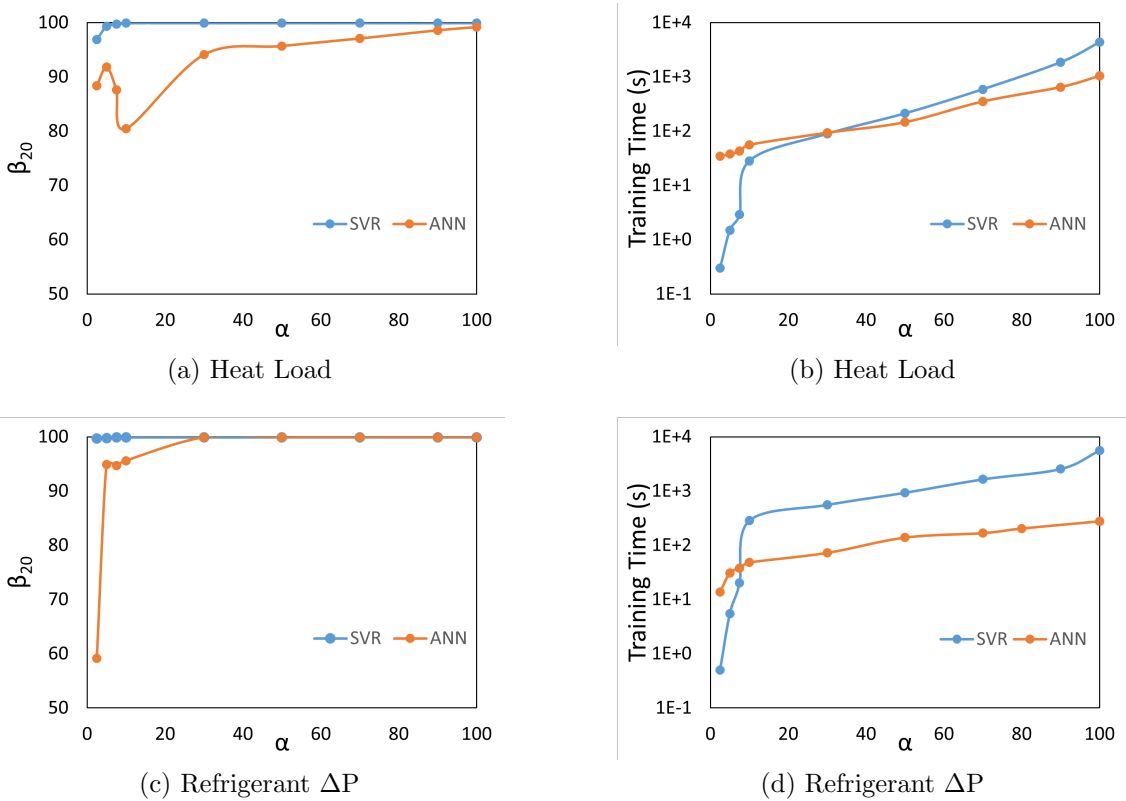


Figure 3.17: Radiator Training Dataset Size Impact

### 3.4 Outcome-based Comparison Framework

Conventionally, ML models are compared based on their prediction capabilities with each model demanding the same level of input in terms of training dataset size [10], [61]. Though this method of comparison provides an understanding of an ML model's capabilities, this form of comparison may not always be useful in identifying the most suitable ML model for a given problem. Thus, an outcome based comparison of ML models is proposed wherein, an attempt is made to gauge the cost incurred by a model in order to achieve a pre-determined degree of prediction accuracy. The steps that make up this outcome-based comparison framework is

shown in the flowchart below (see fig.3.18).

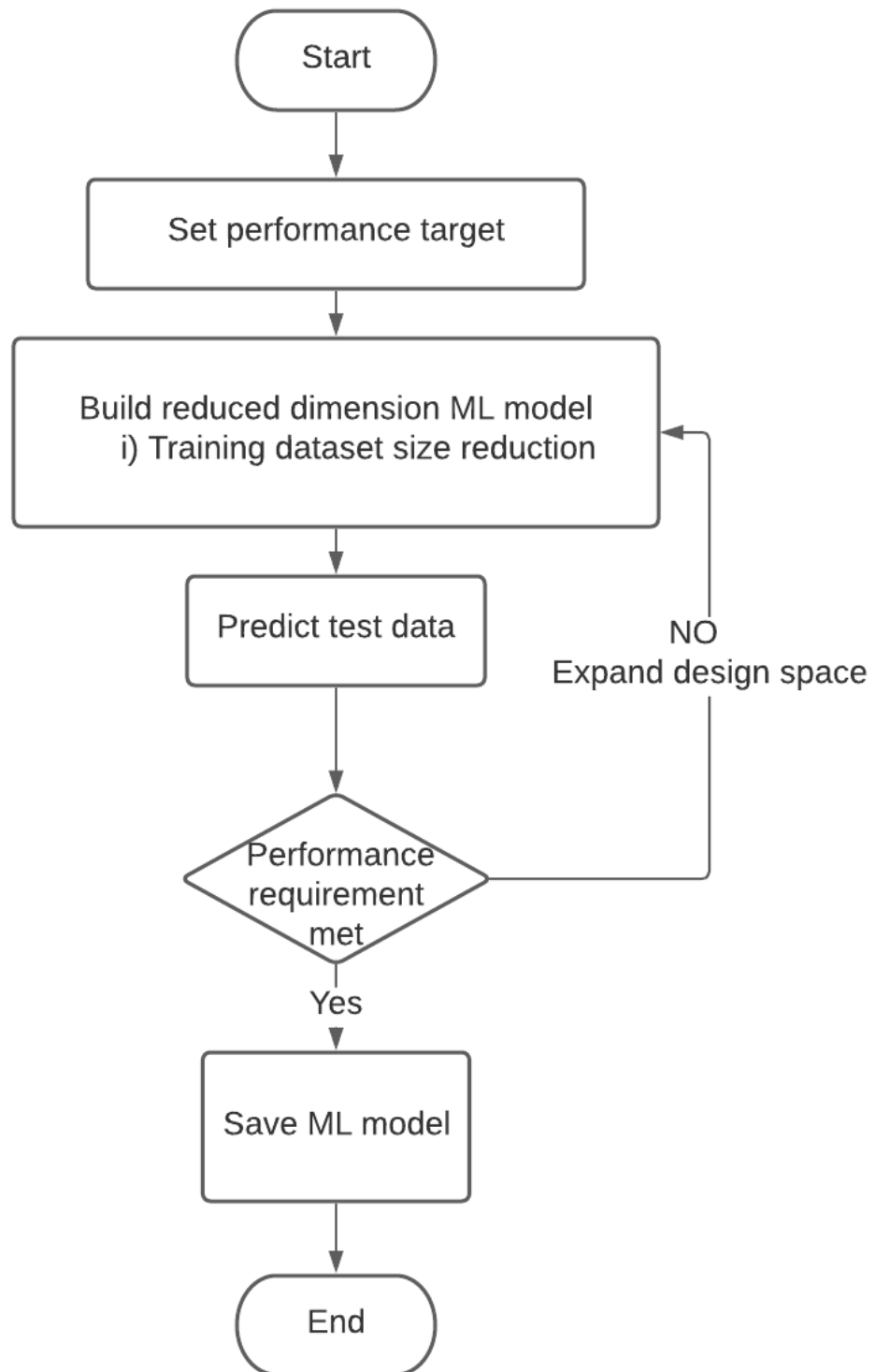


Figure 3.18: Outcome-based Comparison Framework

One of the two research thrusts of this thesis is to determine the cost-accuracy appropriateness of an ML model applied to a particular problem (see section 2.7). An outcome of this thrust is to identify the most efficient ML model for a given problem.

The most efficient ML model is one that yields satisfactory prediction accuracy at a reasonable cost. Either the conventional ML model comparison or the outcome-based comparison can be exercised to deem the suitability of an ML model to the problem at hand. This is depicted in greater detail in fig. 3.19

Application	Preferred model (Conventional Comparison)	Preferred model (Outcome-based Comparison)
Radiator Heat load	Baseline ANN	Reduced domain SVR
Radiator Pressure Drop	Baseline ANN	Reduced domain SVR

Figure 3.19: ML Model Appropriateness

## Chapter 4: ML Model Development of Two-Phase Heat Exchangers

### 4.1 Introduction

A two-phase HX is a device that is involved in the transfer of thermal energy between two fluids by virtue of absorption or release of latent heat of vaporization. The inclusion of latent heat of vaporization greatly enhances the heat transfer in a two-phase HX where at least one of the two fluids undergo a phase change. As part of a Vapor Compression Cycle (VCC), two-phase HXs are utilized either as evaporators or condensers. Two-phase HXs are termed as evaporators when they absorb thermal energy from an external fluid resulting in their evaporation, while they are termed as condensers when they release thermal energy to the external fluid resulting in their condensation. Thus, the change in enthalpy is observed as a change in vapor quality rather than a change in temperature as is the norm in a single-phase HX. As a consequence of their marked superiority over single-phase HXs more than 60% of HXs in the industry operate in two-phase mode [148].

Tube-fin HXs due to their large heat transfer area and compactness are used extensively as condensers and evaporators in HVAC&R systems. Furthermore, studies by Westphalen et al. [2] and Liang et al. [35] communicate the extent to which optimal TFHX designs can yield benefits in terms of energy and cost reduction.

With the objective of reducing the environmental impact of HVAC&R units, there lies an imperative need for the development of quick, cheap and accurate HX performance prediction tools. ML models due to their effective mapping capabilities, thus prove to be a powerful instrument in fulfilling this need.

## 4.2 Solution Methodology

The steps taken to arrive at acceptable predictive ML models are analogous to those exercised in section 3.2. Therefore a detailed description is provided solely in those areas where stark differences with the former (section 3.2) exist.

### 4.2.1 Design Space Identification

The individual design spaces considered for the TF condenser and TF evaporator modeling are shown in figs. 4.1 and 4.2 respectively.

Variables (inputs to the model)				Parameters		
Variables	Units	Range	Nature	Parameter	Units	Value
Refrigerant	-	R410A, R32	Categorical	Air Temperature	K	308.15
Tubes per Bank	EA	10 - 100	Discrete	Air RH	%	10
Tubes per Bank per Circuit	EA	1 - 4	Discrete	Fin Type	-	Flat plate
Tube Banks	EA	1 - 4	Discrete	Fin Thickness	mm	0.1
Tube Length	m	0.25 - 2	Continuous	Tube OD	mm	9.525
Fins per Inch	inch <sup>-1</sup>	11 - 20	Continuous	Tube Thickness	mm	0.26
Air Velocity	ms <sup>-1</sup>	0.5 - 3	Continuous	Horizontal Spacing	mm	22
Refrigerant $\Delta T_{sat}$	K	2 - 30	Continuous	Vertical Spacing	mm	25.4
Refrigerant Mass Flux	kgm <sup>-2</sup> s <sup>-1</sup>	300 - 1200	Continuous	Circuitry Type	-	Full Counter Flow
Refrigerant $T_{dew}$	K	313.15 - 323.15	Continuous			

Figure 4.1: Condenser Design Space

Variables (inputs to the model)				Parameters		
Variables	Units	Range	Nature	Parameter	Units	Value
Refrigerant	-	R410A, R32	Categorical	Air Temperature	K	299.85
Tubes per Bank	EA	10 - 50	Discrete	Air RH	%	50
Tubes per Bank per Circuit	EA	4 - 20	Discrete	Fin Type	-	Flat plate
Tube Banks	EA	1 - 8	Discrete	Fin Thickness	mm	0.1
Tube Length	m	0.25 - 2	Continuous	Tube OD	mm	9.525
Fins per Inch	inch <sup>-1</sup>	11 - 20	Continuous	Tube Thickness	mm	0.26
Air Velocity	ms <sup>-1</sup>	0.5 - 3	Continuous	Horizontal Spacing	mm	22
Refrigerant $T_{\text{bubble}}$	K	278.15 - 288.15	Continuous	Vertical Spacing	mm	25.4
Refrigerant Mass Flux	kgm <sup>-2</sup> s <sup>-1</sup>	300 - 1200	Continuous	Circuitry Type	-	Full Counter Flow
Inlet quality	%	10 - 30	Continuous			

Figure 4.2: Evaporator Design Space

The list of responses attempted to be predicted accurately by both, the TF condenser ML model as well as the TF evaporator ML model is shown in fig. 4.3.

Response (Model Output)	Units
Heat Load	W
Refrigerant $\Delta P$	Pa

Figure 4.3: Machine Learning Model Output

Data pertaining to the condenser and evaporator design space has been obtained from standard guidelines [149] in addition to data made publicly available from an Original Equipment Manufacturer [150].

#### 4.2.2 Design Space Sampling

The same procedure adopted in section 3.2.2 is followed here. Details of the relevant TF condenser and TF evaporator datasets are shown in tables 4.1 and 4.2 respectively.

Table 4.1: Tube-Fin Condenser Data

Application	Training dataset size	Testing dataset size
Tube-fin Condenser	378511	142840

Table 4.2: Tube-Fin Evaporator Data

Application	Training dataset size	Testing dataset size
Tube-fin Evaporator	210008	74870

### 4.2.3 Synthetic Data Generation

As conducted in section 3.2.3, CoilDesigner<sup>®</sup> [4] is made use of to obtain labeled data corresponding to the training and test datasets.

### 4.2.4 Exploratory Data Analysis

A significant difference between the design space considered for single-phase HXs 3.2.1 and that considered for two-phase HXs 4.2.1 is the choice of refrigerant flowing through the HX. While the single-phase HX utilizes only water, the two-phase HXs considered in this thesis utilize R410A (mixture of difluoromethane and pentafluoroethane in equal proportion) and R32 (difluoromethane).

Since we are dealing with two refrigerants or two “classes”, we must identify the existence of an imbalance in class representation. The presence of a class imbalance calls for a modification in our modeling approach as described in the work by Japkowicz [151]. A convenient way of conducting this analysis is through the use of histograms, which additionally serves as a means of investigating the extent of spread and sparsity of the remaining inputs or features pertaining to each of the two-phase HX ML models.

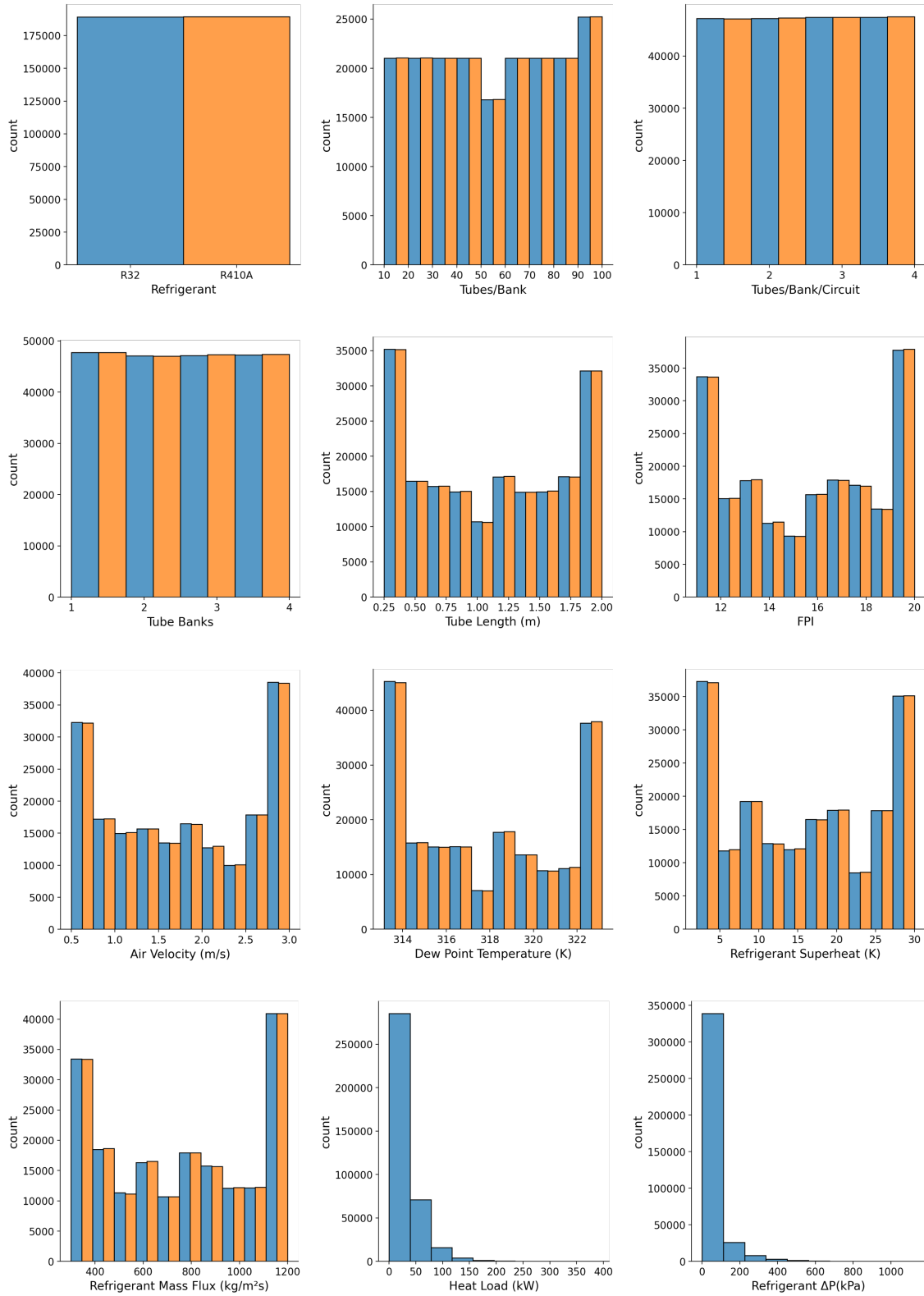


Figure 4.4: TF Condenser Variable Distribution

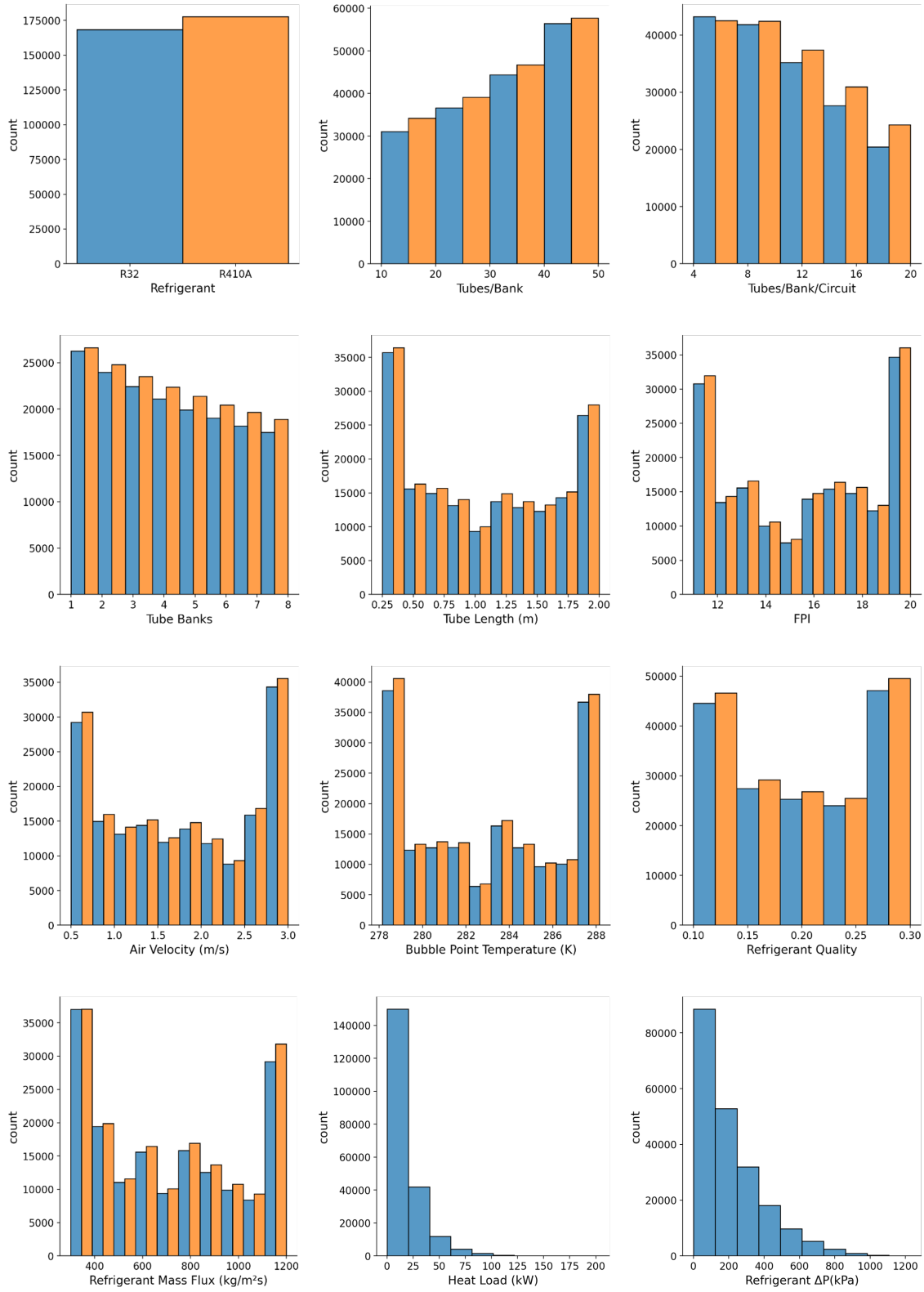
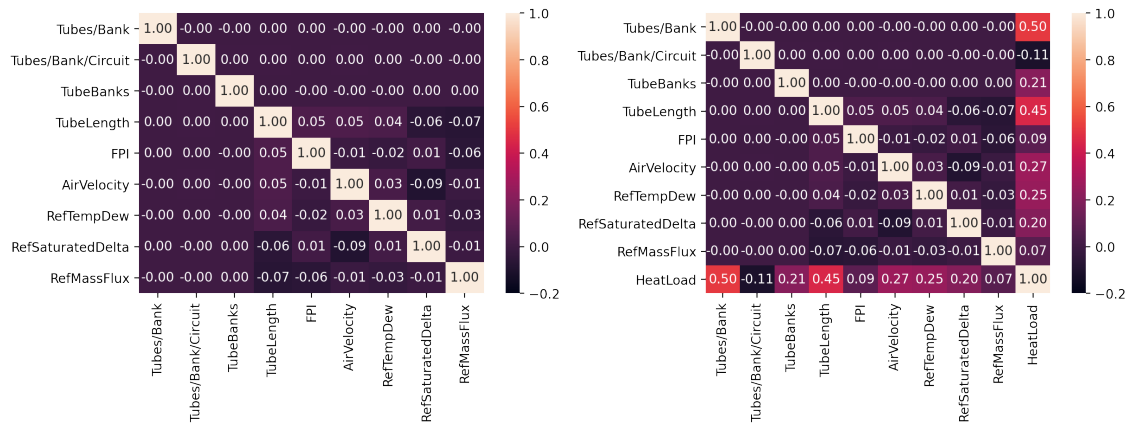


Figure 4.5: TF Evaporator Variable Distribution

The following insights can be drawn from figs. 4.4 and 4.5,

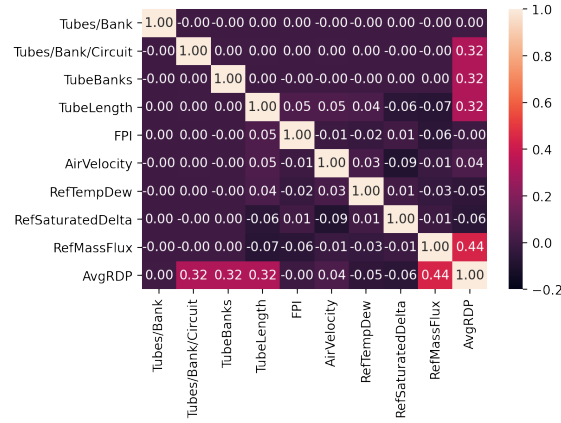
- (i) Both the refrigerants or classes are equally represented.
- (ii) The design variables exhibit a fair spread over their individual ranges.
- (iii) Data representation at the boundaries is larger due to the adoption of the full factorial DOE as described in section 3.2.2.
- (iv) The distribution of Refrigerant  $\Delta P$  is observed to be heavily positively skewed.

Similar to section 3.2.4 a check for multicollinearity among the design variables is conducted with the aid of correlation matrices (figs. 4.6 and 4.7) that indicate the values of Pearson correlation coefficients [135]. As observed previously an absence of multicollinearity between the design variables or inputs is witnessed.



(a) Input-Input Relationship

(b) Input-Output(Q) Relationship



(c) Input-Output( $\Delta P$ ) Relationship

Figure 4.6: Correlation Matrices for TF Condenser

## 4.2.5 Data Preprocessing

The measures considered for preprocessing training and test data pertaining to the TF condenser and TF evaporator are analogous to the steps followed in section 3.2.5. However, one major point of difference is in relation to the transformation of the refrigerant  $\Delta P$  while developing the corresponding ANN models. As opposed to the Box-Cox transformation [139] exercised earlier, the Yeo-Johnson transformation [139] is utilized in this case. The reason for such an alteration is due to the

high degree of compatibility the Yeo-Johnson transformation has with the hyperbolic tangent (see table 2.2) activation function that was obtained as a result of hyperparameter tuning.

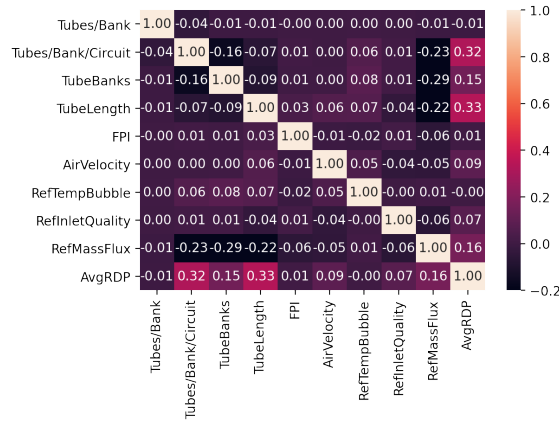
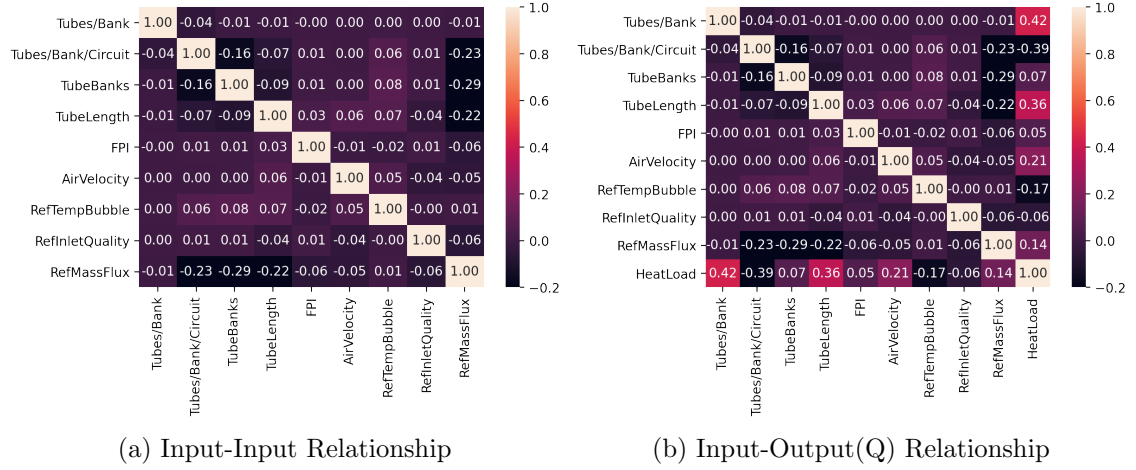


Figure 4.7: Correlation Matrices for TF Evaporator

The Yeo-Johnson transformation is defined as follows:

$$x_i(\lambda, x_i) = \begin{cases} \frac{(x_i+1)^\lambda-1}{\lambda} & \text{if } \lambda \neq 0, x_i \geq 0 \\ \ln(x_i + 1) & \text{if } \lambda = 0, x_i \geq 0 \\ \frac{-[(-x_i+1)^{2-\lambda}-1]}{(2-\lambda)} & \text{if } \lambda \neq 2, x_i < 0 \\ -\ln(-x_i + 1) & \text{if } \lambda = 2, x_i < 0 \end{cases} \quad (4.1)$$

where,  $x_i$  is the value of a numerical variable. Graphically the transformation is observed in fig. 4.8.

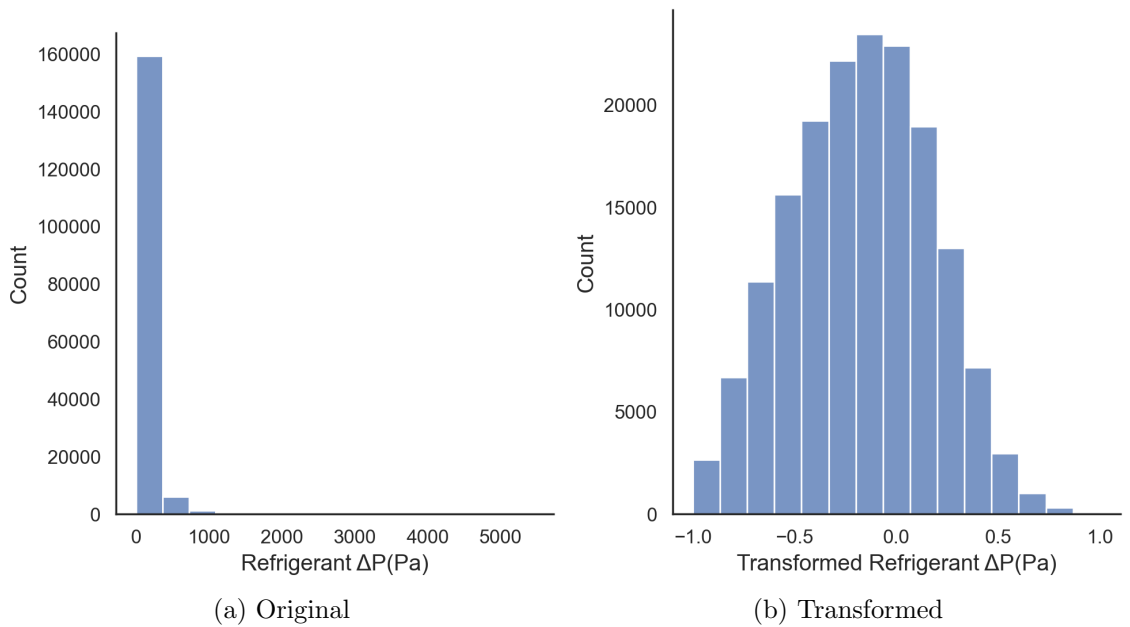


Figure 4.8: Yeo-Johnson Transformation

## 4.2.6 Hyperparameter Tuning

As there exists no difference between the steps adopted as part of the current section and section 3.2.6, only a table of the tuned hyperparameters for both the two-phase HX applications are provided.

Table 4.3: TF Condenser ML model tuned hyperparameters

Model	Hyperparameters	Nature	Tuned Value/Category	
			Q	$\Delta P$
RR	Regularization parameter	Continuous	0.8	1.81
SVR	Deviation tolerance ( $\epsilon$ )	Continuous	0.005	0.007
	Regularization parameter (C)	Continuous	1.4	1.2
	Kernel function	Categorical	RBF	RBF
	Kernel coefficient ( $\gamma$ )	Categorical	0.69	1.8
ANN	Activation function	Categorical	sigmoid	tanh
	Batch size	Discrete	16	16
	Weight initialization scheme	Categorical	glorot-uniform	normal
	Network architecture	[-]	10-10-8-1	10-9-8-9-1

Table 4.4: TF Evaporator ML model tuned hyperparameters

Model	Hyperparameters	Nature	Tuned Value/Category	
			Q	$\Delta P$
RR	Regularization parameter	Continuous	0.28	0.34
SVR	Deviation tolerance ( $\epsilon$ )	Continuous	0.002	0.008
	Regularization parameter (C)	Continuous	2.3	1.1
	Kernel function	Categorical	RBF	RBF
	Kernel coefficient ( $\gamma$ )	Categorical	0.52	0.54
ANN	Activation function	Categorical	sigmoid	tanh
	Batch size	Discrete	16	16
	Weight initialization scheme	Categorical	glorot-uniform	glorot-uniform
	Network architecture	[-]	10-10-9-1	10-9-6-8-1

## 4.2.7 Model Training

The procedure followed and the computing resources used to train each ML model is as described in section 3.2.8, and hence will not be elaborated further.

## 4.2.8 Model Testing

The performance of the developed ML models (RR, SVR, and ANN) on the test dataset of the TF Condenser (see table 4.1) and TF evaporator (see table 4.2) is compared by simultaneously examining their individual verification plots and corresponding performance metrics 3.2.7. It must be noted that unless specified, each performance metric pertains to the test dataset concerned with either HX. For a comparison of heat load predictions, the reader is directed to tables 4.5 and 4.6 and figs. 4.9 and 4.10 respectively.

Inspecting the results for the heat load predictions reveals the ANN outperforming the other ML models considered. As seen in table 3.5, the prediction accuracy of the baseline RR model is poor. While the baseline SVR yields satisfactory heat load predictions, it imposes a massive time penalty. A similar trend is observed in the case of single-phase HX predictions too. ANN estimates provide the much needed compromise between efficient mapping and quick compute time. The ANN predictions result in consistently high values of  $\beta_{20}$ , in spite of requiring only a fraction of the training time needed by the SVR. Attention must be paid to the high values of MAPE owing to each ML model's inability to deliver equally satisfactory performance over the entire design space. Similar to results from section 3.2.10

ANNs suffer from high prediction variance for two-phase HX predictions as well.

Table 4.5: TF Condenser Baseline ML Models Comparison

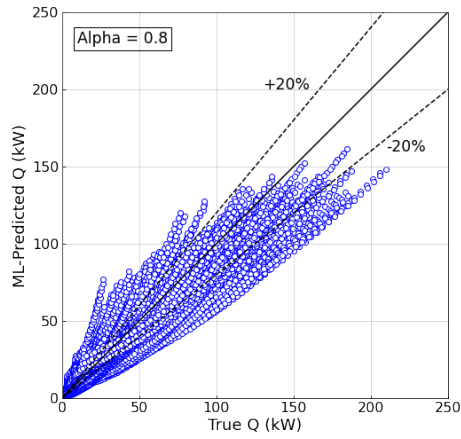
Heat Load Prediction			
Metric	RR	SVR	ANN
RMAE [%]	22.1	3.1	2.7
MAPE [%]	336.1	29.3	56.15
$\sigma_{error}$ [W]	18.6	16.2	104.4
$\beta_5$ [%]	12	82.7	85.3
$\beta_{20}$ [%]	50.2	99.7.4	99.9
Training Time [s]	4.5	53571	1812
Prediction Time [s]	0.005	152	1.6

Table 4.6: TF Evaporator Baseline ML Models Comparison

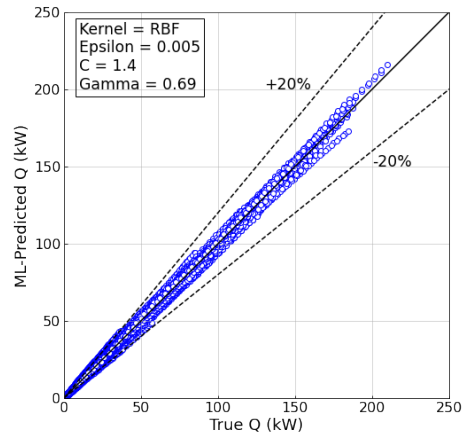
Heat Load Prediction			
Metric	RR	SVR	ANN
RMAE [%]	33.4	7.8	6.9
MAPE [%]	335.1	159.8	67.4
$\sigma_{error}$ [W]	19.1	23	80.7
$\beta_5$ [%]	14.5	47.8	51.4
$\beta_{20}$ [%]	30.78	92.4	94.4
Training Time [s]	2.08	65898	946.2
Prediction Time [s]	0.003	174	0.4

Similarly, relevant results in relation to  $\Delta P$  predictions are presented in tables 4.7 and 4.8 and figs 4.11 and 4.12 respectively. In conformance with earlier trends, the ANN fares significantly better than other competing models for the condenser and evaporator cases. A comparison of the predictions across both HXs indicates that the ML models; SVR and ANN in particular, yield relatively better predictions for condenser  $\Delta P$  as opposed to corresponding estimates of evaporator  $\Delta P$ .

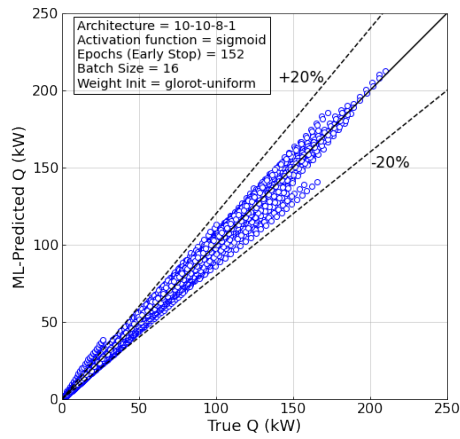
This degradation in prediction performance for the evaporator  $\Delta P$  could be attributed to the existence of a class imbalance pertinent to the following features: Tubes/Bank, Tubes/Bank/Circuit and Tube Banks. Better resampling procedures



(a) Ridge Regression



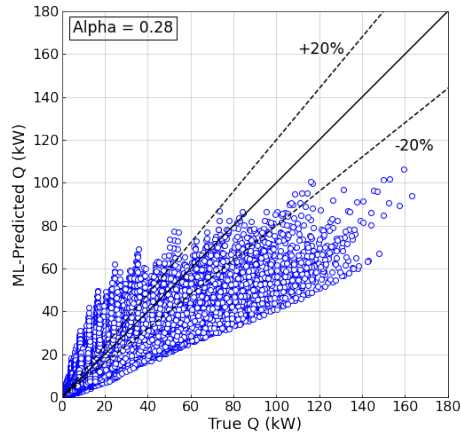
(b) Support Vector Regression



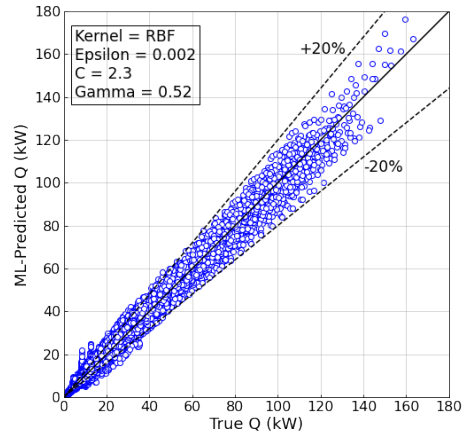
(c) Artificial Neural Network

Figure 4.9: TF Condenser Heat Load Prediction Verification Plots

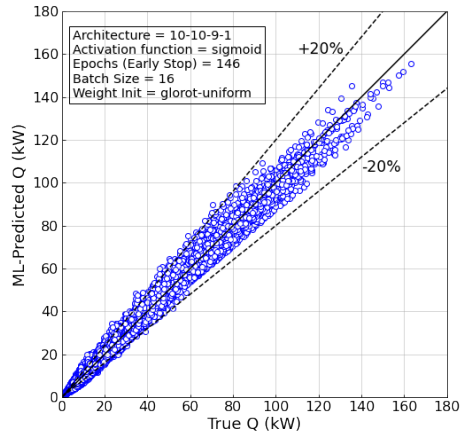
to either over-sample sparse classes or under-sample abundant classes [151] could be adopted, ultimately leading to improved ML model predictions.



(a) Ridge Regression



(b) Support Vector Regression



(c) Artificial Neural Network

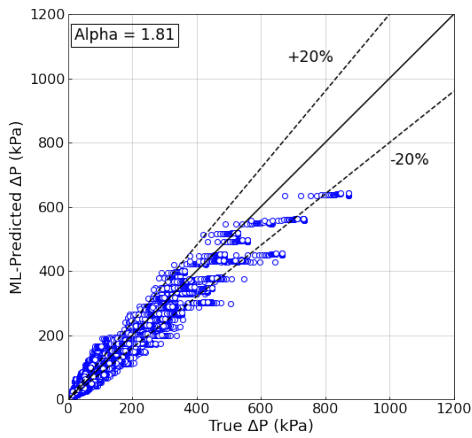
Figure 4.10: TF Evaporator Heat Load Prediction Verification Plots

Table 4.7: TF Condenser Baseline ML Models Comparison

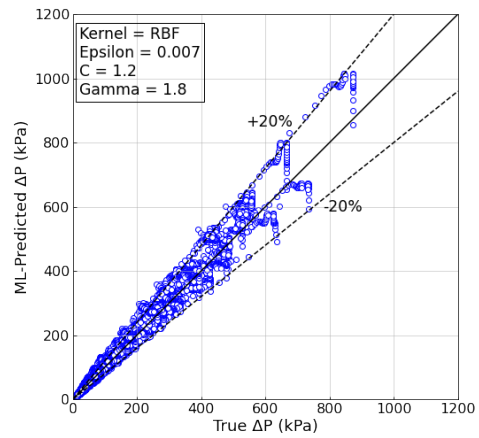
Pressure Drop Prediction			
Metric	RR	SVR	ANN
RMAE [%]	19.9	6.4	4.5
MAPE [%]	187.8	58.9	119.4
$\sigma_{error}$ [Pa]	47.6	154.6	87.7
$\beta_5$ [%]	14.5	51.6	67.6
$\beta_{20}$ [%]	55.51	96.6	98.9
Training Time [s]	2.9	68087	6163
Prediction Time [s]	0.007	513	1.5

Table 4.8: TF Evaporator Baseline ML Models Comparison

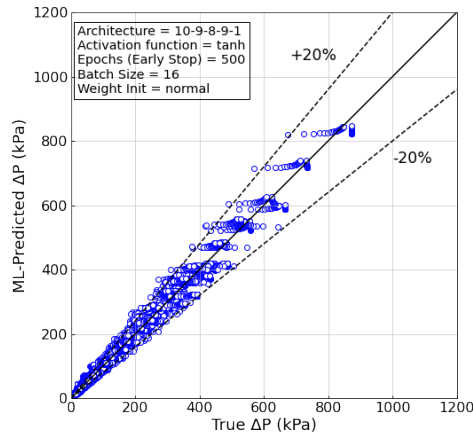
Pressure Drop Prediction			
Metric	RR	SVR	ANN
RMAE [%]	44	11	8.03
MAPE [%]	980.6	284	124.2
$\sigma_{error}$ [Pa]	475	726	784
$\beta_5$ [%]	15.3	38.1	49.1
$\beta_{20}$ [%]	34.9	83.1	91.4
Training Time [s]	1.6	29630	2564
Prediction Time [s]	0.004	137	1.5



(a) Ridge Regression

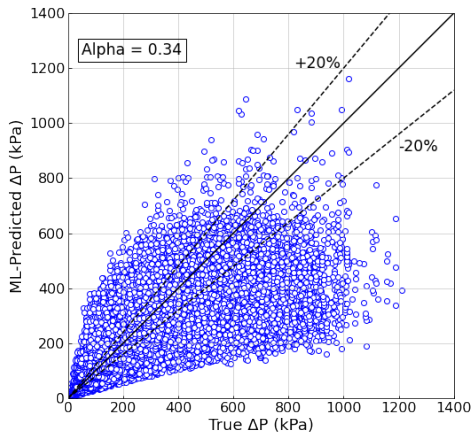


(b) Support Vector Regression

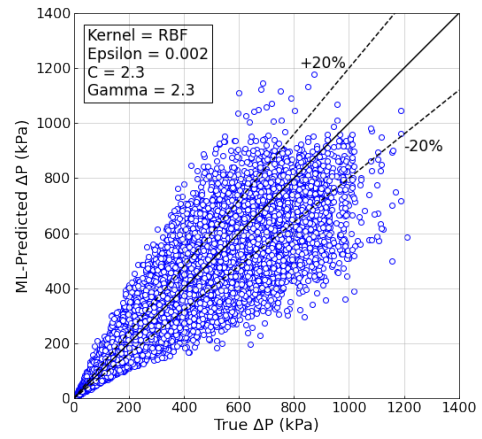


(c) Artificial Neural Network

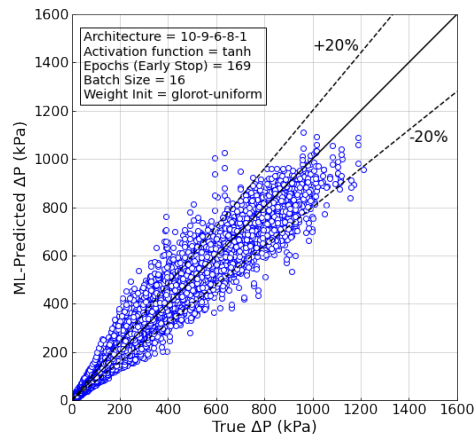
Figure 4.11: TF Condenser Pressure Drop Prediction Verification Plots



(a) Ridge Regression



(b) Support Vector Regression



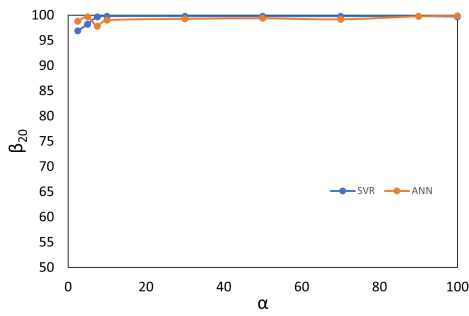
(c) Artificial Neural Network

Figure 4.12: TF Evaporator Pressure Drop Prediction Verification Plots

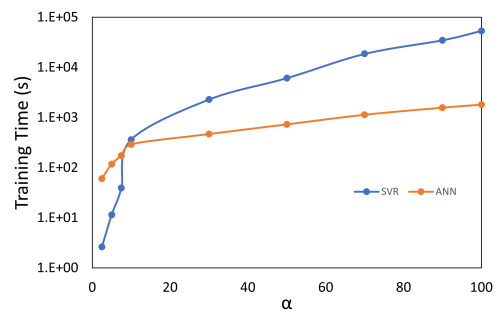
### 4.3 Training Dataset Size Impact

Similar to section 3.3, the impact of training the ML models over different dataset sizes is explored for the cases of the condenser and the evaporator that were investigated previously in sections 4.2 - 4.2.8. The results of this exercise are exhibited in figs 4.13 and 4.14. Considering the case of the condenser heat load, results similar to the baseline are observed in that the SVR and ANN models are able to achieve high prediction accuracies. For the refrigerant  $\Delta P$  however, an interesting occurrence takes place. The SVR predictions seem to be degrading as the dataset size increases. This phenomenon may be attributed to the onset of overfitting as the dataset size increases, indicating that the hyperparameter tuning conducted proved to be unsatisfactory. In terms of training times; trends similar to the radiator dataset size impact is observed.

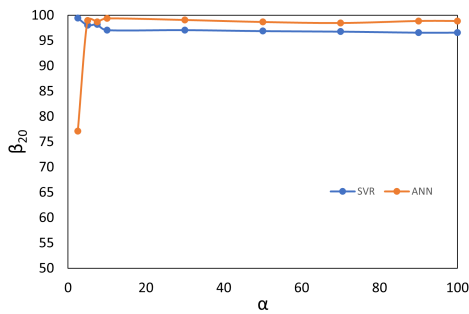
An observation of fig. 4.14 offers the following insight. Barring estimates of refrigerant  $\Delta P$  at  $\alpha \leq 5$ , the ANN predictions of heat load and refrigerant  $\Delta P$  are consistently superior to that delivered by the SVR. This is also exhibited in the baseline model performances, where the ANN fares better. A slight anomaly is observed in the training time comparison for heat load. Unlike previous cases, the SVR training time is always greater than the corresponding ANN training time in this particular instance, indicating the inappropriateness of the SVR model for this application.



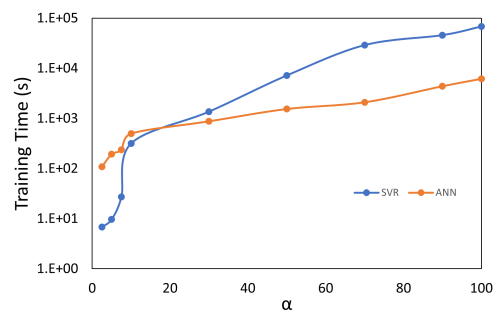
(a) Heat Load



(b) Heat Load

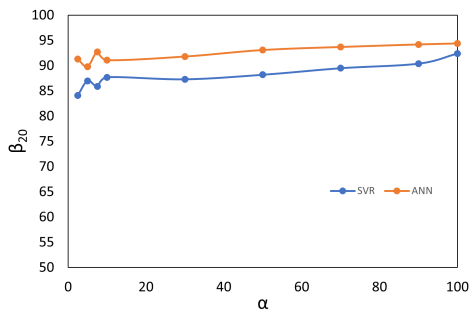


(c) Refrigerant  $\Delta P$

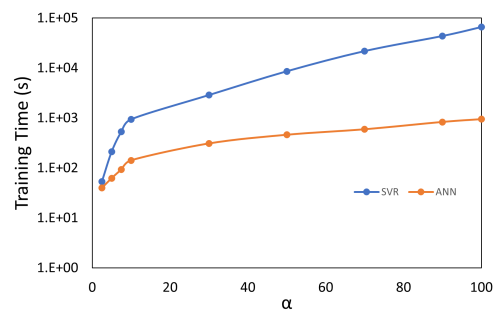


(d) Refrigerant  $\Delta P$

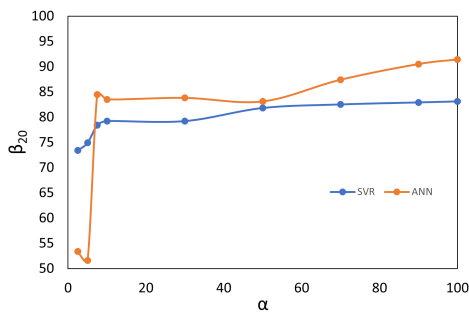
Figure 4.13: Condenser Training Dataset Size Impact



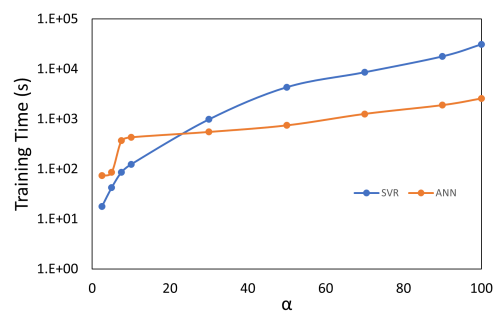
(a) Heat Load



(b) Heat Load



(c) Refrigerant  $\Delta P$



(d) Refrigerant  $\Delta P$

Figure 4.14: Evaporator Training Dataset Size Impact

## 4.4 Outcome-based Comparison

As the framework was explained in section 3.4, only results pertaining to the two-phase HXs are shown here in fig 4.15

Application	Preferred model (Conventional Comparison)	Preferred model (Outcome-based Comparison)
Condenser Heat load	Baseline ANN	Reduced domain SVR
Condenser Pressure Drop	Baseline ANN	Reduced domain SVR
Evaporator Heat load	Baseline ANN	Baseline ANN
Evaporator Pressure Drop	Baseline ANN	Baseline ANN

Figure 4.15: ML Model Appropriateness

## Chapter 5: Conclusion

### 5.1 Summary

This section comprises a brief summary of each research objective pertaining to this thesis

- (i) Performance prediction of single and two-phase Heat exchangers with a high degree of accuracy: Chapters 3 and 4 consist of the methodologies adopted to develop Machine Learning (ML) based tube-fin heat exchanger (TFHX) models. Three ML techniques namely, Ridge Regression (RR), Support Vector Regression (SVR) and Artificial Neural Networks (ANN) are implemented with the aim of predicting the heat transfer capacity ( $Q$ ) and refrigerant pressure drop ( $\Delta P$ ) associated with a given HX. Each model is subsequently verified by a distinct dataset previously unseen by during the model training phase. Performance metrics are used to determine their capabilities and comparisons are finally made.
- (ii) Determine the cost-accuracy appropriateness of an ML model applied to a particular problem: Chapters 3 and 4 examine the potential of SVR and ANN models to deliver previously exhibited levels of prediction accuracy when

trained on datasets consisting of fewer samples and design variables. Comparisons are first made between the reduced-domain models and their corresponding baseline models with the intent of checking for performance degradation. This is followed by a comparison of the reduced-domain SVR and ANN models. Finally through the aid of an outcome-based comparison framework, the most suitable ML technique for a given problem is identified.

Please note that RR models are not included in the reduced domain comparisons as their baseline performance was poor.

## 5.2 Conclusions

Concluding remarks associated with each objective is presented in this section.

### HX Performance Prediction

Some of the common trends observed across each of the three HXs considered are as follows:

- (i) Linear models namely RR yields unsatisfactory predictions for both heat load and refrigerant pressure drop.
- (ii) Each of the ML models suffer from relatively high maximum absolute performance error.
- (iii) The training time required by the SVR model is significantly higher than the other two models for both heat load and refrigerant pressure drop.

Observations specific to each HX is enumerated below:

(i) TF Radiator

- SVR and ANN models predict  $> 99\%$  of Radiator performance within  $\pm 20\%$  for both heat load and refrigerant pressure drop.
- For predictions of heat load, the ANN exhibits comparatively low robustness.
- Similar prediction trends of heat transfer and refrigerant pressure drop phenomena across physics-based and ML models are exhibited.

(ii) TF Condenser

- Across both heat load and refrigerant pressure drop, ANN models predict  $> 99\%$  of condenser performance within  $\pm 20\%$ , while SVR models predict no lesser than 96.6%.
- The ANN models for heat load and refrigerant pressure drop are found to have low prediction robustness.

(iii) TF Evaporator

- Evaporator refrigerant pressure drop predictions are poor across all ML models.
- For predictions of refrigerant pressure drop, satisfactory performance is achieved only by the ANN with  $\beta_{20}$  equalling 91.4%. The SVR model on the other hands is able to achieve a  $\beta_{20}$  value of 83.1% only.

- The robustness of each predictive model for refrigerant pressure drop is extremely poor. Additionally ANNs also exhibit low robustness while predicting heat load.

#### Cost-Accuracy Appropriateness of ML models

- Conventional comparison of baseline models indicates ANNs as the preferred choice for performance prediction.
- Reduced domain models are superior to baseline models in 4 out of 6 cases.
- Outcome-based comparison shows SVR can outperform ANN in certain cases.

### 5.3 Contributions

The main contributions of this thesis are

- (i) A detailed literature survey of investigations pertaining to ML techniques applied to heat transfer.
- (ii) ML based TFHX models capable of quickly predicting performance with a high degree of accuracy.
- (iii) An outcome-based comparison framework for ML models - This serves as a guide to determine the ML model to adopt while estimating HX performance.

## 5.4 Future Work

While this thesis addresses a couple of gaps present in the literature, it also opens up avenues for further research and development:

- Improve prediction capabilities: especially refrigerant pressure drop of a TF evaporator by integrating first principles of heat transfer.
- Generalize investigations conducted: an emphasis must be placed to include a larger family of refrigerants, with a focus on those that possess low Ozone Depletion and Global Warming Potential.
- Extend the capabilities of this investigation to other classes of HXs. Compact HXs are receiving greater attention while Shell-and-Tube HXs and Plate HXs find greater prominence in the process industry. Thus it would be beneficial to possess a tool suitable to these classes of heat transfer equipment.

## Bibliography

- [1] USA EIA. U.S. Energy Information Administration, “Annual Energy Outlook 2020”, U.S. Department of Energy, Washington DC, 2020. Technical report, 2020.
- [2] Detlef Westphalen and James Brodrick. Heat Transfer Enhancement. *ASHRAE Journal*, page 3, 2006.
- [3] John Judge and Reinhard Radermacher. A heat exchanger model for mixtures and pure refrigerant cycle simulations. *International Journal of Refrigeration*, 20(4):244–255, June 1997.
- [4] Haobo Jiang, Vikrant Aute, and Reinhard Radermacher. CoilDesigner: a general-purpose simulation and design tool for air-to-refrigerant heat exchangers. *International Journal of Refrigeration*, 29(4):601–610, June 2006.
- [5] Varun Singh, Vikrant Aute, and Reinhard Radermacher. A heat exchanger model for air-to-refrigerant fin-and-tube heat exchanger with arbitrary fin sheet. *International Journal of Refrigeration*, 32(7):1724–1735, November 2009.
- [6] M. Mohanraj, S. Jayaraj, and C. Muraleedharan. Applications of artificial neural networks for thermal analysis of heat exchangers – A review. *International Journal of Thermal Sciences*, 90:150–172, April 2015.
- [7] M. I. Jordan and T. M. Mitchell. Machine learning: Trends, perspectives, and prospects. *Science*, 349(6245):255–260, July 2015.
- [8] Z.G. Wu, J.Z. Zhang, Y.B. Tao, Y.L. He, and W.Q. Tao. Application of artificial neural network method for performance prediction of a gas cooler in a CO<sub>2</sub> heat pump. *International Journal of Heat and Mass Transfer*, 51(21-22):5459–5464, October 2008.
- [9] Hao Peng and Xiang Ling. Predicting thermal–hydraulic performances in compact heat exchangers by support vector regression. *International Journal of Heat and Mass Transfer*, 84:203–213, May 2015.

- [10] A. Khosravi, J.J.G. Pabon, R.N.N. Koury, and L. Machado. Using machine learning algorithms to predict the pressure drop during evaporation of R407C. *Applied Thermal Engineering*, 133:361–370, March 2018.
- [11] Kwang-Tzu Yang. Artificial Neural Networks (ANNs): A New Paradigm for Thermal Science and Engineering. *Journal of Heat Transfer*, 130(9), July 2008.
- [12] Mihir Sen and K T Yang. Applications of Artificial Neural Networks and Genetic Algorithms in Thermal Engineering. In *CRC Handbook of Thermal Engineering*, F. Kreith, ed, pages 4–620 – 4–661. CRC, Boca Raton, FL, 2000.
- [13] Chungen Yin, Lasse Rosendahl, and Zhongyang Luo. Methods to improve prediction performance of ANN models. *Simulation Modelling Practice and Theory*, 11(3-4):211–222, July 2003.
- [14] Vikrant C Aute. A Review of State of the Art in Modeling of Air-to-Refrigerant Heat Exchangers for HVAC&R Applications. page 11, 2016.
- [15] Omer Sarfraz, Christian K Bach, and Craig Bradshaw. A Literature Review of Numerical Modeling Techniques for Vapor Compression Systems with Focus on Heat Exchanger Modeling. page 11, 2018.
- [16] José A. R. Parise. Simulation of vapour-compression heat pumps. *SIMULATION*, 46(2):71–76, February 1986. Publisher: SAGE Publications Ltd STM.
- [17] James Edward Braun. Methodologies for the Design and Control of Central Cooling Plants. page 434, 1988.
- [18] Chwalowski et al. Verification of evaporator computer models and analysis of performance of an evaporator coil, 1989.
- [19] Hui Jin and Jeffrey D Spitler. A Parameter Estimation Based Model of Water-to-Water Heat Pumps for Use in Energy Calculation Programs. *ASHRAE Transactions*, page 16, 2002.
- [20] G. Zhou, Y. Ye, J. Wang, W. Zuo, Y. Fu, and X. Zhou. Modeling air-to-air plate-fin heat exchanger without dehumidification. *Applied Thermal Engineering*, 143:137–148, October 2018.
- [21] J E Braun, S A Klein, and J W Mitchell. Effectiveness Models for Cooling Towers and Cooling Coils. *ASHRAE Transactions*, 95:11, 1989.
- [22] N B NL Stefanuk, J D Apevich, and M Renkszbuut. Modeling and simulation of a superheat-controlled water-to-water heat pump. page 13, 1992.
- [23] Shenglan Xuan, Vikrant Aute, and Reinhard Radermacher. Generic Dynamic Model for Heat Exchangers. page 8, 2006.

- [24] Omar AbdelAziz, Vikrant Aute, and Reinhard Radermacher. Effect of Void Fraction Model on the Dynamic Performance of Moving Boundary Heat Exchanger. page 8, 2008.
- [25] Ian Bell. ACHP Documentation. page 122, 2012.
- [26] Hongtao Qiao, Christopher R. Laughman, Vikrant Aute, and Reinhard Radermacher. An advanced switching moving boundary heat exchanger model with pressure drop. *International Journal of Refrigeration*, 65:154–171, May 2016.
- [27] Piotr A Domanski. EVSIM- an evaporator simulation model accounting for refrigerant and one dimensional air distribution. Technical Report NIST IR 89-4133, National Institute of Standards and Technology, Gaithersburg, MD, 1989.
- [28] Piotr Domanski. Simulation of an Evaporator with Nonuniform One-Dimensional Air Distribution. 1991. Publisher: ASHRAE Transactions.
- [29] Jangho Lee and P.A. Domanski. IMPACT OF AIR AND REFRIGERANT MALDISTRIBUTIONS ON THE PERFORMANCE OF FINNED-TUBE EVAPORATORS WITH R-22 AND R-407C, 1997.
- [30] Jian Liu, WenJian Wei, GouLiang Ding, Chunlu Zhang, Masaharu Fukaya, Kaijian Wang, and Takefumi Inagaki. A general steady state mathematical model for fin-and-tube heat exchanger based on graph theory. *International Journal of Refrigeration*, 27(8):965–973, December 2004.
- [31] David Richardson. AN OBJECT ORIENTED SIMULATION FRAMEWORK FOR STEADY-STATE ANALYSIS OF VAPOR COMPRESSION REFRIGERATION SYSTEMS AND COMPONENTS. page 184, 2006.
- [32] D.A. Yashar, S. Lee, and P.A. Domanski. Rooftop air-conditioning unit performance improvement using refrigerant circuitry optimization. *Applied Thermal Engineering*, 83:81–87, May 2015.
- [33] Ammar M. Bahman and Eckhard A. Groll. Application of interleaved circuitry to improve evaporator effectiveness and COP of a packaged AC system. *International Journal of Refrigeration*, 79:114–129, July 2017.
- [34] Todd Rossi. Detection, Diagnosis and Evaluation of Faults in Vapor Compression Cycle Equipment, 1995.
- [35] S.Y. Liang, T.N. Wong, and G.K. Nathan. Numerical and experimental studies of refrigerant circuitry of evaporator coils. *International Journal of Refrigeration*, 24(8):823–833, December 2001.

- [36] C Oliet, C D Perez-Segarra, S Danov, and A Oliva. Numerical Simulation Of Dehumidifying Fin-And-Tube Heat Exchangers. Model Strategies And Experimental Comparisons. page 9, 2002.
- [37] Haobo Jiang, Vikrant Aute, and Reinhard Radermacher. R5-1 A USER-FRIENDLY SIMULATION AND OPTIMIZATION TOOL FOR. page 8, 2002.
- [38] Ip Seng Iu. DEVELOPMENT OF AIR-TO-AIR HEAT PUMP SIMULATION PROGRAM WITH ADVANCED HEAT EXCHANGER CIRCUITRY ALGORITHM, 2007.
- [39] Varun Singh, Vikrant Aute, and Reinhard Radermacher. Numerical approach for modeling air-to-refrigerant fin-and-tube heat exchanger with tube-to-tube heat transfer. *International Journal of Refrigeration*, 31(8):1414–1425, December 2008.
- [40] Omer Sarfraz, Christian K. Bach, and Craig R. Bradshaw. A novel technique for computationally efficient consideration of cross-fin conduction in fin-and-tube heat exchanger models. *International Journal of Refrigeration*, 107:73–83, November 2019.
- [41] T W Simpson, J D Peplinski, P N Koch, and J K Allen. Metamodels for Computer-based Engineering Design: Survey and recommendations. page 22, 2001.
- [42] G. Gary Wang and S. Shan. Review of Metamodeling Techniques in Support of Engineering Design Optimization. *Journal of Mechanical Design*, 129(4):370–380, May 2006.
- [43] T. Hastie, R. Tibshirani, and J.H. Friedman. *The Elements of Statistical Learning: Data Mining, Inference, and Prediction*. Springer series in statistics. Springer, 2009.
- [44] Fabian Pedregosa, Gaël Varoquaux, Alexandre Gramfort, Vincent Michel, Bertrand Thirion, Olivier Grisel, Mathieu Blondel, Peter Prettenhofer, Ron Weiss, Vincent Dubourg, Jake Vanderplas, Alexandre Passos, David Cournapeau, Matthieu Brucher, Matthieu Perrot, and Édouard Duchesnay. Scikit-learn: Machine Learning in Python. *Journal of Machine Learning Research*, 12(85):2825–2830, 2011.
- [45] François Chollet and others. Keras, 2015.
- [46] Corinna Cortes and Vladimir Vapnik. Support-vector networks. *Machine Learning*, 20(3):273–297, September 1995.
- [47] Alex J. Smola and Bernhard Schölkopf. A tutorial on support vector regression. *Statistics and Computing*, 14(3):199–222, August 2004.

- [48] Soteris A Kalogirou. Applications of artificial neural-networks for energy systems. *Applied Energy*, page 19, 2000.
- [49] Mohammad Ghalandari, Misagh Irandoost Shahrestani, Akbar Maleki, Mostafa Safdari Shadloo, and Mamdouh El Haj Assad. Applications of intelligent methods in various types of heat exchangers: a review. *Journal of Thermal Analysis and Calorimetry*, 145(4):1837–1848, August 2021.
- [50] Matthew T. Hughes, Girish Kini, and Srinivas Garimella. Status, Challenges, and Potential for Machine Learning in Understanding and Applying Heat Transfer Phenomena. *Journal of Heat Transfer*, 143(12):120802, December 2021.
- [51] Gerardo Diaz, Mihir Sen, K. T. Yang, and Rodney McClain. Simulation of Heat Exchanger Performance by Artificial Neural Networks. *HVAC&R Research*, 5(3):195–208, July 1999.
- [52] Arturo Pacheco-Vega, Mihir Sen, K T Yang, and Rodney L McClain. Neural network analysis of fin-tube refrigerating heat exchanger with limited experimental data. *Int. J. Heat Mass Transfer*, page 8, 2001.
- [53] Arturo Pacheco-Vega, Gerardo Di ´az, Mihir Sen, K. T. Yang, and Rodney L. McClain. Heat Rate Predictions in Humid Air-Water Heat Exchangers Using Correlations and Neural Networks. *Journal of Heat Transfer*, 123(2):348–354, April 2001.
- [54] Guo-Liang Ding, Chun-Lu Zhang, and Tao Zhan. An approximate integral model with an artificial neural network for heat exchangers. *Heat Transfer?Asian Research*, 33(3):153–160, May 2004.
- [55] C.K. Tan, J. Ward, S.J. Wilcox, and R. Payne. Artificial neural network modelling of the thermal performance of a compact heat exchanger. *Applied Thermal Engineering*, 29(17-18):3609–3617, December 2009.
- [56] Liang Yang, Ze-Yu Li, Liang-Liang Shao, and Chun-Lu Zhang. Model-based dimensionless neural networks for fin-and-tube condenser performance evaluation. *International Journal of Refrigeration*, 48:1–9, December 2014.
- [57] Z. Tian, B. Gu, L. Yang, and F. Liu. Performance prediction for a parallel flow condenser based on artificial neural network. *Applied Thermal Engineering*, 63(1):459–467, February 2014.
- [58] Santanu Prasad Datta, Prasanta Kumar Das, and Siddhartha Mukhopadhyay. An optimized ANN for the performance prediction of an automotive air conditioning system. *Science and Technology for the Built Environment*, 25(3):282–296, March 2019.

- [59] FAYE C McQUISTON. CORRELATION OF HEAT, MASS AND MOMENTUM TRANSPORT COEFFICIENTS FOR PLATE-FIN-TUBE HEAT TRANSFER SURFACES WITH STAGGERED TUBES. page 16.
- [60] D. L. Gray, Ralph L. Webb, and USA 1986 International Heat Transfer Conference 8 San Francisco, 17-22 August. HEAT TRANSFER AND FRICTION CORRELATIONS FOR PLATE FINNED-TUBE HEAT EXCHANGERS HAVING PLAIN FINS. In *International Heat Transfer Conference 8*, pages 2745–2750. Begell House Inc., 1986.
- [61] Anurag Kumra, Nikhil Rawal, and Pijush Samui. Prediction of Heat Transfer Rate of a Wire-on-Tube Type Heat Exchanger: An Artificial Intelligence Approach. *Procedia Engineering*, 64:74–83, 2013.
- [62] Wei Yan, Meijing Li, Xin Pan, Guorong Wu, and Liping Liu. Application of support vector regression cooperated with modified artificial fish swarm algorithm for wind tunnel performance prediction of automotive radiators. *Applied Thermal Engineering*, 164:114543, January 2020.
- [63] Ransisi Huang, Jiazhen Ling, and Vikrant Aute. Comparison of approximation-assisted heat exchanger models for steady-state simulation of vapor compression system. *Applied Thermal Engineering*, 166:114691, February 2020.
- [64] H.M. Ertunc and M. Hosoz. Artificial neural network analysis of a refrigeration system with an evaporative condenser. *Applied Thermal Engineering*, 26(5-6):627–635, April 2006.
- [65] H. Metin Ertunc and Murat Hosoz. Comparative analysis of an evaporative condenser using artificial neural network and adaptive neuro-fuzzy inference system. *International Journal of Refrigeration*, 31(8):1426–1436, December 2008.
- [66] Helena Haas Reichert, Rodrigo Ghiorzzi Donni, Paulo Smith Schneider, and Ivoni Carlos Acunha Junior. Data driven assessment of a small scale evaporative condenser based on a combined artificial neural network with design of experiment approach. *International Journal of Refrigeration*, 115:139–147, July 2020.
- [67] Pooria Behnam, Meysam Faegh, Mohammad Behshad Shafii, and Mehdi Khiadani. A comparative study of various machine learning methods for performance prediction of an evaporative condenser. *International Journal of Refrigeration*, 126:280–290, June 2021.
- [68] Asghar Alizadehdakhel, Masoud Rahimi, Jafar Sanjari, and Ammar Abdulaziz Alsairafi. CFD and artificial neural network modeling of two-phase flow pressure drop. *International Communications in Heat and Mass Transfer*, 36(8):850–856, October 2009.

- [69] Nirjhar Bar, Sudip Kumar Das, and Manindra Nath Biswas. Prediction of Frictional Pressure Drop Using Artificial Neural Network for Air-water Flow through U-bends. *Procedia Technology*, 10:813–821, 2013.
- [70] Alireza Zendejboudi and Xianting Li. A robust predictive technique for the pressure drop during condensation in inclined smooth tubes. *International Communications in Heat and Mass Transfer*, 86:166–173, August 2017.
- [71] Juan Jose Garcia, Franklin Garcia, José Bermúdez, and Luiz Machado. Prediction of pressure drop during evaporation of R407C in horizontal tubes using artificial neural networks. *International Journal of Refrigeration*, 85:292–302, January 2018.
- [72] J.M. Barroso-Maldonado, J.A. Montañez-Barrera, J.M. Belman-Flores, and S.M. Aceves. ANN-based correlation for frictional pressure drop of non-azeotropic mixtures during cryogenic forced boiling. *Applied Thermal Engineering*, 149:492–501, February 2019.
- [73] Yue Qiu, Deepak Garg, Sung-Min Kim, Issam Mudawar, and Chirag R. Kharrangate. Machine learning algorithms to predict flow boiling pressure drop in mini/micro-channels based on universal consolidated data. *International Journal of Heat and Mass Transfer*, 178:121607, October 2021.
- [74] Sung-Min Kim and Issam Mudawar. Universal approach to predicting two-phase frictional pressure drop for mini/micro-channel saturated flow boiling. *International Journal of Heat and Mass Transfer*, 58(1-2):718–734, March 2013.
- [75] Keivan Ardam, Behzad Najafi, Andrea Lucchini, Fabio Rinaldi, and Luigi Pietro Maria Colombo. Machine Learning based Pressure Drop Estimation of Evaporating R134a Flow in Micro-fin Tubes: Investigation of the Optimal Dimensionless Feature Set. *International Journal of Refrigeration*, page S0140700721003005, July 2021.
- [76] Benbella A. Shannak. Frictional pressure drop of gas liquid two-phase flow in pipes. *Nuclear Engineering and Design*, 238(12):3277–3284, December 2008.
- [77] Seok-Jin Oh, Kwan-Soo Lee, and Seung-Jae Moon. Optimal Design of a Parallel-Flow Heat Exchanger Using a Response Surface Methodology. *Numerical Heat Transfer, Part A: Applications*, 49(4):411–426, August 2006.
- [78] Lei Sun and Chun-Lu Zhang. Evaluation of elliptical finned-tube heat exchanger performance using CFD and response surface methodology. *International Journal of Thermal Sciences*, 75:45–53, January 2014.
- [79] Kurt Hornik, Maxwell Stinchcombe, and Halbert White. Multilayer feedforward networks are universal approximators. *Neural Networks*, 2(5):359–366, January 1989.

- [80] K. Jambunathan, S.L. Hartle, S. Ashforth-Frost, and V.N. Fontama. Evaluating convective heat transfer coefficients using neural networks. *International Journal of Heat and Mass Transfer*, 39(11):2329–2332, July 1996.
- [81] Afshin J. Ghajar, Lap Mou Tam, and Sik Chung Tam. Improved Heat Transfer Correlation in the Transition Region for a Circular Tube with Three Inlet Configurations Using Artificial Neural Networks. *Heat Transfer Engineering*, 25(2):30–40, March 2004.
- [82] Hakan Demir, Özden Ağra, and Ş. Özgür Atayılmaz. Generalized neural network model of alternative refrigerant (R600a) inside a smooth tube. *International Communications in Heat and Mass Transfer*, 36(7):744–749, August 2009.
- [83] M. Balcilar, A.S. Dalkilic, and S. Wongwises. Artificial neural network techniques for the determination of condensation heat transfer characteristics during downward annular flow of R134a inside a vertical smooth tube. *International Communications in Heat and Mass Transfer*, 38(1):75–84, January 2011.
- [84] M. Balcilar, K. Aroonrat, A.S. Dalkilic, and S. Wongwises. A numerical correlation development study for the determination of Nusselt numbers during boiling and condensation of R134a inside smooth and corrugated tubes. *International Communications in Heat and Mass Transfer*, 48:141–148, November 2013.
- [85] Sadra Azizi and Ebrahim Ahmadloo. Prediction of heat transfer coefficient during condensation of R134a in inclined tubes using artificial neural network. *Applied Thermal Engineering*, 106:203–210, August 2016.
- [86] Yue Qiu, Deepak Garg, Liwei Zhou, Chirag R. Kharangate, Sung-Min Kim, and Issam Mudawar. An artificial neural network model to predict mini/micro-channels saturated flow boiling heat transfer coefficient based on universal consolidated data. *International Journal of Heat and Mass Transfer*, 149:119211, March 2020.
- [87] Liwei Zhou, Deepak Garg, Yue Qiu, Sung-Min Kim, Issam Mudawar, and Chirag R. Kharangate. Machine learning algorithms to predict flow condensation heat transfer coefficient in mini/micro-channel utilizing universal data. *International Journal of Heat and Mass Transfer*, 162:120351, December 2020.
- [88] D. R. E. Ewim, A. O. Adelaja, E. J. Onyiriuka, J. P. Meyer, and Z. Huan. Modelling of heat transfer coefficients during condensation inside an enhanced inclined tube. *Journal of Thermal Analysis and Calorimetry*, 146(1):103–115, October 2021.

- [89] M.M. Shah. A general correlation for heat transfer during film condensation inside pipes. *International Journal of Heat and Mass Transfer*, 22(4):547–556, April 1979.
- [90] Donald P Traviss, Anton B Baron, and Warren M Rohsenow. FORCED-CONVECTION CONDENSATION INSIDE TUBES. page 107.
- [91] Sung-Min Kim and Issam Mudawar. Universal approach to predicting saturated flow boiling heat transfer in mini/micro-channels – Part II. Two-phase heat transfer coefficient. *International Journal of Heat and Mass Transfer*, 64:1239–1256, September 2013.
- [92] Sung-Min Kim and Issam Mudawar. Universal approach to predicting heat transfer coefficient for condensing mini/micro-channel flow. *International Journal of Heat and Mass Transfer*, 56(1-2):238–250, January 2013.
- [93] L. M. Tam, A. J. Ghajar, H. K. Tam, and S. C. Tam. Development of a Heat Transfer Correlation for the Transitional Flow in a Horizontal Tube Using Support Vector Machines. In *Heat Transfer: Volume 1*, pages 527–536, Jacksonville, Florida, USA, January 2008. ASMEDC.
- [94] Hou Kuan Tam, Lap Mou Tam, and Afshin J. Ghajar. Heat Transfer Correlation for Two-Phase Flow in Vertical Pipes Using Support Vector Machines. *Heat Transfer Engineering*, 32(11-12):1047–1052, October 2011.
- [95] Mohammad Reza Jafari Nasr and Ali Habibi Khalaj. Heat Transfer Coefficient and Friction Factor Prediction of Corrugated Tubes Combined With Twisted Tape Inserts Using Artificial Neural Network. *Heat Transfer Engineering*, 31(1):59–69, January 2010.
- [96] Saeb M. Besarati, Philip D. Myers, David C. Covey, and Ali Jamali. Modeling friction factor in pipeline flow using a GMDH-type neural network. *Cogent Engineering*, 2(1):1056929, December 2015.
- [97] A. Çebi, E. Akdoğan, A. Celen, and A. S. Dalkilic. Prediction of friction factor of pure water flowing inside vertical smooth and microfin tubes by using artificial neural networks. *Heat and Mass Transfer*, 53(2):673–685, February 2017.
- [98] Basma Souayah, Suvanjan Bhattacharyya, Najib Hdhiri, and Mir Waqas Alam. Heat and Fluid Flow Analysis and ANN-Based Prediction of A Novel Spring Corrugated Tape. *Sustainability*, 13(6):3023, March 2021.
- [99] W. Zhang, T. Hibiki, and K. Mishima. Correlations of two-phase frictional pressure drop and void fraction in mini-channel. *International Journal of Heat and Mass Transfer*, 53(1-3):453–465, January 2010.

- [100] Behzad Najafi, Keivan Ardam, Andrej Hanušovský, Fabio Rinaldi, and Luigi Pietro Maria Colombo. Machine learning based models for pressure drop estimation of two-phase adiabatic air-water flow in micro-finned tubes: Determination of the most promising dimensionless feature set. *Chemical Engineering Research and Design*, 167:252–267, March 2021.
- [101] Gregory J. Zdaniuk, Louay M. Chamra, and D. Keith Walters. Correlating heat transfer and friction in helically-finned tubes using artificial neural networks. *International Journal of Heat and Mass Transfer*, 50(23-24):4713–4723, November 2007.
- [102] Gongnan Xie, Bengt Sunden, Qiuwang Wang, and Linghong Tang. Performance predictions of laminar and turbulent heat transfer and fluid flow of heat exchangers having large tube-diameter and large tube-row by artificial neural networks. *International Journal of Heat and Mass Transfer*, 52(11-12):2484–2497, May 2009.
- [103] Saeel S. Pai, Dhvaneel Visaria, and Justin A. Weibel. A Machine-Learning-Based Surrogate Model for Internal Flow Nusselt Number and Friction Factor in Various Channel Cross Sections. In *2021 20th IEEE Intersociety Conference on Thermal and Thermomechanical Phenomena in Electronic Systems (iTherm)*, pages 1024–1029, San Diego, CA, USA, June 2021. IEEE.
- [104] Alejandro López-Belchí, Fernando Illán-Gómez, José Manuel Cano-Izquierdo, and José Ramón García-Cascales. GMDH ANN to optimise model development: Prediction of the pressure drop and the heat transfer coefficient during condensation within mini-channels. *Applied Thermal Engineering*, 144:321–330, November 2018.
- [105] Matthew T. Hughes, Brian M. Fronk, and Srinivas Garimella. Universal condensation heat transfer and pressure drop model and the role of machine learning techniques to improve predictive capabilities. *International Journal of Heat and Mass Transfer*, 179:121712, November 2021.
- [106] M Malayeri, H Mullersteinhagen, and J Smith. Neural network analysis of void fraction in air/water two-phase flows at elevated temperatures. *Chemical Engineering and Processing*, 42(8-9):587–597, August 2003.
- [107] Sadra Azizi, Ebrahim Ahmadloo, and Mohamed M. Awad. Prediction of void fraction for gas-liquid flow in horizontal, upward and downward inclined pipes using artificial neural network. *International Journal of Multiphase Flow*, 87:35–44, December 2016.
- [108] Huajun Li, Haifeng Ji, Zhiyao Huang, Baoliang Wang, Haiqing Li, and Guohua Wu. A New Void Fraction Measurement Method for Gas-Liquid Two-Phase Flow in Small Channels. *Sensors*, 16(2):159, January 2016.

- [109] C. Riverol and V. Napolitano. ESTIMATION OF THE OVERALL HEAT TRANSFER COEFFICIENT IN A TUBULAR HEAT EXCHANGER UNDER FOULING USING NEURAL NETWORKS. APPLICATION IN A FLASH PASTEURIZER. *International Communications in Heat and Mass Transfer*, 29(4):453–457, May 2002.
- [110] Lingfang Sun, Yingying Zhang, Xinpeng Zheng, Shanrang Yang, and Yukun Qin. Research on the Fouling Prediction of Heat Exchanger Based on Support Vector Machine. In *2008 International Conference on Intelligent Computation Technology and Automation (ICICTA)*, pages 240–244, changsha, Hunan, October 2008. IEEE.
- [111] Lingfang Sun, Yingying Zhang, and Rina Saqi. Research on the fouling prediction of heat exchanger based on Support Vector Machine optimized by Particle Swarm Optimization algorithm. In *2009 International Conference on Mechatronics and Automation*, pages 2002–2007, Changchun, August 2009. IEEE.
- [112] Ehsan Davoudi and Behzad Vaferi. Applying artificial neural networks for systematic estimation of degree of fouling in heat exchangers. *Chemical Engineering Research and Design*, 130:138–153, February 2018.
- [113] Sreenath Sundar, Manjunath C. Rajagopal, Hanyang Zhao, Gowtham Kuntumalla, Yuquan Meng, Ho Chan Chang, Chenhui Shao, Placid Ferreira, Nenad Miljkovic, Sanjiv Sinha, and Srinivasa Salapaka. Fouling modeling and prediction approach for heat exchangers using deep learning. *International Journal of Heat and Mass Transfer*, 159:120112, October 2020.
- [114] Hüseyin Kurt and Muhammet Kayfeci. Prediction of thermal conductivity of ethylene glycol–water solutions by using artificial neural networks. *Applied Energy*, 86(10):2244–2248, October 2009.
- [115] Shuai Deng, Wen Su, and Li Zhao. A neural network for predicting normal boiling point of pure refrigerants using molecular groups and a topological index. *International Journal of Refrigeration*, 63:63–71, March 2016.
- [116] Alireza Baghban, Mohammad Bahadori, Jake Rozyn, Moonyong Lee, Ali Abbas, Alireza Bahadori, and Arash Rahimali. Estimation of air dew point temperature using computational intelligence schemes. *Applied Thermal Engineering*, 93:1043–1052, January 2016.
- [117] Gaurav Krishnayatra, Sulekh Tokas, and Rajesh Kumar. Numerical heat transfer analysis & predicting thermal performance of fins for a novel heat exchanger using machine learning. *Case Studies in Thermal Engineering*, 21:100706, October 2020.
- [118] Niccolo Giannetti, Mark Anthony Redo, Sholahudin, Jongsoo Jeong, Seiichi Yamaguchi, Kiyoshi Saito, and Hyunyoung Kim. Prediction of two-phase flow

- distribution in microchannel heat exchangers using artificial neural network. *International Journal of Refrigeration*, 111:53–62, March 2020.
- [119] Y. Mi, M. Ishii, and L.H. Tsoukalas. Vertical two-phase flow identification using advanced instrumentation and neural networks. *Nuclear Engineering and Design*, 184(2-3):409–420, August 1998.
- [120] Y. Mi, M. Ishii, and L.H. Tsoukalas. Flow regime identification methodology with neural networks and two-phase flow models. *Nuclear Engineering and Design*, 204(1-3):87–100, February 2001.
- [121] T. Tambouratzis and I. Pázsit. Non-invasive on-line two-phase flow regime identification employing artificial neural networks. *Annals of Nuclear Energy*, 36(4):464–469, May 2009.
- [122] Tatiana Tambouratzis and Imre Pázsit. A general regression artificial neural network for two-phase flow regime identification. *Annals of Nuclear Energy*, 37(5):672–680, May 2010.
- [123] Paul J. Kreitzer, Michael Hanchak, and Larry Byrd. Flow Regime Identification of Horizontal Two Phase Refrigerant R-134a Flow Using Neural Networks. In *Volume 7B: Fluids Engineering Systems and Technologies*, page V07BT08A059, San Diego, California, USA, November 2013. American Society of Mechanical Engineers.
- [124] M.K. Seal, S.M.A. Noori Rahim Abadi, M. Mehrabi, and J.P. Meyer. Machine learning classification of in-tube condensation flow patterns using visualization. *International Journal of Multiphase Flow*, 143:103755, October 2021.
- [125] Yunlong Zhou, Fei Chen, and Bin Sun. Identification Method of Gas-Liquid Two-phase Flow Regime Based on Image Multi-feature Fusion and Support Vector Machine. *Chinese Journal of Chemical Engineering*, 16(6):832–840, December 2008.
- [126] Gustavo M. Hobold and Alexandre K. da Silva. Machine learning classification of boiling regimes with low speed, direct and indirect visualization. *International Journal of Heat and Mass Transfer*, 125:1296–1309, October 2018.
- [127] Dan Li, Xuefeng Yang, Shouren Wang, Derong Duan, Zhuang Wan, Guofeng Xia, and Wenbo Liu. Experimental research on vibration-enhanced heat transfer of fin-tube vehicle radiator. *Applied Thermal Engineering*, 180:115836, November 2020.
- [128] Yiwen Jian, Zishuai Yu, Zhaohui Liu, Yi Li, and Rui Li. Simulation Study of Impacts of Radiator Selection on Indoor Thermal Environment and Energy Consumption. *Procedia Engineering*, 146:466–472, 2016.

- [129] M. Embaye, R.K. AL-Dadah, and S. Mahmoud. Numerical evaluation of indoor thermal comfort and energy saving by operating the heating panel radiator at different flow strategies. *Energy and Buildings*, 121:298–308, June 2016.
- [130] Qinguo Zhang, Liangfei Xu, Jianqiu Li, and Minggao Ouyang. Performance prediction of plate-fin radiator for low temperature preheating system of proton exchange membrane fuel cells using CFD simulation. *International Journal of Hydrogen Energy*, 42(38):24504–24516, September 2017.
- [131] AHRI. AHRI\_standard\_410-2001\_with\_addenda\_1.2&3.pdf, June 2011.
- [132] Modine Manufacturing Company. Modine Commercial Fin Tube Radiation, February 2020.
- [133] M. D. McKay, R. J. Beckman, and W. J. Conover. A Comparison of Three Methods for Selecting Values of Input Variables in the Analysis of Output From a Computer Code. *Technometrics*, 42(1):55–61, February 2000.
- [134] Edward R. Mansfield and Billy P. Helms. Detecting Multicollinearity. *The American Statistician*, 36(3a):158–160, August 1982. Publisher: Taylor & Francis.
- [135] Larry L. Havlicek and Nancy L. Peterson. Robustness of the Pearson Correlation against Violations of Assumptions. *Perceptual and Motor Skills*, 43(3-suppl):1319–1334, December 1976. Publisher: SAGE Publications Inc.
- [136] S B Kotsiantis, D Kanellopoulos, and P E Pintelas. Data Preprocessing for Supervised Learning. 1(1):7, 2006.
- [137] T. Jayalakshmi and A. Santhakumaran. Statistical Normalization and Back Propagation for Classification. *International Journal of Computer Theory and Engineering*, pages 89–93, 2011.
- [138] Dalwinder Singh and Birmohan Singh. Investigating the impact of data normalization on classification performance. *Applied Soft Computing*, 97:105524, December 2020.
- [139] Sanford Weisberg. Yeo-Johnson Power Transformations. page 4, October 2001.
- [140] Li Yang and Abdallah Shami. On hyperparameter optimization of machine learning algorithms: Theory and practice. *Neurocomputing*, 415:295–316, November 2020.
- [141] James Bergstra and Yoshua Bengio. Random Search for Hyper-Parameter Optimization. page 25, February 2012.

- [142] M. Stone. Cross-Validatory Choice and Assessment of Statistical Predictions. *Journal of the Royal Statistical Society: Series B (Methodological)*, 36(2):111–133, January 1974.
- [143] Frank J Massey. The Kolmogorov-Smirnov Test for Goodness of Fit. 46(253):12, March 1951.
- [144] Kaichao You, Mingsheng Long, Jianmin Wang, and Michael I. Jordan. How Does Learning Rate Decay Help Modern Neural Networks? *arXiv:1908.01878 [cs, stat]*, September 2019. arXiv: 1908.01878.
- [145] Eduardo Sontag and H Sussman. Backpropagation Can Give Rise to Spurious Local Minima Even for Networks without Hidden Layers, 1989.
- [146] M. Gori and A. Tesi. On the problem of local minima in backpropagation. *IEEE Transactions on Pattern Analysis and Machine Intelligence*, 14(1):76–86, January 1992.
- [147] Chunteng Bao, Lihong Xu, Erik D. Goodman, and Leilei Cao. A novel non-dominated sorting algorithm for evolutionary multi-objective optimization. *Journal of Computational Science*, 23:31–43, November 2017.
- [148] F. Mayinger. Classification and Applications of Two-Phase Flow Heat Exchangers. In Sadik Kakaç, Arthur E. Bergles, and E. Oliveira Fernandes, editors, *Two-Phase Flow Heat Exchangers: Thermal-Hydraulic Fundamentals and Design*, pages 3–27. Springer Netherlands, Dordrecht, 1988.
- [149] AHRI. AHRI\_standard\_550-590\_i-P\_2020, 2020.
- [150] Modine Manufacturing Company. Modine Commercial Coolers General Catalog, 2015.
- [151] Nathalie Japkowicz. The Class Imbalance Problem: Significance and Strategies. page 7, 2000.